UNIVERSITY OF CALIFORNIA
SANTA CRUZ

**Metal Oxide and Group III-nitride Nanomaterials for Photoelectrochemical Water Splitting**

Dissertation submitted in partial satisfaction
of the requirements for the degree of

DOCTOR OF PHILOSOPHY

in

CHEMISTRY

by

**Yi Yang**

September 2016

The Dissertation of Yi Yang is approved:

_____
Professor Yat Li, chair

_____
Professor Ilan Benjamin

_____
Professor Jin Z. Zhang

_____
Tyrus Miller
Vice Provost and Dean of Graduate Studies

## Table of Contents

## List of Figures

### Chapter 1



### Chapter 2

**Figure 2.6.** (a) SEM image of InN nanowires on carbon cloth substrate. (b) TEM image of InN nanowire. (c) Lattice-resolved TEM of InN nanowire. (d) Diameter histogram collected from 150 InN nanowires. The solid line is the Gaussian fitting curve.

**Figure 2.7.** (a) I-V curvecollected for Si-doped GaN-1000 nanowires on carbon cloth under light on/off chops (100 mW/cm$^2$, AM 1.5G). (b) I-t curves collected at 0.7 V vs. Ag/AgCl for 3600s.

**Chapter 3**

**Figure 3.1.** (a) Schematic diagram illustrates the growth procedure for rutile $TiO_2$ and H-R-$TiO_2$ nanowire arrays. (b) SEM image of rutile $TiO_2$ nanowires. (c) XRD spectra collected for rutile $TiO_2$ and H-R-$TiO_2$ nanowires prepared at the hydrogenation temperatures of 350, 450, and 550 $^oC$

**Figure 3.2.** (a) Linear sweeps voltammograms collected for pristine $TiO_2$ (red) and H-R-$TiO_2$ nanowires hydrogenated at 350 $^oC$ (blue), 450 $^oC$ (orange), and 550 $^oC$ (purple). (b) Amperometric *I-t* curves collected at 0.2 V vs. Ag/AgCl for 1 hour for H-R-$TiO_2$ nanowire hydrogenated at 350 $^oC$. (c) IPCE spectra of pristine $TiO_2$ and H-R-$TiO_2$ nanowires (350 $^oC$). (d) Mott-Schottky plots collected at a frequency of 10 kHz in the dark for the pristine $TiO_2$ and H-R-$TiO_2$ nanowires. Inset: magnified Mott-Schottky plots of H-R-$TiO_2$ nanowires hydrogenated at different temperatures.

**Figure 3.3.**(a) Schemeof the growth procedure for anatase $TiO_2$ and H-A-

$TiO_2$nanowires. (b) SEM image of anatase $TiO_2$ nanowires. (c) Linear sweeps voltammograms collected for pristine $TiO_2$ (red) and H-A-$TiO_2$ nanowires hydrogenated at 350 $^oC$ (blue), 450 $^oC$ (orange), and 550 $^oC$ (purple).(d) Mott-Schottky plots collected at the frequency of 10 kHz in the dark for pristine anatase $TiO_2$ and H-A-$TiO_2$ nanowires.

**Figure 3.4.** IPCE spectra of pristine anatase $TiO_2$ and H-A-$TiO_2$ nanowires hydrogenated at 550 $^oC$

**Figure 3.5.**(a) Schematic diagram demonstrated the growth procedure for the mixed phase $TiO_2$ and H-M-$TiO_2$ nanowires. Inset: SEM image of H-M-$TiO_2$ nanowires. (b) XRD spectra collected for pristine mixed phase $TiO_2$ and H-M-$TiO_2$ nanowires hydrogenated at various temperatures (350, 450, and 550 $^oC$). (c) Linear sweep voltammograms collected for the mixed phase $TiO_2$ and H-M-$TiO_2$ nanowires. (d) Mott-Schottky plots collected at a frequency of 10kHz in the dark for the mixed phase $TiO_2$ and H-M-$TiO_2$ nanowires.

**Chapter 4**

**Figure 4.1.**(a) I-t curves of rutile $TiO_2$ and H-$TiO_2$ photoanode for 12 hours. (b) I-V curves collected at 50 mV/s for rutile $TiO_2$ and H-$TiO_2$ before (solid lines) and following (dash lines) test.Amperometric *I–t* curve of (c) anatase $TiO_2$ nanotube and (d) P25 nanoparticle film photoanodes.

**Figure 4.2**. XRD spectra collected for $TiO_2$ nanowire photoanode before and

**Abstract**

**Metal Oxide and Group III-nitride Nanomaterials for Photoelectrochemical Water Splitting**

By

Yi Yang

Photoelectrochemical (PEC)cell is a device generated hydrogen fuel through an environmentally friendly method. The earliest report should date back to 1972. Honda and Fujishima firstdemonstrated solar water splitting by using titanium dioxide as photoanode in the cell. Then extensive efforts have been devotedto improving the solar-to-hydrogen (STH) conversionefficiency and decreasing thecost. However, current the efficiency of PEC device was limited on finding out a suitable photoanode material. The ideal photoanode material should have a good bandgap, favorable bandgap position, chemically stable and low cost. Therefore, this thesis would focus on studying different photoanode materials including GaN, $TiO_2$ and $Fe_2O_3$ to achieve high PECwater oxidation performance. In this thesis, I first designed GaN nanowires on carbon cloth via a chemical vapor deposition (CVD) method and demonstrated significant photoactivity for photoelectrochemical water oxidation. In addition, our group used to report a facile and general strategy to fundamentally improve the performance of $TiO_2$ nanowires for PEC water splitting.However, there are some

concerns about the real effects under higher hydrogen treated temperature as well as the stability of oxygen vacancies in $TiO_2$. Therefore I investigated the effect of hydrogenation temperature and the stability of oxygen vacancies in $TiO_2$ photoanodes. Furthermore, there are few reports about the study on the long term stability of $TiO_2$ photoanode even though most scholars used to think $TiO_2$ belongs to one of the most stable photoanode materials. Therefore,I carried out the first long term photostability measurement on various phases $TiO_2$ photoanodes including rutile, anatase and mixed phased and found $TiO_2$ photoanodes were not stable as expected. Then I investigated the mechanism of the instability of $TiO_2$ and carried out two strategies to stabilize $TiO_2$ materials in the PEC cell. Finally, I created a facile acid treated method on hematite to substantially enhance the PEC activity. I found the enhanced photocurrent is due to improved efficiency of charge separation as well as possible passivation of surface electron traps.

## Dedication

**DEDICATED**
**TO**
**MY FAMILY**

**Acknowledgements**

During the five years in my PhD program, I really appreciate all the people who used to help me.

Firstly, I want to thank my advisor, Prof. Yat Li.Without his offer, I could not come to UCSC to have the chance to pursue my PhD degree here and learn the culture of US. Furthermore, he used great patience to teach me how to do the research in an efficient and logic way, including how to find out the novelty and key points and how to design experiments in a project. After some time, I found it was a really good way to train me to create a meaningful project, and complete a project independently and perfectly. In addition, he always gave me many meaningful suggestions on presentating my own work in the presentation. I also thank him gave me advices and enough freedom on jobhunting.Furthermore, he also tought me how to get along well with different types of people. Besides, I wouldlike to thank Prof. Li's wife, Dr. Fang Qian. I appreciate all her favors on my research, jobhuntings as well as sharing life experience.

Secondly, I would like to thank my comittees, Prof. Ilan Benjamin and Prof. Jin Z. Zhang.Thanks to their high standard on my second year seminar, oral and review exams so I can be a qualified Doctor. Especially, I want to thank Prof. Jin Z. Zhang. He spent a lot of time helping me prepare my exams as well as my

jobhuntings.

Thirdly, I would like to thank Yat's first student, Dr. Gongming Wang. He offered me so much help not only in research but also in life when I came to UC Santa Cruz. Besides, I need to thank Yat's second student, Dr. Yichuan Ling. I appreciate all his favors on my research. In addition, I would also like to thank all the former and current members in Li lab,including, Dr. Hunyu Wang, Prof. Xihong Lu, Feng Luan, Prof.Dingshen Yuan, Prof. Xiaoxia Liu, Dr. Ying-Chih Pu, Tianyu Liu, Teng Zhai, Yang Yang, Wei-Hao Lin, Tianyi Kou, Yu Song, Bin Yao, Mingyang Li and Jing Zhang. Thank for their helps in my research projects. Furthermore, I also want to express my thanks to my friends in Shaowei's lab and Jin's lab, including Dr. Xiongwu Kang, Peiguang Hu, Limei Chen, Gaby Lu, Staci Adams, Prof. Haixia Ma, Binbin Luo.

Finally, I really need thank my parents, Zhongkui Yang and Yaru Sun. Without theirsupport, I could not come to UC Santa Cruz and finish my PhD program. I really appreciate all theirunderstandings on each of my decisions these years. Besides, I also need to thank my older sister, Liang Yang and her husband Bo Fu. Without them to take care of my parents, I can't pursue my degree without any concerns.

The text of this dissertation includes reprints of the following previously

published or subsequently published materials.

1. “Growth of Gallium Nitride and Indium Nitride Nanowires on Conductive and Flexible Carbon Cloth Substrate”,**Yang Y.**, Ling Y, Wang G., Lu X., Tong Y. and Li Y., *Nanoscale*, 2013, 5, 1820-1824
2. “The Effect of Hydrogenation Temperature on TiO2 Nanostructures for Photoelectrochemical Water Oxidation”,**Yang Y.**, Ling Y., Wang G. and Li Y., *Eur. J. Inorg. Chem.*, 2014, 760-766
3. “ Photo-hole Induced Corrosion of Titanium Dioxide: Mechanism and Solutions”,**Yang Y.**, Ling Y.,Wang G., Liu T., Wang F., Zhai T., Tong Y., Li Y., *Nano Lett.*, 2015, 15, 7051-7057
4. “Acid Treatment Enables Suppression of Electron-Hole Recombination in Hematite for Photoelectrochemical Water Splitting”,**Yang Y.**, Forster M., Ling Y., Wang G., Zhai T., Tong Y., Cowan A. J. and Li Y.,*Angew. Chem. Int. Ed.*, 2016, 128, 3464-3468

# Chapter 1

## Introduction of Photoanode Nanomaterials for Photoelectrochemical Water Splitting


### Abstract

Hydrogen is a clean and renewable fuel with high energy density, which has great potential to address the surgent problem due to the rapid increase demand for energy. Photoelectrochemical (PEC) water splitting is a promising method to convert solar energy to storable chemical fuels such as hydrogen ($H_2$).However, the current efficiency of solar to hydrogen is still very low. The performance was mainly limited by the bandgap, diffusion length, carrier lifetime and stability of the photoelectrode materials. In addition, the efficiency of photoanode materials is far behind of the efficiency of photocathode materials. My research mainly focused on the study of photoanode semiconductor materials.Although nanostructured semiconductors could increase electrolyte accessible area and shorten carrier diffusion distance, so that improve the PEC performance to some extent,these nanostructurescould not change their intrinsic electronic properties. In the chapter, I give an overview of the basic mechanism of photoelectrochemical water splitting, the general requirement and current study on the photoanode materials, and PEC performance measurements.

## Introduction

The growth of the global population and the standard of living has resulted in a constantly increased energy demanding. Nowadays, the energy crisis has become one of the most urgent issues in the society. Based on this, looking for renewable and sustainable energy sources is believed to be a potential solution to solve the serve energy issues. Among the sustainable energy sourcesincluding solar, wind, and hydropower,converting solar energy into chemical fuelhas attracted large attentions due to the abundance of energy source.For instance, the total solar energy reached the Earth's surface is around 125,000 TW, whichis sufficient to cover global energy requirement. Among the solar energy conversion devices, photoelectrochemical (PEC) cell is one of the most attractive devices is to convert solar energy into chemical fuels such as hydrogen as hydrogen hashigh energydensity of ~140 MJ/Kg.[1]Furthermore, hydrogen is the popular source in a hydrogen fuel cell to generate electricity, and water is the only side production. Therefore, PEC water spilitting is an environment-friendly and effective method to address the energy shortage issues.

### 1.1 The Principle of Photoelectrochemical Water Splitting

PEC water splitting is anenvironmentally friendly and low cost reaction to generate hydrogen fuel.[2-7] The reaction is :

$$H_2O_{(l)} \rightarrow H_{2(g)} + \tfrac{1}{2}O_{2(g)} \ (\Delta G \approx 237.2 \text{ kJ mol}^{-1}, E^0 = 1.23 \text{ V } \textit{vs.} \text{ NHE})$$

This process could be achieved in a PEC cell by using an-type semiconductor

asthe photoanode and p-type semiconductor as photocathode**(Figure 1.1a)**.[8] The charge transfer between semiconductor and electrolyte results in charging of the surface layer of the semiconductor. The charge transfer from the *n* type semiconductor to the electrolyte would result in upwards band bending. The potential barrier at the interface could helpcharge separation and facilitate charger's transportation at the band bending layers. For water splitting, it requires at least 1.23 V to drive the reaction.To drive the water splitting, the photoelectrodes must absorb light with photon energies larger than 1.23 eV. In addition, for sustainable water splitting, the bandgap larger than 1.23 eV bandgap is not enough. In most cases, overpotential should also be considered to drive the reaction. Therefore, the minium bandgap should be around1.7 ~ 1.8eV.[7,9-10]

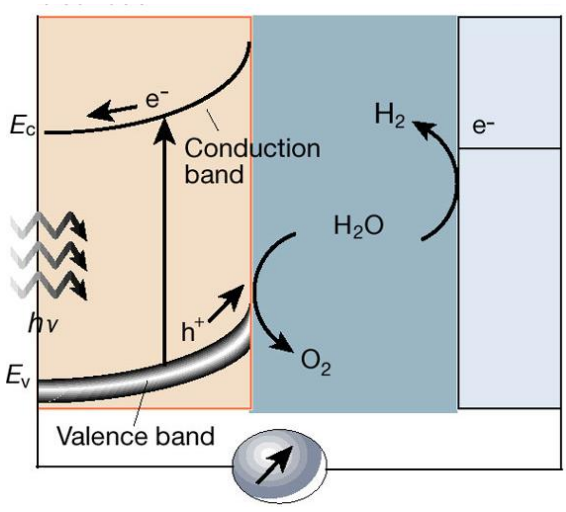


**Figure 1.1** Scheme of photoelectrochemical cell based on *n*-type semiconductor photoanode.[8]

## 1.2 General Photoanode Materials on Photoelectrochemical Water Splitting

Currently, the STH conversion efficiency of PEC device is mainly limited by the

low performance of photoanode.Therefore, large number of scholars devoted great efforts to investigate the study on photoanode materials.Figure 1.2 shows the band structure potentials of typical semiconductors versus vacuum potential and their corresponded bandgaps. [32] Actually,large amount of*n*-type metal oxide semiconductors including $TiO_2$, [11-14] ZnO,[15-18]$WO_3$,[19-22] hematite [27-31]and $BiVO_4$, [23-26] have been studied as photoanode materials for water splitting. Basicly, the bandgap of the n type semiconductor should be larger than 1.23 eV and cover the water reduction and oxidation potentials. As shown in Figure 1.2, onlylarge bandgap metal oxides such as $TiO_2$, $SrTiO_3$ and ZnO can meet this requirement. However, the large bandgap could only absorb the UV light, which is only 3% in the ground level sunlight. For those metal oxides with small bandgap such as $Fe_2O_3$ and $WO_3$, their conduction band potentials are not negative enough to reduce water, so external bias should be applied to drive water splitting. Furthermore, the conductivity of $Fe_2O_3$ is bad and its carrier diffusion length is really short. [28]Besides the metal oxide photoanode materials, metal sulfides such as CdS and CdSe can satisfy this requirement. However, they suffer great severe stability issue due to the easy oxidation to metal oxides. [33-36] Furthermore, silicon could absorb large portion of solar spectrum due to it small bandgap (1.1 eV)[37]However, external bias is needed because the valence band is not positive enough to oxidize water.[38-41]In addition, the instability is also an important issue for silicon photoanodedue to eht surface oxidation by the photogenerated holes.

42

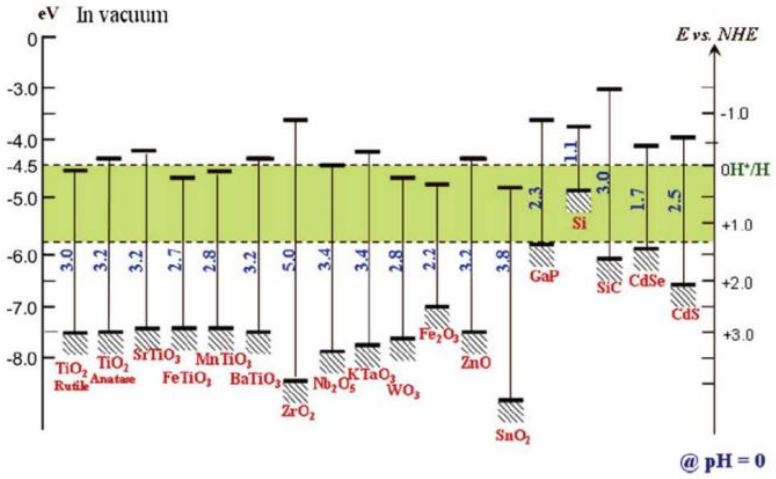


**Figure 1.2.** The bandgap and band structure potentials of n type semiconductor photoanode materials. [32]

### 1.3 PEC Performance Measurement

A three-electrode PEC cell is normally used to measure the PEC performance of photoanodes. (Figure 1.3) The designed photoanode materials were applied as the working electrodes. A coiled Pt sheetand an Ag/AgCl (1M KCl) electrode were used as counter electrode and reference electrode, respectively. The Electrolyte could be basic, neutralor acidic aqueous solution according to the requirement of the photoelectrodes.In addition, the electrolyte was deaerated by purging $N_2$ gas. The PEC measurements were recorded by an electrochemical workstation (Model CHI 660D, CH instruments, Inc., Austin, TX); and a solar simulator (Newport, Model 69907) coupled to a filter (AM 1.5G) with a 150 W Xenon lamp as the white light source.

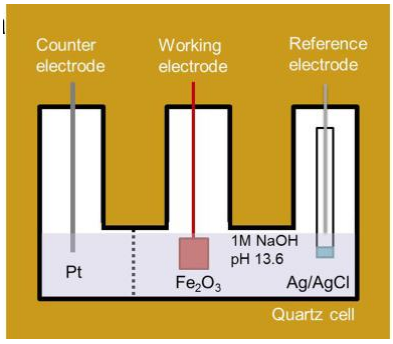


**Figure 1.3**Scheme of a three-electrode PEC cell.

## References


1. Li, Y.; Zhang, J. Z. *Laser & Photonics Reviews* **2010,** 4, (4), 517-528.
2. Wheeler, D. A.; Wang, G.; Ling, Y.; Li, Y.; Zhang, J. Z. *Energy Environ. Sci.* **2012,** 5, (5), 6682-6702.
3. Gratzel, M. *Nature* **2001,** 414, (6861), 338-344.
4. Sivula, K.; Zboril, R.; Le Formal, F.; Robert, R.; Weidenkaff, A.; Tucek, J.; Frydrych, J.; Gratzel, M. *J Am Chem Soc* **2010,** 132, (21), 7436-7444.
5. Sivula, K.; Le Formal, F.; Grätzel, M. *ChemSusChem* **2011,** 4, (4), 432-449.
6. Wang, G.; Ling, Y.; Li, Y. *Nanoscale* **2012,** 4, (21), 6682-6691.
7. Wang, G.; Ling, Y.; Wang, H.; Xihong, L.; Li, Y. *Journal of Photochemistry and Photobiology C: Photochemistry Reviews* **2014,** 19, (0), 35-51.
8. Grätzel M., *Nature,* **2001**, 414, 338-344
9. Coridan, R. H.; Shaner, M.; Wiggenhorn, C.; Brunschwig, B. S.; Lewis, N. S. *The Journal of Physical Chemistry C* **2013,** 117, (14), 6949-6957.

10. Liu, C.; Tang, J.; Chen, H. M.; Liu, B.; Yang, P. *Nano Lett* **2013,** 13, (6), 2989-2992.

11. Park, H. S.; Lee, H. C.; Leonard, K. C.; Liu, G.; Bard, A. J. *Chemphyschem* **2013,** 14, (10), 2277-2287.

12. Heller, A. *Science* **1984,** 223, (4641), 1141-1148.

13. Wang, H.; Wang, G.; Ling, Y.; Lepert, M.; Wang, C.; Zhang, J. Z.; Li, Y. *Nanoscale* **2012,** 4, (5), 1463-1466.

14. Aharon-Shalom, E.; Heller, A. *J Electrochem Soc* **1982,** 129, (12), 2865-2866.

15. Hensel, J.; Wang, G.; Li, Y.; Zhang, J. Z. *Nano Lett.* **2010,** 10, 478-483.

16. Wang, G.; Wang, H.; Ling, Y.; Tang, Y.; Yang, X.; Fitzmorris, R. C.; Wang, C.; Zhang, J. Z.; Li, Y. *Nano Lett* **2011,** 11, (7), 3026-3033.

17. Boettcher, S. W.; Warren, E. L.; Putnam, M. C.; Santori, E. A.; Turner-Evans, D.; Kelzenberg, M. D.; Walter, M. G.; McKone, J. R.; Brunschwig, B. S.; Atwater, H. A.; Lewis, N. S. *J Am Chem Soc* **2011,** 133, (5), 1216-1219.

18. Hwang, Y. J.; Hahn, C.; Liu, B.; Yang, P. *ACS Nano* **2012,** 6, (6), 5060-5069.

19. Su, J. Z.; Guo, L. J.; Bao, N. Z.; Grimes, C. A. *Nano Lett* **2011,** 11, (5), 1928-1933.

20. Wang, G.; Ling, Y.; Wang, H.; Yang, X.; Wang, C.; Zhang, J. Z.; Li, Y.

*Energy Environ. Sci.* **2012,** 5, (3), 6180-6187.

21. Zhang, X.; Lu, X.; Shen, Y.; Han, J.; Yuan, L.; Gong, L.; Xu, Z.; Bai, X.; Wei, M.; Tong, Y.; Gao, Y.; Chen, J.; Zhou, J.; Wang, Z. L. *Chem. Commun. (Camb.)* **2011,** 47, (20), 5804-5806.
22. Jin, T.; Diao, P.; Wu, Q.; Xu, D.; Hu, D.; Xie, Y.; Zhang, M. *Applied Catalysis B: Environmental* **2014,** 148-149, 304-310.
23. Sayama, K.; Nomura, A.; Arai, T.; Sugita, T.; Abe, R.; Yanagida, M.; Oi, T.; Iwasaki, Y.; Abe, Y.; Sugihara, H. *The Journal of Physical Chemistry B* **2006,** 110, (23), 11352-11360.
24. Wang, G.; Ling, Y.; Lu, X.; Qian, F.; Tong, Y.; Zhang, J. Z.; Lordi, V.; Rocha Leao, C.; Li, Y. *The Journal of Physical Chemistry C* **2013,** 117, (21), 10957-10964.
25. Sivula, K. *The Journal of Physical Chemistry Letters* **2013,** 4, (10), 1624-1633.
26. Zhou, M.; Wu, H. B.; Bao, J.; Liang, L.; Lou, X. W.; Xie, Y. *Angew. Chem. Int. Ed.* **2013,** 52, (33), 8579-8583.
27. Wang, G.; Ling, Y.; Wheeler, D. A.; George, K. E. N.; Horsley, K.; Heske, C.; Zhang, J. Z.; Li, Y. *Nano Lett* **2011,** 11, (8), 3503-3509.
28. Ling, Y.; Wang, G.; Reddy, J.; Wang, C.; Zhang, J. Z.; Li, Y. *Angew. Chem.* **2012,** 124, (17), 4150-4155.
29. Lin, Y.; Zhou, S.; Sheehan, S. W.; Wang, D. *J. Am. Chem. Soc.* **2011,** 133,

2398-2401.

30. Lin, Y.; Yuan, G.; Sheehan, S.; Zhou, S.; Wang, D. *Energy Environ. Sci.* **2011,**4, (12), 4862-4869.

31. Li, L.; Yu, Y.; Meng, F.; Tan, Y.; Hamers, R. J.; Jin, S. *Nano Lett* **2012,** 12, (2), 724-731.

32. Jing, D. W.; Guo, L. J.; Zhao, L. A.; Zhang, X. M.; Liu, H. A.; Li, M. T.; Shen, S. H.; Liu, G. J.; Hu, X. W.; Zhang, X. H.; Zhang, K.; Ma, L. J.; Guo, P. H., *Int. J. Hydrogen Energy* **2010,** 35, 7087-7097

33. Hensel, J.; Wang, G. M.; Li, Y.; Zhang, J. Z., *Nano Lett.* **2010,** 10, 478-483.

34. Wang, G. M.; Yang, X. Y.; Qian, F.; Zhang, J. Z.; Li, Y., *Nano Lett.* **2010,** 10, 1088-1092.

35. Liu, L. P.; Wang, G. M.; Li, Y.; Li, Y. D.; Zhang, J. Z., *Nano Res.* **2011,** 4, 249-258.

36. Larsen, G. K.; Fitzmorris, B. C.; Longo, C.; Zhang, J. Z.; Zhao, Y. P., *J. Mater. Chem.* **2012,** 22, 14205-14218.

37. Walter, M. G.; Warren, E. L.; McKone, J. R.; Boettcher, S. W.; Mi, Q. X.; Santori, E. A.; Lewis, N. S., *Chem. Rev.* **2010,** 110, 6446-6473.

38. Shin, K.; Yoo, J. B.; Park, J. H., *J. Power Sources* **2013,** 225, 263-268.

39. Swierk, J. R.; Mallouk, T. E., *Chem. Soc. Rev.* **2013,** 42, 2357-2387.

40. Khaselev, O.; Turner, J. A., *Science* **1998,** 280, 425-427.

41. Brillet, J.; Yum, J. H.; Cornuz, M.; Hisatomi, T.; Solarska, R.; Augustynski,

J.; Graetzel, M.; Sivula, K., *Nature Photon.* **2012,** 6, 823-827.

42. Chen, Y. W.; Prange, J. D.; Duhnen, S.; Park, Y.; Gunji, M.; Chidsey, C. E. D.; McIntyre, P. C., *Nature Mater.* **2011,** 10, 539-544.

# Chapter 2

## Growth of Gallium Nitride and Indium Nitride Nanowires on Conductive and Flexible Carbon Cloth Substrate


### Abstract

In this chapter I demonstrate a general strategy for synthesis of gallium nitride (GaN) and indium nitride (InN) nanowires on conductive and flexible substrates-carbon cloth. The GaN and InN nanowires were with Ga and In metal as group III precursors and ammonia as group V precursorsynthesizedthrough a home built chemical vapor deposition (CVD) system. We found the morphology, density and growth mechanism of these nanowires are determined by the growth temperature and the group III-nitride nanowires are single crystalline wurtzite structures. Furthermore, we applied the GaN nanowires on carbon cloth substrate as a photoelectrode and shown pronounced photoactivity for photoelectrochemical water oxidation. The ability to grow group III-nitride nanowires on conductive and flexible substrate could open up new opportunities for nanoscale photonic, electrochemical and electronic devices.


### 2.1 Introduction

Semiconductor nanowireshave been studied widely on active nanoscale electronic and photonic devices.[1-4] Among them, group III-nitride[5-8]nanomaterials havedemonstratedgreat potentialsin device applications,such as field-effect transistors,[9-11] light-emittingdiodes,[12-16]and lasers.[17-22]For practical

applications, it is highly desirable to have high yield nanowires assembled on a conductive, flexible and low-cost substrate that connects all the nanowires to form scalable and wearable electronic and photonic devices. Normally, the synthesis of group III-nitride nanowires are always demonstrated on a variety of sapphire substrates.[5]Yang and coworkers also reported the growth of high density vertically aligned GaN nanowire arrays on γ-$LiAlO_2$ and MgO substrates.[23]However, sapphires are not conductive that restricted the applications of the group III-nitride nanodevices. To address this issue, considerable efforts has been placed over the past years in preparing group III-nitrides nanowires on conductive substrates such as silicon,[24, 25] $ZrB_2$,[26] $(Mn,Zn)Fe_2O_4$,[27] SiC,[28]and stainless steel.[29] However, these substratesare either expensive or not flexible. In addition, carbon cloth have been extensively used as electrode materials in applications such as fuel cells and supercapacitors due to their low cost, excellent conductivity, corrosion resistance, and flexibility.[30-33]These works motivated us to explore the potential of carbon cloth as growth substrate for group III-nitride materials, which could potentially address the limitation of conventional substrates. Here we reportthe high yield synthesis ofGaN and InN nanowires on carbon cloth substrates using chemical vapor deposition (CVD) method for the first time. Importantly, we demonstrated that GaN nanowire arrays grown on the carbon cloth substrate can be served as photoelectrode for photoelectrochemical water oxidation.

## 2.2 Experimental Section

### 2.2.1 Synthesis of GaN nanowires

Carbon cloth (AvCarb 1071 HCB 40cm×40cm) was cleaned by ethanol and followed by deionized water. Then the substrate was soaked in zinc acetate (0.02 M) ethanol solution and further heated on a hot plate at 550°C for 10 min to form a layer of ZnO seeds. The ZnO seeded carbon cloth substrate was then dipped into the $Ni(NO_3)_2$ ethanol solution (0.2 M) and was heated to forma NiO catalyst layer. GaN nanowires were grown in a horizontal tube furnace ata temperature range between 800 and 1100 °C and a fixed pressure of 100 torr for 30 min.Gallium metal (99.999%, Alfa Aesar) and ammonia (15 sccm) were Ga and N precursors, respectively. The carbon cloth substrate was covered on the gallium metal (99.999%, Alfa Aesar) and holded by a mica plate. The carrier gas was ultrahigh purity hydrogen gas (30 sccm). In addition, Si-doped GaN nanowires were synthesized with the similar method with the injection of silane as the Si dopant source with a flow rate of 5sccm into the CVD system.

### 2.2.2 Synthesis of InN nanowires

The pre-cleaned carbon cloth substrate was dropped the gold colloidal solution and allows to air dry. InN nanowires were grown at 550 °C and 150 torr for 30 min.Indium metal (99.999%, Alfa Aesar) and ammonia (200 sccm) were applied as In and N precursors, respectively. The indium metal was contained in a ceramic boat and the carbon cloth substrate was covered on the top. The carrier gas was $N_2$(100 sccm).

### 2.2.3 Photoelectrochemical measurements of nanowire photoanodes

The Si-doped GaN nanowires grown on carbon cloth substrate were fashioned into electrodes by securing the carbon cloth substrate to a copper wire. Edges of the substrate were then sealed with epoxy resin. The effective area of the working electrode is around 0.30 $cm^2$. All the photoelectrochemical measurements were performed by a CHI 660D electrochemical station, using Ag/AgCl (1 M KCl) as reference electrode, Pt sheet as counter electrode, and 0.5M $Na_2SO_4$ aqueous solution (pH = 6.8) as an electrolyte, under a simulated sunlight (100 $mW/cm^2$) generated with a 150W xenon lamp (Newport 6255) coupled with an AM 1.5 global filter (Newport 81094). The power density of the incident light was measured with a digital power-meter. The electrolyte was 0.5M $Na_2SO_4$ solution with a pH value of 7.

### 2.2.4 Material Characterization

X-ray diffraction (XRD) spectra were measured at room temperature on a Rigaku Americas Miniflex Plus powder diffractometer from a 2θ angle of 20 to 70 degree with a step size of 0.04 degree at a rate of 1 degree/min. Scanning electron microscopy (SEM) images were collected by a field-emission SEM (Hitachi S-4800 II). High resolution transmission electron microscopy images were collected by a TEM (Tecnai F20 UT) operated at 200 kV.

## 2.3 Results and Discussion

GaN nanowires were synthesized on ZnO seeded carbon cloth substrate in hydrogen atmosphere by CVD method (Figure 2.1), using gallium metal and

ammonia as Ga and N precursors, respectively. Nickel (II) nitrate was used as catalyst for the growth. We obtained high yield GaN nanowires in a range of temperatures between 800 and 1100 °C. Scanning electron microscopy (SEM) images show that the nanowiremorphology and size are closely associated with the growth temperatures (Figure 2.2). As shown in Figure 2.2a and 2.2e, nanowiresprepared at 800 °C exhibit a broad distribution of wire diameter. In addition, these nanowires are thin and kinked with a typical diameter less than 50 nm and a length in the range of 1 to 4 μm. When the growth temperature increased to 900 °C, uniform nanowires were obtained (Figure 2.2b and 2.2f). These nanowires have a typical length in a range of 2 to 5 μm, slightly longer than the wires obtained at 800 °C. Furthermore, nanoparticles were observed on the tipsof nanowires obtained at800 and 900 °C,suggesting the growth mechanism was vapor-liquid-solid (VLS) growth process.[34, 35]When the growth temperature further increased to 1000 °C (Figure 2.2c and 2.2g), the nanowires became even thicker and longer (6 to 25 μm). Andnanoparticles were not observed on the tips of nanowires obtained at 1000 °C, indicating the nanowire growth mechanism changed as the temperature increase from 900 to 1000 °C. At 1100 °C, the anisotropic growth of 1D structure is no longer favorable and the formation of microcrystals was observed.

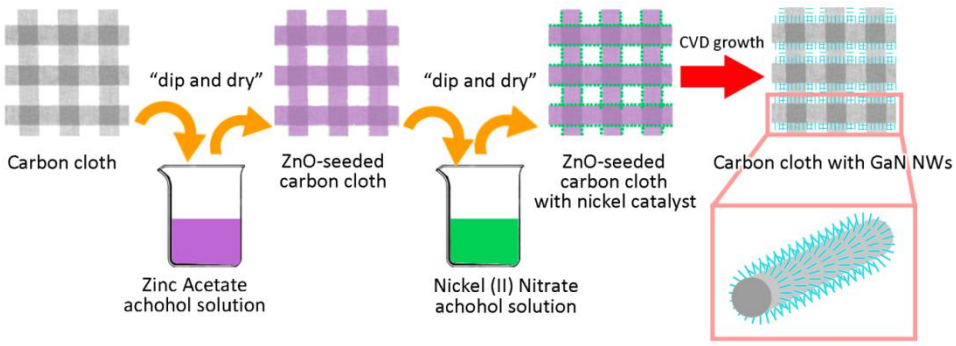

**Figure 2.1.** Scheme of the growth procedure for GaN nanowires on carbon cloth substrate.

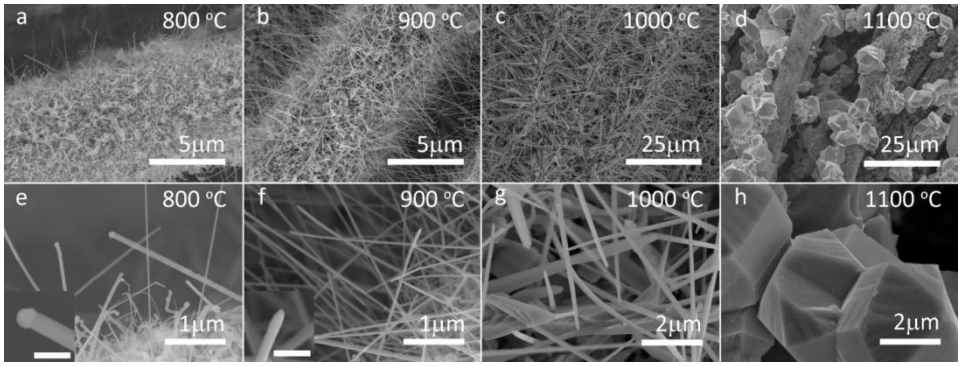


**Figure 2.2.** SEM images collected for the GaN nanowires prepared at different growth temperatures. Inset: SEM images collected at the tip of GaN nanowires obtained at800 and 900 °C. Scale bars in insets are 200 nm.

Powder X-ray diffraction spectra were collected from GaN nanowires grown at 900 °C and 1000°C, which denoted as GaN-900 and GaN-1000, and a blank carbon cloth substrate treated under the same growth conditions in the absence of Ga metal precursor (Figure 3.3a). The dashed lines are the peaks highlight to wurtzite GaN structure (PDF # 65-3410). These sharp diffraction peaks suggest the good crystallinity of GaN. Furthermore, we also observed the diffraction peaks that can be indexed to Ga metal, which is possible to bedeposited on the substrate during the growth process. In addition, GaN-900 and GaN-1000 show distinct size distribution. Diameter histograms were collected for GaN-900 (Figure 2.3b) and GaN-1000 (Figure 2.3c) nanowires based on the 150 nanowires fromSEM analysis. The Gaussian fittings based on these histograms revealed that the average diameters of GaN-900 and GaN-1000 nanowires

arearound 50 nm and 200 nm, respectively.

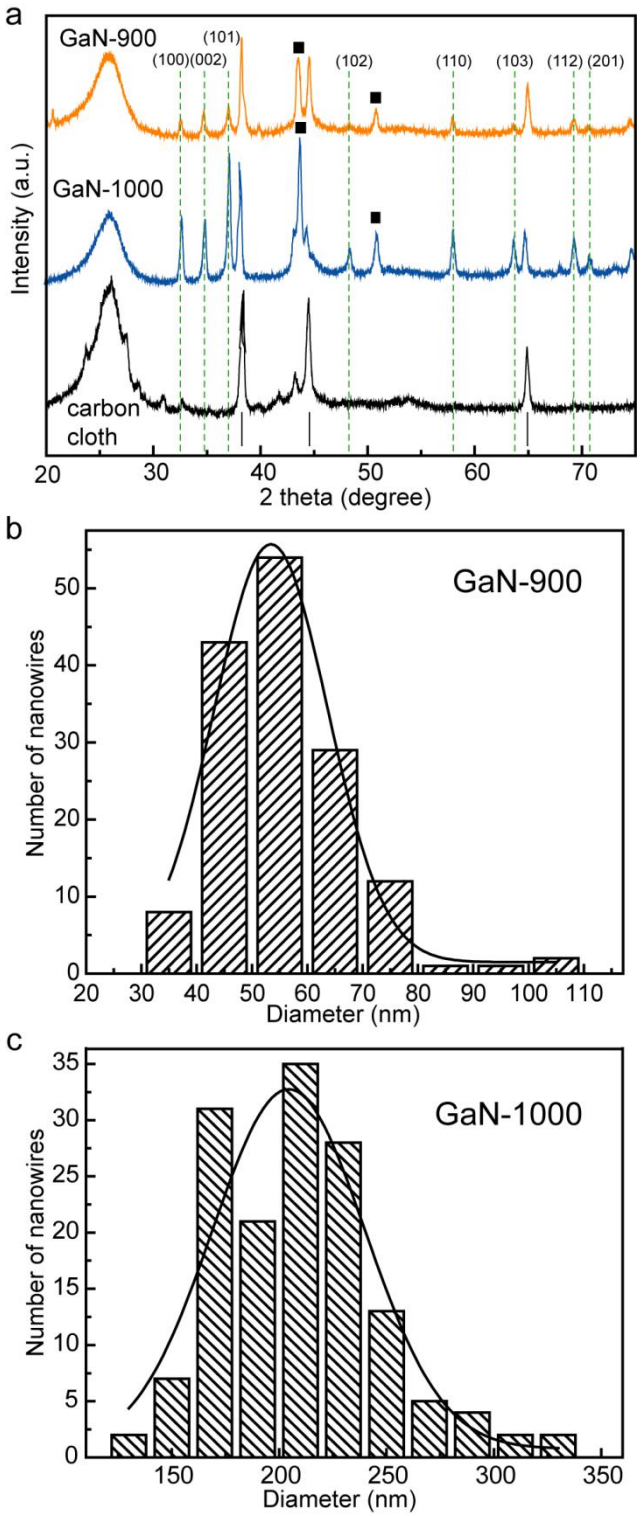


**Figure 2.3.** (a) XRD spectra collected from GaN-900 and GaN-1000 nanowires on carbon cloth substrate anda blank carbon cloth substrate. (b,c) Diameter

histograms collected from150 GaN-900 and GaN-1000 nanowires.The solid linesare the Gaussian fitting.

TEM analyses were used to further characterize the structure and the growth mechanism of GaN-900 and GaN-1000 nanowires. The TEM image collected for GaN-900 nanowire showed that the nanowire diameter is essentially the same as the diameter of Ni nanocluster, as expected for the VLS process (Figure 2.4a).[34] The lattice spacing of the catalyst was measured to be 0.20 nm, consistent with the d-spacing of the Ni (111) plane (Figure 2.4c). The homogeneous contrast along the wire suggests that the nanowire is single crystalline material. The HRTEM image revealed the lattice fringes with interplanar spacings of 0.25 and 0.24 nm, correspond to the (002) and (101) planes of wurtzite GaN, respectively. The angles between these lattice planes and thelattice plane perpendicular to the nanowire growth axis are 90° and 28.05°, suggesting the GaN-900 nanowire grows along the [100] direction. Additionally, TEM image shows that GaN-1000 nanowire is asingle-crystal with sharp nanowire end (Figure 2.4b). Interestingly, we did not observe any Ni catalyst for all the GaN-1000 nanowires. The absence of catalyst indicates that the growth of the GaN-1000 nanowires could be drived by self-catalytic vapor-solid process[36] or defect induced growth mechanism,[37]instead of the VLS mechanism observed for GaN-900 nanowires. The TEM image also reveals that the lattice fringes that perpendicular to the nanowire growth axis has an interplanar spacing of 0.28 nm, which is consistent with the wurtzite GaN (100) plane and therefore confirms the GaN-1000 nanowires also grow along [100]

direction.

On the other hand, we found that the ZnO seeds also play an important role in the VLS growth of GaN-900 nanowires. Figure 2.5 shows the SEM images collected for GaN nanowires grown on carbon cloth substrate without ZnO coating. While nanowires were still obtained in the growth temperature window between 800 and 1000 °C, the density of GaN nanowires obtained at 800 and 900 °C were substantially lower than that obtained on the ZnO seeded substrate at the same temperatures. Additionally, most of these GaN nanowires are twisted, which is different from the morphology observed on the ZnO seeded substrate. Ni catalysts were found at the tip of these nanowires. Meanwhile, the morphology and density of GaN nanowires prepared at 1000 °C are similar to the GaN-1000 nanowires.These results suggest that the ZnO seeds could facilitate the VLS growth of GaN nanowires at the temperature 900 °C or below.

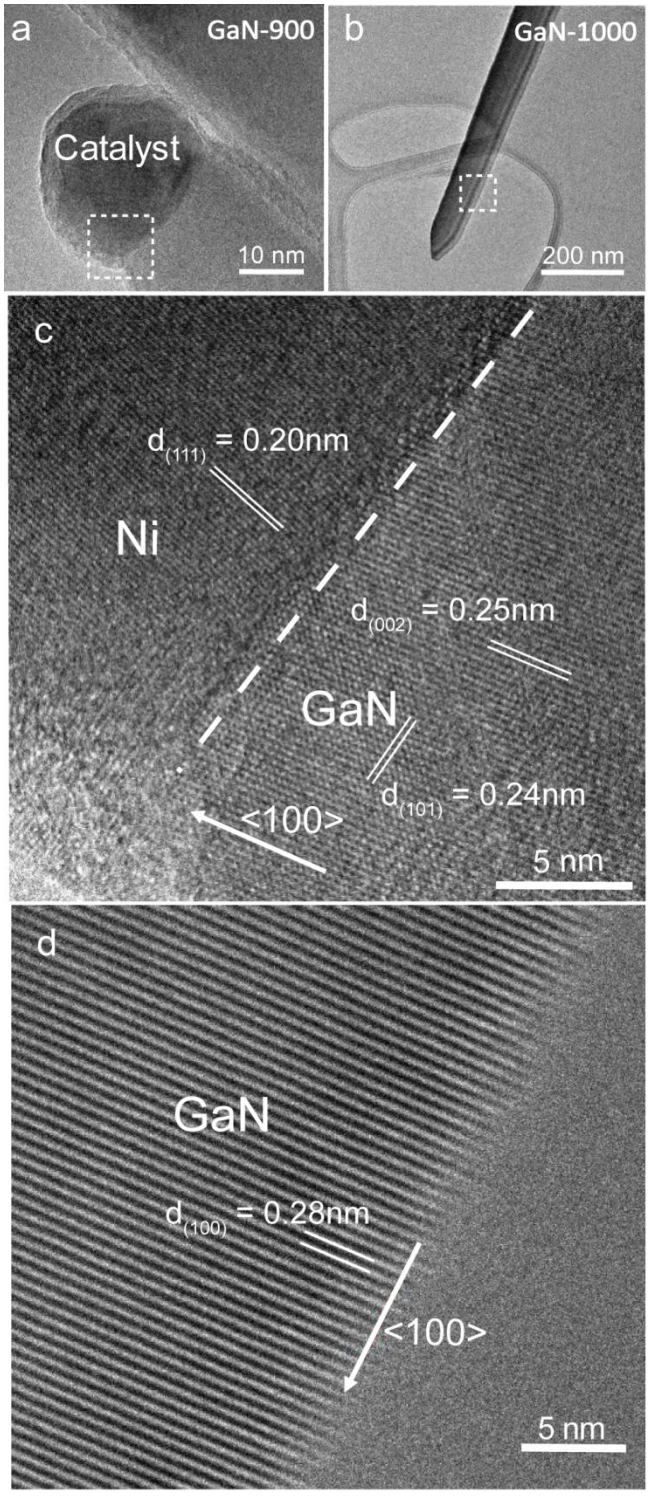


**Figure 2.4.** TEM images of (a) GaN-900 and (b) GaN-1000 nanowires. (c) Lattice-resolved TEM images recorded at the interface of GaN-900 nanowire and nickel catalyst. (d) Lattice-resolved TEM images of GaN-1000 nanowire.

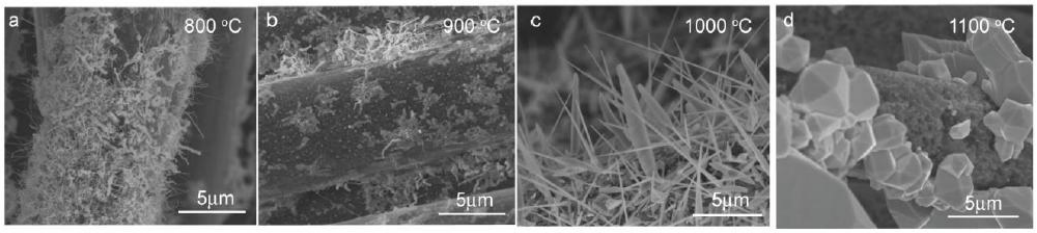


**Figure 2.5.** SEM images collected for GaN nanowires prepared at different temperatures without ZnO seed.

We further extended this growth approach to prepare another important group III-nitride materialon carbon cloth substrate-InN nanowires. As shown in Figure 2.6a, the carbon fibers were uniformly covered by InN nanowires, and the lengths were between 500 nm and 2 μm. A diameter histogram was plotted from the 150 InN nanowires(Figure 2.6d). These nanowires exhibit uniform diameters, with an average diameter of 40 nm. Meanwhile, a gold nanoparticle was found on the tip of the InN nanowire,as shown in Figure 2.6b. It indicates that the InN growth is also drived by VLS process. The lattice-resolved TEM image was collected at the interface between gold nanoparticle and InN nanowire. The interplanar spacings in the nanowire and the particle were measured to be 0.283 nm and 0.235 nm, corresponding to the wurtzite InN (002) plane and gold (111) plane, respectively. Additionally, the InN (002) plane perpendicular to the nanowire growth axis, indicating the InN nanowire grew along [002] direction.

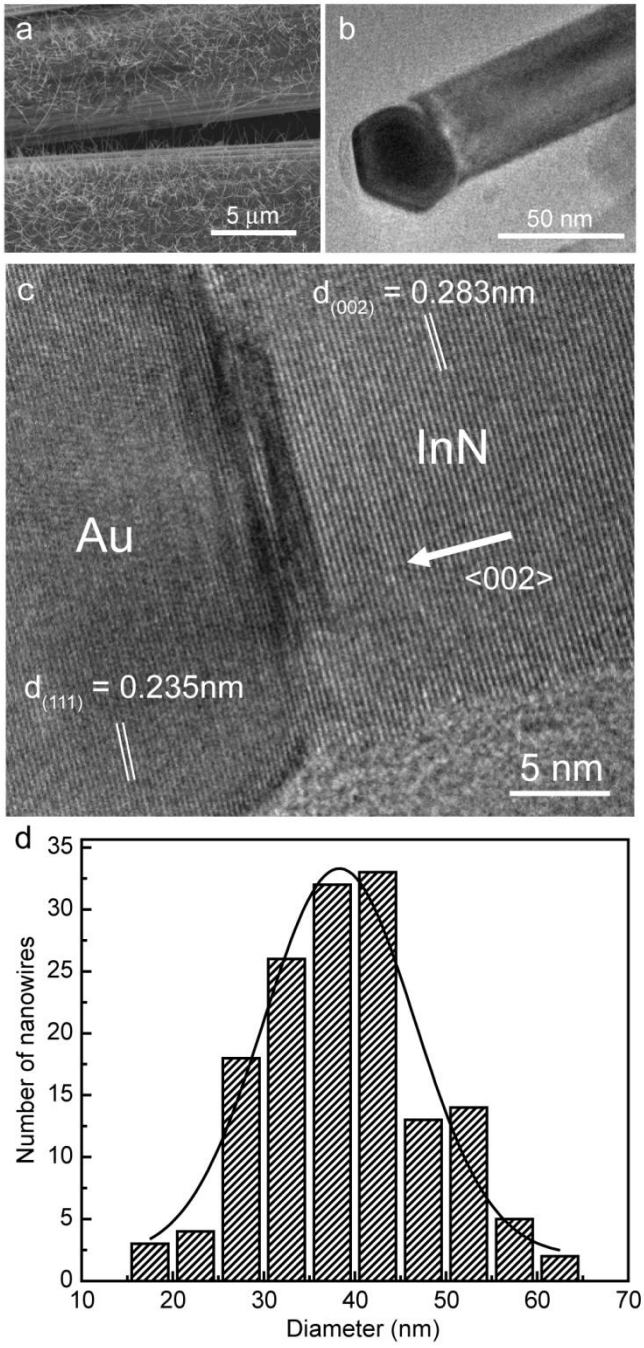


**Figure 2.6.** (a) SEM image of InN nanowires on carbon cloth substrate. (b) TEM image of InN nanowire. (c) Lattice-resolved TEM of InN nanowire. (d) Diameter histogram collected from 150 InN nanowires. The solid line is the Gaussian fitting curve.

The growth of group III-nitrides nanowires on flexible conducting substrate could open up new opportunities for device fabrication and applications. Here we exemplified this idea by employing Si-doped GaN nanowire arrays grown on carbon cloth as a photoelectrode for PEC water oxidation. GaN has been studied for photocatalytic water splitting applications because of its favorable bandedge position, in which the conduction band and valence band straddle the hydrogen reduction ($H^+/H_2$) and water oxidation ($H_2O/O_2$) potentials.[38, 39] Silicon is known to be a shallow donor that can increase the electrical conductivity of GaN nanowires.[40] Si-doped GaN nanowires were prepared on carbon cloth substrate using the same conditions for GaN-1000 nanowires, with the addition of diluted silane gas (100 ppm in ultrahigh purity hydrogen) at a rate of 5 sccm during the growth. PEC measurements were performed in a three-electrode system, using the nanowire-arrayed electrode as working electrode, platinum sheet and Ag/AgCl (1M KCl) as the counter and the reference electrode, respectively. 0.5M $Na_2SO_4$ solution (pH = 7) was used as electrolyte because photoanodic etching of GaN could occur in both strong basic and acidic electrolytes.[41]The photoactivity of the nanowire electrode was measured under the simulated solar illumination at 100 mW/cm$^2$. Figure 2.7a shows the I-V curvecollected for the Si-doped GaN-1000 nanowire electrode with light on/off cycles in a potential range of -0.1 to 0.9 V vs. Ag/AgCl. The results confirmed that these GaN nanowires exhibit pronounced photoresponse under white light illumination. To examine the photostability of GaN nanowires for water oxidation, I–t curves were collected at 0.7 V vs. Ag/AgCl with light on/off cycles at 100mW/cm$^2$ (Figure 2.7b). We observed the photocurrent density slightly decay from 31 to

25μA/cm$^2$ after 3600s, indicating that Si-doped GaN nanowire photoanode was relatively stable for photoelectrochemical water oxidation.

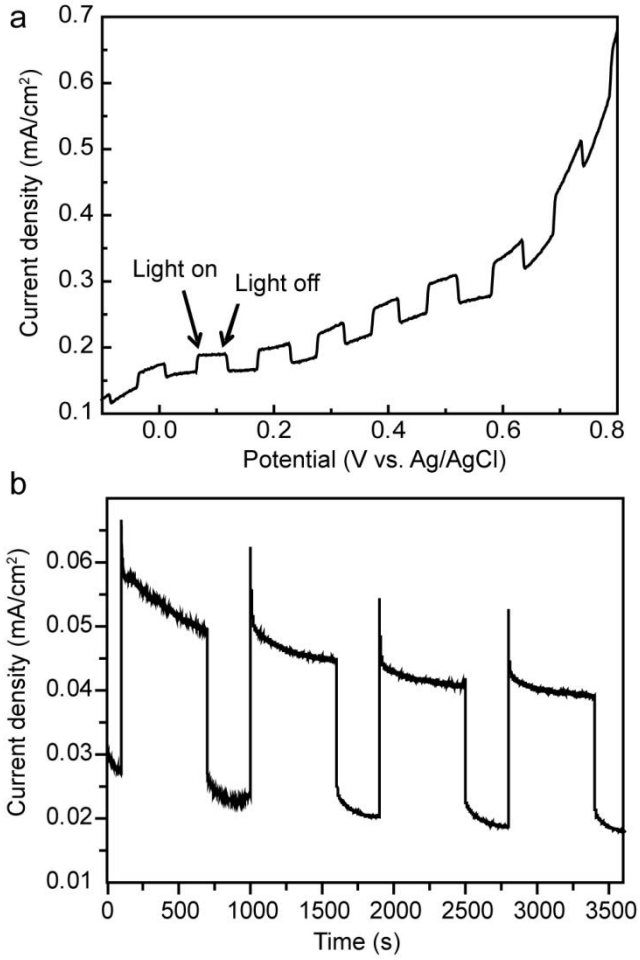


**Figure 2.7.** (a) I-V curvecollected for Si-doped GaN-1000 nanowires on carbon cloth under light on/off chops (100 mW/cm$^2$, AM 1.5G). (b) I-t curves collected at 0.7 V vs. Ag/AgCl for 3600s.

## 2.4 Conclusion

In summary, we have reported a simple and general method to prepare high yield GaN and InN nanowires on a low cost, conductivity and flexible carbon cloth substrate. The densities, lengths and diameters of nanowirescan be controlled by adjusting growth temperatures. The Si-doped GaN nanowires

grown on carbon cloth can serve a photoanode and shownpronounced photoactivities for photoelectrochemical water oxidation. Carbon cloth substrates serve as a promising conductive and flexible substrate for group-III nitride nanomaterials, which could open up new opportunities for nanoscale photonic, electronic and electrochemical devices.

References


1. C. M. Lieber, *MRS Bull.*, 2003, **28**, 486-491.
2. Y. Li, F. Qian, J. Xiang and C. M. Lieber, *Materials Today*, 2006, **9**, 18-27.
3. X. C. Jiang, Q. H. Xiong, S. Nam, F. Qian, Y. Li and C. M. Lieber, *Nano Letters*, 2007, **7**, 3214-3218.
4. L. S. Li, Y. H. Yu, F. Meng, Y. Z. Tan, R. J. Hamers and S. Jin, *Nano Letters*, 2012, **12**, 724-731.
5. O. Ambacher, *Journal of Physics D-Applied Physics*, 1998, **31**, 2653-2710.
6. S. K. Lim, M. Brewster, F. Qian, Y. Li, C. M. Lieber and S. Gradecak, *Nano Letters*, 2009, **9**, 3940-3944.
7. S. A. Dayeh, C. Soci, X. Y. Bao and D. L. Wang, *Nano Today*, 2009, **4**, 347-358.
8. Y. J. Dong, B. Z. Tian, T. J. Kempa and C. M. Lieber, *Nano Letters*, 2009, **9**, 2183-2187.

9. Y. Li, J. Xiang, F. Qian, S. Gradecak, Y. Wu, H. Yan, H. Yan, D. A. Blom and C. M. Lieber, *Nano Letters*, 2006, **6**, 1468-1473.

10. M. Azize, A. L. Hsu, O. I. Saadat, M. Smith, X. Gao, S. P. Guo, S. Gradecak and T. Palacios, *Ieee Electron Device Letters*, 2011, **32**, 1680-1682.

11. S. A. Dayeh, D. Susac, K. L. Kavanagh, E. T. Yu and D. Wang, *Nano Letters*, 2008, **8**, 3114-3119.

12. X. F. Duan, Y. Huang, Y. Cui, J. F. Wang and C. M. Lieber, *Nature*, 2001, **409**, 66-69.

13. Z. H. Zhong, F. Qian, D. L. Wang and C. M. Lieber, *Nano Letters*, 2003, **3**, 343-346.

14. H. M. Kim, Y. H. Cho, H. Lee, S. I. Kim, S. R. Ryu, D. Y. Kim, T. W. Kang and K. S. Chung, *Nano Letters*, 2004, **4**, 1059-1062.

15. F. Qian, Y. Li, S. Gradecak, D. L. Wang, C. J. Barrelet and C. M. Lieber, *Nano Letters*, 2004, **4**, 1975-1979.

16. Y. Huang, X. F. Duan and C. M. Lieber, *Small*, 2005, **1**, 142-147.

17. M. H. Huang, S. Mao, H. Feick, H. Q. Yan, Y. Y. Wu, H. Kind, E. Weber, R. Russo and P. D. Yang, *Science*, 2001, **292**, 1897-1899.

18. J. C. Johnson, H. J. Choi, K. P. Knutsen, R. D. Schaller, P. D. Yang and R. J. Saykally, *Nature Materials*, 2002, **1**, 106-110.

19. X. F. Duan, Y. Huang, R. Agarwal and C. M. Lieber, *Nature*, 2003, **421**,

241-245.

20. R. Agarwal, C. J. Barrelet and C. M. Lieber, *Nano Letters*, 2005, **5**, 917-920.

21. F. Qian, Y. Li, S. Gradecak, H. G. Park, Y. J. Dong, Y. Ding, Z. L. Wang and C. M. Lieber, *Nature Materials*, 2008, **7**, 701-706.

22. F. Qian, M. Brewster, S. K. Lim, Y. C. Ling, C. Greene, O. Laboutin, J. W. Johnson, S. Gradecak, Y. Cao and Y. Li, *Nano Letters*, 2012, **12**, 3344-3350.

23. T. Kuykendall, P. J. Pauzauskie, Y. F. Zhang, J. Goldberger, D. Sirbuly, J. Denlinger and P. D. Yang, *Nature Materials*, 2004, **3**, 524-528.

24. S. H. Lee, Y. H. Mo, K. S. Nahm, E. K. Suh and K. Y. Lim, *Phys. Stat. Sol. (c)*, 2002, **0**, 148-151.

25. W. Guo, M. Zhang, P. Bhattacharya and J. Heo, *Nano Lett.*, 2011, **11**, 1434-1438.

26. Y. Tomida, S. Nitta, S. Kamiyama, H. Amano, I. Akasaki, S. Otani, H. Kinoshita, R. Liu, A. Bell and F. A. Ponce, *Applied Surface Science*, 2003, **216**, 502-507.

27. J. Ohta, H. Fujioka and M. Oshima, *Applied Physics Letters*, 2003, **83**, 3060-3062.

28. J. R. LaRoche, B. Luo, F. Ren, K. H. Baik, D. Stodilka, B. Gila, C. R. Abernathy, S. J. Pearton, A. Usikov, D. Tsvetkov, V. Soukhoveev, G.

Gainer, A. Rechnikov, V. Dimitriev, G. T. Chen, C. C. Pan and J. I. Chyi, *Solid-State Electronics*, 2004, **48**, 193-196.

29. C. Pendyala, J. B. Jasins, J. H. Kim, V. K. Vendra, S. Lisenkov, M. Menon and M. K. Sunkara, *Nanoscale*, 2012, **4**, 6269-6275.

30. S. H. Jo, D. Z. Wang, J. Y. Huang, W. Z. Li, K. Kempa and Z. F. Ren, *Applied Physics Letters*, 2004, **85**, 810-812.

31. X. H. Zhang, L. Gong, K. Liu, Y. Z. Cao, X. Xiao, W. M. Sun, X. J. Hu, Y. H. Gao, J. A. Chen, J. Zhou and Z. L. Wang, *Advanced Materials*, 2010, **22**, 5292-5296.

32. Q. Cheng, J. Tang, J. Ma, H. Zhang, N. Shinya and L. C. Qin, *Journal of Physical Chemistry C*, 2011, **115**, 23584-23590.

33. G. Wang, X. Lu, Y. Ling, T. Zhai, H. Wang, Y. Tong and Y. Li, *ACS Nano*, 2012, **6**, 10296-10302.

34. X. F. Duan and C. M. Lieber, *Journal of the American Chemical Society*, 2000, **122**, 188-189.

35. T. Kuykendall, P. Pauzauskie, S. K. Lee, Y. F. Zhang, J. Goldberger and P. D. Yang, *Nano Letters*, 2003, **3**, 1063-1066.

36. C. Liu, Z. Hu, Q. Wu, X. Z. Wang, Y. Chen, H. Sang, J. M. Zhu, S. Z. Deng and N. S. Xu, *Journal of the American Chemical Society*, 2005, **127**, 1318-1322.

37. Z. Chen, C. B. Cao and H. S. Zhu, *Journal of Physical Chemistry C*,

2007, **111**, 1895-1899.

38. H. S. Jung, Y. J. Hong, Y. Li, J. Cho, Y. J. Kim and G. C. Yi, *Acs Nano*, 2008, **2**, 637-642.

39. D. F. Wang, A. Pierre, M. G. Kibria, K. Cui, X. G. Han, K. H. Bevan, H. Guo, S. Paradis, A. R. Hakima and Z. T. Mi, *Nano Letters*, 2011, **11**, 2353-2357.

40. W. Gotz, N. M. Johnson, C. Chen, H. Liu, C. Kuo and W. Imler, *Applied Physics Letters*, 1996, **68**, 3144-3146.

41. I. M. Huygens, K. Strubbe and W. P. Gomes, *Journal of the Electrochemical Society*, 2000, **147**, 1797-1802.

# Chapter 3

## The Effect of Hydrogenation Temperature on $TiO_2$ Nanostructures for Photoelectrochemical Water Oxidation


### Abstract

Hydrogen treatment strategy has recently beendemonstrated as a simple and effective strategy to improve the performance of $TiO_2$photoande for the PEC water oxidation. However,the performance of those hydrogenated $TiO_2$photoandedecreasedsignificantly when the treated temperature is above 350 $^oC$due to degradation of thefluorine-doped tin oxide (FTO) substrate.To eliminate the influence of substrate on the performance of $TiO_2$photoanode, in this chapter, I report the PEC performance with the titanium dioxide ($TiO_2$) photoanodesas a function of hydrogenation temperatureon titanium (Ti) foil.These $TiO_2$ nanowires were hydrogenated in a range of temperatures between 350 and 550$^oC$, in which the resistance of Ti foil remained unchanged. We found that the rutile and anatase hydrogen treated $TiO_2$photoanodes achieved the optimalperformance at 350 $^oC$ and 550$^oC$, respectively. The optimal hydrogenation temperature is believed to be related to the carrier density of hydrogen treated $TiO_2$.These results could provide important insights to improve the performance $TiO_2$ photoelectrodes for photoelectrochemical water oxidation as well as other solar energy conversion devices.

## 3.1 Introduction

$TiO_2$ has been investigated extensively as photoanode for PEC water oxidation because of their superior chemical stability,favorable band-edge positions, and low material cost. [1-4] However, the solar conversion efficiency of $TiO_2$ is relatively low due to large band-gap, low electrical conductivity, and fast electron-hole recombination. Therefore, alot of methods have been demonstrated to address these limitations. For instance, $TiO_2$ nanostructures were also intentionally doped with non-metal elements to narrow the band-gap, [7, 10] and/or sensitized with small band gap semiconductors to improve the solar energy utilization. [11-13]Additionally,one-dimensional (1D) $TiO_2$ nanostructures were synthesized to reduce the electron-hole recombination loss by minimizing the diffusion length of minority carriers.[5-8, 9] Furthermore, intrinsic defects such as oxygen vacancies and/or hydrogen impurities can be created to increase the electrical conductivity of metal oxidesand its PEC performance.[14-20]Recently,hydrogenation has been reported as a simple and effective strategy to introduce as shallow donors into $TiO_2$ materials.[21-23]The hydrogen-treated rutile $TiO_2$ nanowire photoanode grown on FTO substrate could achieve the photocurrent density as high as 2.5 $mA/cm^2$ at 0.23 V vs. Ag/AgCl under white light illumination, which was five times higher than pristine $TiO_2$photoelectrode at the same bias.[21] The enhanced photocurrent was attributed to the improved charge collection efficiency as a result of increased carrier density. The carrier

density can be controlled by the hydrogenation temperature. 350 $^{o}$C was found to be the optimal hydrogenation temperature. However, the photoanode performance decreased rapidly beyond 350 $^{o}$C. While the reason for the decreased performance under high hydrogenation temperature was stillunclear. The increased resistance of FTO substrate was believed to be a possible reason.[21]Since the performance of $TiO_2$ nanowire photoanode could be limited by the substrate conductivity, 350 $^{o}$C may not be the optimal hydrogenation temperature and the intrinsic performance of hydrogen treated $TiO_2$ nanowires could be further enhanced.

In this chapter, the rutile, anatase, and the mixed rutile-anatase phase $TiO_2$ nanowires grown on titanium (Ti) foil as a function of hydrogenation temperature on PEC have been studied. The Ti foils treated under various hydrogenation temperatures maintained good conductivity. The results shown the rutile and anatase hydrogenated $TiO_2$ photoanodes achieved their optimal PEC performance at hydrogenation temperatures of 350 $^{o}$C and 550 $^{o}$C, respectively. The optimal hydrogenation temperature is believed to be related to the carrier density of $TiO_2$.

## 3.2 Experimental section:

### 3.2.1 Preparation of rutile $TiO_2$ nanowire arrays

Rutile $TiO_2$ nanowire arrays were grown on a Ti foil using a hydrothermal method reported previously. [24] The Ti foil (1.5cm×1.5cm, 99.5%, Alfa Aesar) approximately 0.25 mm thick was initially cleaned with ethanol, rinsed with deionized (DI) water, and finally dried in air. The Ti precursor solution was prepared by mixing 6 ml concentrated hydrochloric acid with 6 ml DI water and 0.5 ml titanium n-butoxide in a 100 ml beaker. The Ti precursor solution and the clean Ti foil were transferred into the Teflon-lined stainless steel autoclave (30 ml). The autoclave was heated in an oven at 150 °C for 8 hours. The autoclave was cooled down at room temperature. The substrate was taken out and cleaned with DI water, and annealed in air at 550 °C for 3 hours.

### 3.2.2 Preparation of anatase $TiO_2$ nanowires

Anatase $TiO_2$ nanowires were prepared on the titanium foil using the hydrothermal method.[33]The Ti foil (1.5 cm×1.5 cm) was precleaned with ethanol, followed by DI water. Then the Ti foil was placed into a 30 ml Teflon-lined stainless steel autoclave filled with 20 ml 1 M NaOH aqueous solution. The sealed autoclave was heated at 180 $^oC$ for 7 hours. After the autoclave cooled down at room temperature, the Ti foil was taken out and washed with DI water. The Ti foil was covered with nanowires, and then it was immersed into a 1M HCl aqueous solution for 10 min, rinsed with DI water and air dried. Finally, the Ti foil with nanowires was annealed in air at 500 °C for 3 hours.

### 3.2.3 Preparation of mixed phase $TiO_2$ nanowire arrays

The mixed phase $TiO_2$ nanowire arrays were prepared by etching method. The precleaned Ti foil (1.5 cm×1.5 cm) was immersed into a 20 ml $H_2O_2$ aqueous solution. The solution was heated at 80 °C for 24 hours. After the solution cooled down to room temperature, the Ti foil was taken out and cleaned with DI water. Finally, the Ti foil was annealed in air at 550 °C for 3 hours.

### 3.2.4 Hydrogenation

All $TiO_2$ nanomaterials were annealed in a home-built tube furnace in hydrogen atmosphere (50 sccm, 740 torr) at 350, 450 or 550 °C for 30 minutes.

### 3.2.5 Photoelectrochemical measurements

$TiO_2$ and hydrogenated $TiO_2$ nanowire arrays were manufactured into photoanodes through soldering the copper wire on a bare part of Ti foil substrate. The metal contact and the substrate edges were covered with the insulating epoxy resin. The exposed effective area for the working electrode is around 0.20 $cm^2$. All the photoelectrochemical measurements were performed by a CHI 660D electrochemical station, using Pt plate as counter electrode, Ag/AgCl (1 M KCl) as reference electrode, and 1 M KOH aqueous solution as electrolyte, under a simulated sunlight (100 $mW/cm^2$) generated with a 150W xenon lamp (Newport 6255) coupled with an AM 1.5G filter (Newport 81094). The power density of the incident light was measured with a digital power-meter (Molectron, PM5100).. Mott-Schottky plots were measured at a frequency of 10 kHz with the same CHI 660D electrochemical station in the dark. The incident-photon-to-current-conversion-efficiencies (IPCE) were collected by a Solartron 1280B electrochemical station with a solar simulator (Newport 69920, 1000 W

xenon lamp), coupled with aligned monochromator (Oriel Cornerstone 130 1/8 m) and an infrared water filter (Oriel 6127).

### 3.2.6 Material Characterization

Scanning electron microscopy (SEM) images were collected by a field-emission SEM (Hitachi S-4800 II). X-ray diffraction (XRD) spectra were measured at room temperature on a Rigaku Americas Miniflex Plus powder diffractometer from a 2θ angle of 20 to 90 degree with a step size of 0.04 degree at a rate of 1 degree/min.

## 3.3 Results and Discussion

The pristine $TiO_2$ and hydrogen treated $TiO_2$ (H-$TiO_2$) samples at various hydrogenation temperatures were cut from the same piece of Ti foil to minimize the variation of nanowire morphology and density between these samples. The rutile $TiO_2$ nanowire arrays were synthesized by a hydrothermal method.[24] As shown in Figure 3.1a, a pre-cleaned Ti foil was put into an autoclave with a mixture solution of titanium n-butoxide and hydrochloric acid. Then the autoclave was heated at 150 $^oC$ for 5 hours. Finally, the as-prepared nanowires were first annealed in the air at 550 $^oC$ for 3 hours, following by annealing in pure hydrogen atmosphere for additional 30 minutes under various temperatures of 350, 450 and 550 $^oC$. SEM analysis revealed that the nanowire bundles were vertically aligned on the Ti foil substrate (Figure 3.1b). XRD spectra were

collected from the $TiO_2$ and H-$TiO_2$ nanowire arrays prepared under various hydrogenation temperatures. In Figure 3.1c, the dashed lines highlight the diffraction peaks of rutile $TiO_2$ structure (JCPDS 65-0190). The results also showed that all hydrogen-treated $TiO_2$ nanowires have the same rutile structure (denoted as H-R-$TiO_2$), suggesting no crystal phase change after hydrogenation.

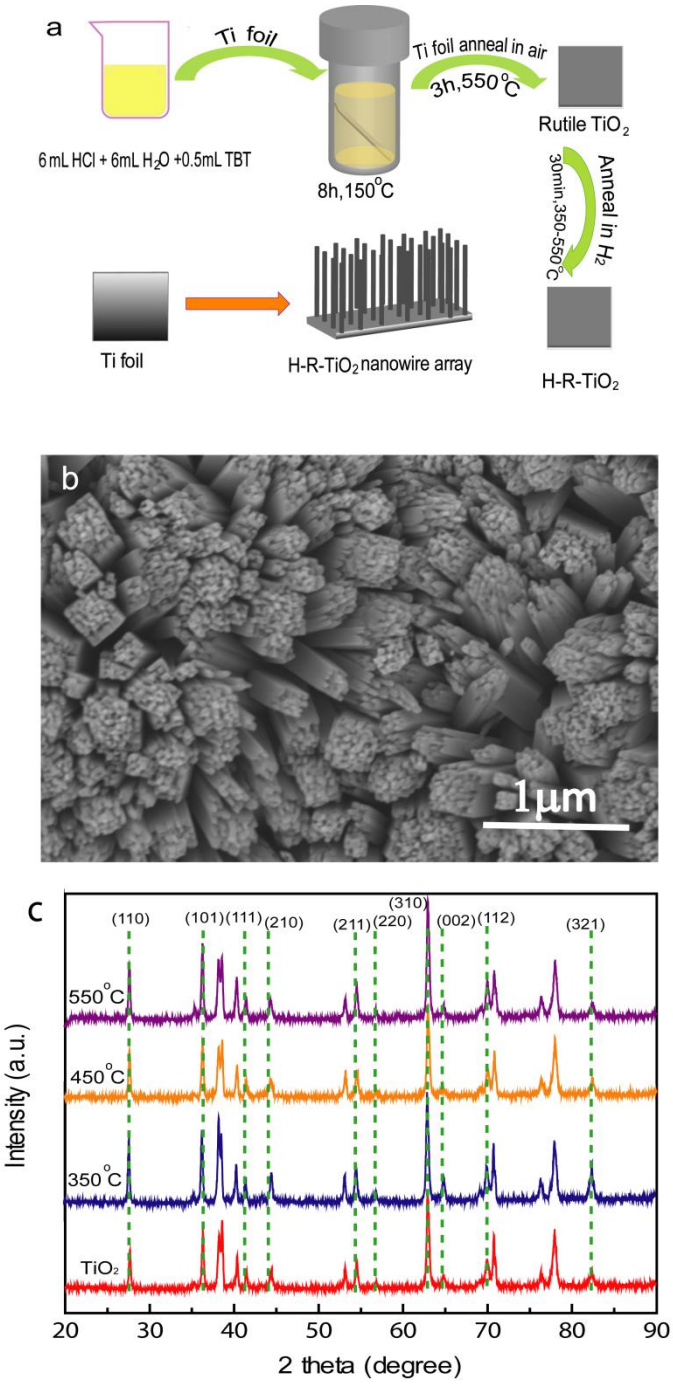


**Figure 3.1.** (a) Schematic diagram illustrates the growth procedure for rutile $TiO_2$and H-R-$TiO_2$ nanowire arrays. (b) SEM image of rutile $TiO_2$ nanowires. (c) XRD spectra collected for rutile $TiO_2$ and H-R-$TiO_2$ nanowires prepared at the hydrogenation temperatures of 350, 450, and 550 °C.

Pristine rutile $TiO_2$ and H-R-$TiO_2$ nanowire arrays were fabricated into photoanodes and tested for PEC performance. All PEC measurements were performed in a three-electrode electrochemical cell using 1 M KOH solution as electrolyte. The nanowire photoelectrodes were used as working electrode; platinum sheet and Ag/AgCl (1 M KCl) were employed as the counter and reference electrode, respectively. The photoactivity of all nanowire photoelectrodes were measured under the simulated solar illumination at 100 $mW/cm^2$ from a 150 W xenon lamp coupled with an AM 1.5G filter. Figure 3.2a shows the linear sweep voltammograms collected from pristine rutile $TiO_2$ and H-R-$TiO_2$ nanowire photoelectrodes hydrogenated at various temperatures in a potential window between -1.0 and 0.5 V vs. Ag/AgCl. The results showed that the photocurrent densities of all H-R-$TiO_2$ samples were substantially higher than that of pristine $TiO_2$, proved hydrogen treatment was an effective strategy for enhancing the PEC performance. Among all the H-R-$TiO_2$ nanowire samples, the sample hydrogenated at 350 $^oC$ exhibited the highest photocurrent density, which is consistent with the previous results obtained from H-R-$TiO_2$ nanowires grown on FTO substrate. [21] Amperometric *I-t* studies collected at 0.2 V vs. Ag/AgCl showed that the photocurrent of H-R-$TiO_2$ (350 $^oC$) was stable under illumination for one hour (Figure 3.2b). To ensure the PEC performance of H-R-$TiO_2$ photoanodes was not affected by the substrate conductivity, we measured

the resistances of Ti foils after hydrogenation. Importantly, the Ti foils hydrogenated at temperatures between 350 and 550 $^{o}$C have comparable resistances (0.5 - 0.9 Ohm). These results suggested that the photocurrent reduction at hydrogenation temperatures beyond 350 $^{o}$C was not due to the decrease of substrate conductivity.

To quantitatively evaluate the photoactivity as a function of incident light wavelength, we measured the incident photon-to-current conversion efficiency (IPCE) for both H-R-$TiO_2$ (350 $^{o}$C) and pristine $TiO_2$ photoanodes at 0.2 V vs. Ag/AgCl (Figure 3.2c). IPCE values were calculated from the photocurrent densities obtained under different wavelengths in a range from 300 to 600 nm, and expressed as the following equation:

$$IPCE = (1240\ I) / (\lambda\ J_{light}) \qquad (1)$$

where $I$ (mA/cm$^2$) is the photocurrent density, $\lambda$ (nm) is the incident wavelength, and $J_{light}$ (mw/cm$^2$) is the power density of irradiance at the specific wavelength. H-R-$TiO_2$ nanowires hydrogenated at 350 $^{o}$C showed significantly enhanced IPCE values compared to pristine $TiO_2$ in the entire UV region between 300 nm and 420 nm. The sample yielded a maximum IPCE value of 55% at 320 nm, and then gradually dropped to zero at wavelengths beyond 430 nm, which is consistent with the band-gap energy of rutile $TiO_2$ (3.0 eV). The IPCE results revealed that the enhanced photocurrent of H-R-$TiO_2$ was due to improved photoactivity in UV region.

Additionally, we conducted the electrochemical impedance measurements for the rutile $TiO_2$ and H-R-$TiO_2$ samples to investigate their electrochemical properties. All the samples were measured at a frequency of 10 kHz in the dark. Figure 3.2d shown the Mott-Schottky plots of $TiO_2$ and H-R-$TiO_2$ nanowire samples. All of them exhibit positive slopes, as expected for *n*-type semiconductor. The carrier densities of these nanowires were calculated by using Mott-Schottky equation:

$$N_d = (2/e_0\varepsilon\varepsilon_0)\,[d\,(1/C^2)/dV]^{-1} \quad (2)$$

Where $e_0$ is the electron charge; $\varepsilon_0$ is the permittivity of vacuum; $\varepsilon$ (=170) is the dielectric constant of $TiO_2$. [25] $N_d$ is the donor density; and V is the applied bias. Because the depletion layer does not increase when the capacitance reached a plateau, we chose the linearly increasing region to calculate the carrier densities. The region has been highlighted by the dashed line in Figure 3.2d. The electron densities of the rutile $TiO_2$ and H-R-$TiO_2$ (350 $^oC$, 450 $^oC$, and 550 $^oC$) nanowire arrays were calculated to be $6.1\times10^{17}$, $2.2\times10^{19}$, $4.7\times10^{19}$, and $1.2\times10^{20}$ $cm^{-3}$, respectively. The donor density of $TiO_2$ increased substantially with the hydrogenation temperature. The results suggest the improved photoactivity of H-R-$TiO_2$ nanowire photoanodes could be due to their increased carrier densities, which can enhance the charge transport and reduce the *IR* drop of the PEC device. The electron mobility is expected to decrease with the increase density of defects, which are believed to be electron scattering centers. On the other

hand, it is known that the introduction of defects such as hydrogen impurities and oxygen vacancies could increase the density of trap states and increase electron-hole recombination loss.[26-28]nWhen the donor density reaches a certain threshold that the electron-hole recombination effect becomes a dominant effect, the efficiency of electron collection decreases. This can explain the gradual reduction of photocurrent for the $TiO_2$ samples hydrogenated at temperatures beyond 350 °C.

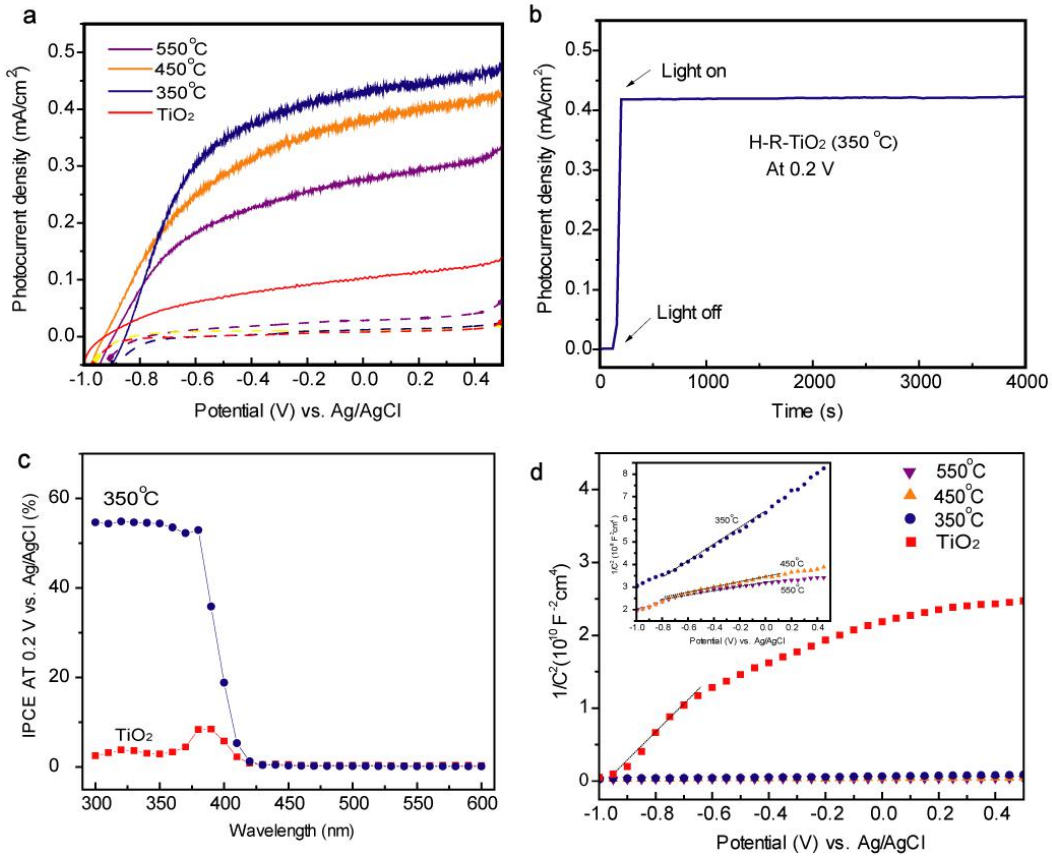


**Figure 3.2.** (a) Linear sweeps voltammograms collected for pristine $TiO_2$ (red)

and H-R-$TiO_2$ nanowires hydrogenated at 350 $^oC$ (blue), 450 $^oC$ (orange), and 550 $^oC$ (purple). (b) Amperometric *I-t* curves collected at 0.2 V vs. Ag/AgCl for 1 hour for H-R-$TiO_2$ nanowire hydrogenated at 350 $^oC$. (c) IPCE spectra of pristine $TiO_2$ and H-R-$TiO_2$ nanowires (350 $^oC$). (d) Mott-Schottky plots collected at a frequency of 10 kHz in the dark for the pristine $TiO_2$ and H-R-$TiO_2$ nanowires. Inset: magnified Mott-Schottky plots of H-R-$TiO_2$ nanowires hydrogenated at different temperatures.

Furthermore, we extended this temperature-dependent hydrogenation study to anatase $TiO_2$, which has been extensively used for photocatalysis, photoelectrochemical and photovoltaic devices.[29-31] The formation energies and locations of defects in anatase structure are expected to be different from rutile structure,[32] and thus, the effect of hydrogenation temperature on anatase $TiO_2$ could be different. Anatase $TiO_2$ nanowires were prepared on Ti foil by a hydrothermal method reported previously (Figure 3.3a).[33]A Ti foil was placed in an autoclave containing 1 M sodium hydroxide solution and heated at 180 $^oC$ for 7 hours. In this process, a layer of $Na_2Ti_2O_4(OH)_2$ nanowire film was formed on the Ti foil. The foil was soaked into a diluted hydrochloric acid solution to replace $Na^+$ with $H^+$ to form $H_2Ti_2O_4(OH)_2$, which was annealed in the air at 500 $^oC$ for 3 hours to form anatase $TiO_2$. These anatase $TiO_2$ nanowires were further annealed at the temperatures between 350 $^oC$ and 550 $^oC$ in hydrogen atmosphere for additional 30 min to form hydrogen-treated anatase

$TiO_2$(denoted as H-A-$TiO_2$). SEM image showed that the Ti foil was covered with high density of nanowires (Figure 3.3b). The average diameter and length of the anatase $TiO_2$ nanowires are estimated to around 20 nm and 5 μm, respectively.

Figure 3.3c shows the linear sweep voltammograms of $TiO_2$ and H-A-$TiO_2$ nanowires. Significantly, the H-A-$TiO_2$ nanowires showed substantial enhancement in photocurrent density compared to the pristine anatase $TiO_2$ nanowires at the same potential. Interestingly, the nanowire sample hydrogenated at 550 $^oC$ showed the highest photocurrent density among the three H-A-$TiO_2$ samples, and achieved 0.2 mA/$cm^2$ at 0.2 V vs. Ag/AgCl. The trend is different from that obtained for rutile $TiO_2$, which has the optimal hydrogen temperature of 350 $^oC$. We believed this is related to the degree of enhancement of carrier density in H-A-$TiO_2$ and H-R-$TiO_2$ samples, which will be discussed later. IPCE spectra were collected for H-A-$TiO_2$ (550 $^oC$) and pristine anatase $TiO_2$ photoanodes as a function of incident light wavelength at 0.2 V vs. Ag/AgCl (Figure 3.4). In comparison to pristine anatase $TiO_2$ nanowires, the H-A-$TiO_2$ nanowires exhibited enhanced photoactivity over the entire UV region. The IPCE values decreased gradually to zero at wavelength beyond 400 nm, which is consistent with the band-gap energy of anatase (3.2 eV).

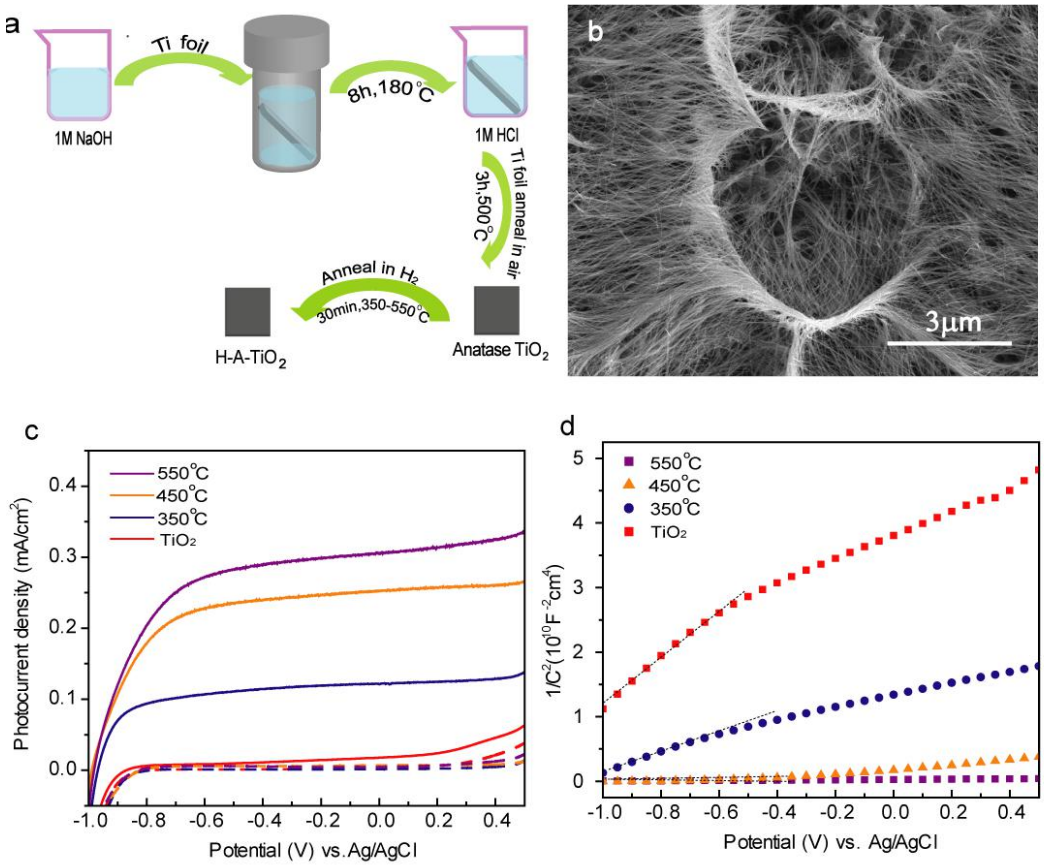


**Figure 3.3.**(a) Schemeof the growth procedure for anatase $TiO_2$ and H-A-$TiO_2$ nanowires. (b) SEM image of anatase $TiO_2$ nanowires. (c) Linear sweeps voltammograms collected for pristine $TiO_2$ (red) and H-A-$TiO_2$ nanowires hydrogenated at 350 °C (blue), 450 °C (orange), and 550 °C (purple).(d) Mott-Schottky plots collected at the frequency of 10 kHz in the dark for pristine anatase $TiO_2$ and H-A-$TiO_2$ nanowires.

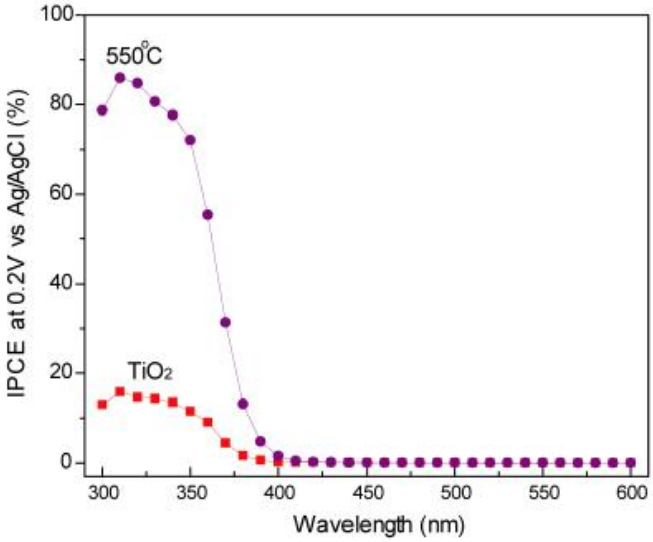


**Figure 3.4.** IPCE spectra of pristine anatase $TiO_2$ and H-A-$TiO_2$ nanowires hydrogenated at 550 $^oC$.

Mott-Schottky plotswere collected for anatase $TiO_2$ and H-A-$TiO_2$ samples. Figure 3.3d shows that the carrier density of $TiO_2$ increases with the hydrogenation temperature. The carrier densities of pristine anatase $TiO_2$ and H-A-$TiO_2$ nanowires were estimated to be $1.5\times10^{17}$, $6.0\times10^{17}$, $8.7\times10^{18}$, and $3.2\times10^{19}$ $cm^{-3}$ Notably, the enhancement factor of carrier density between anatase pristine $TiO_2$ and H-A-$TiO_2$ is considerably less than that observed for rutile $TiO_2$ nanowires. For instance, when anatase $TiO_2$ hydrogenated at 350 $^oC$, the carrier density was enhanced by a factor of two only, while the carrier density of rutile $TiO_2$ increased by two orders of magnitude at the same hydrogenation temperature. This could be due to the difference in formation energies of defects and impurities in rutile and anatase $TiO_2$ materials. The data

also suggest that the performance of anatase $TiO_2$ was not optimized at hydrogenation temperature of 350 $^oC$ could be due to the relatively small enhancement of carrier density. Therefore, the anatase $TiO_2$ showed better performance when it was treated at the higher hydrogenation temperature of 550 $^oC$. However, we were not able to further increase the hydrogenation temperature because the Ti foil substrate became fragile when the annealing temperature was beyond 550 $^oC$.

Finally, we also prepared $TiO_2$ nanowire samples containing both rutile and anatase phases. The mixed phase $TiO_2$ nanowires were synthesized by using chemical etching method reported previously.[34]As shown in Figure 3.5a, the Ti foil was placed in an autoclave containing 30 wt% $H_2O_2$ solution and heated at 80 $^oC$ for 24 hours. The mixed phase $TiO_2$ was prepared through dissolution precipitation mechanism. During the process, the Ti foil was oxidized to Ti (IV) ion and then redeposit to form crystalline $TiO_2$. The Ti foil was then annealed in air at 550 $^oC$ for 3 hours to form mixed phase $TiO_2$ nanowires. These mixed phase $TiO_2$ were hydrogenated at the temperatures between 350 $^oC$ and 550 $^oC$ for additional 30 min to form hydrogen-treated samples (H-M-$TiO_2$). SEM image showed that the Ti foil was covered with nanowires with average diameter of 50 nm (Figure 3.5a inset). XRD spectra confirmed the sample was a mixture of rutile and anatase $TiO_2$ nanowires (Figure 3.5b). The linear sweep voltammograms showed the H-M-$TiO_2$ nanowire samples exhibit significantly

higher photocurrent density than pristine mixed phase $TiO_2$ (Figure 3.5c). The photocurrent density increases with the increasing hydrogenation temperature from 350 to 550 $^oC$, and the H-M-$TiO_2$ nanowires hydrogenated at 550 $^oC$ achieved the highest photocurrent density of ~0.78 mA/$cm^2$ under illumination (AM 1.5G, 100 mW/$cm^2$) (Figure 3.5c). The effect of hydrogenation temperature on the H-M-$TiO_2$ is consistent with the H-A-$TiO_2$ samples. The carrier densities of pristine anatase $TiO_2$ and H-A-$TiO_2$ nanowires were estimated to be $1.5\times10^{16}$, $6.1\times10^{17}$, $7.7\times10^{18}$, and $1.6\times10^{20}$ $cm^{-3}$, according to the Mott-Schottky plots (Figure 3.5d). Likewise, the sample hydrogenated at 550 $^oC$ has the highest donor density among all the H-M-$TiO_2$ samples. This data is also consistent with the Mott-Schottky results obtained from anatase $TiO_2$ samples. And it again suggested the optimal hydrogenation temperature is closely related to the carrier density of $TiO_2$ materials.

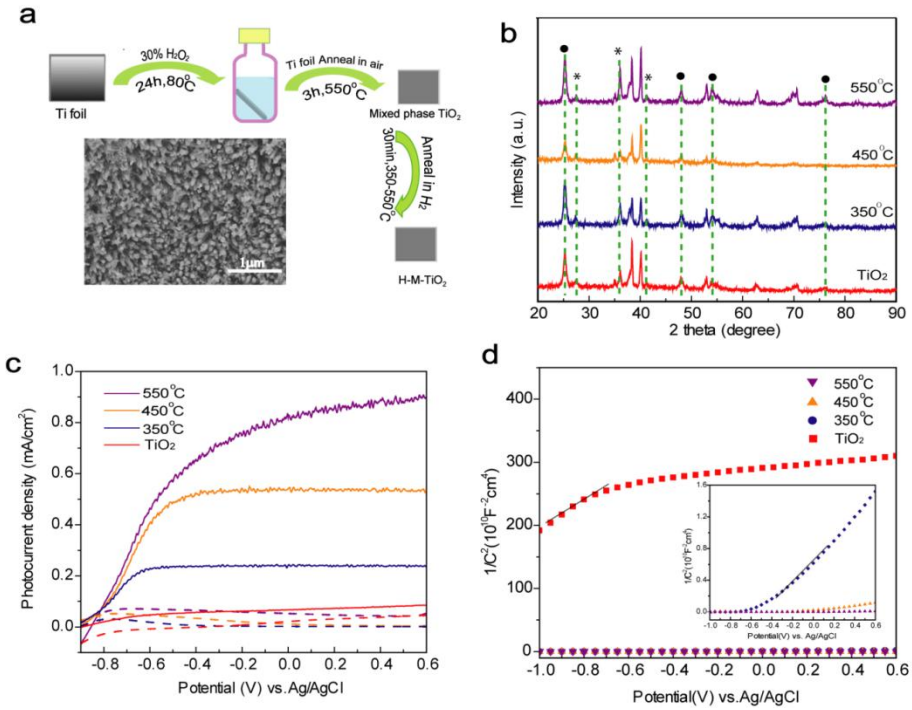


**Figure 3.5.**(a) Schematic diagram demonstrated the growth procedure for the mixed phase $TiO_2$ and H-M-$TiO_2$ nanowires. Inset: SEM image of H-M-$TiO_2$ nanowires. (b) XRD spectra collected for pristine mixed phase $TiO_2$ and H-M-$TiO_2$ nanowires hydrogenated at various temperatures (350, 450, and 550 $^oC$). (c) Linear sweep voltammograms collected for the mixed phase $TiO_2$ and H-M-$TiO_2$ nanowires. (d) Mott-Schottky plots collected at a frequency of 10kHz in the dark for the mixed phase $TiO_2$ and H-M-$TiO_2$ nanowires.

### 3.4 Conclusion

In summary, we investigated the hydrogenation temperature effect on $TiO_2$ photoanodes for PEC water oxidation. We grew rutile, anatase and mixed phase

$TiO_2$ nanowires on Ti foil. The metal foil substrate couldeliminate the substrate issue. We found the optimal hydrogenation temperatures for $TiO_2$ nanomaterials are related to the degree of enhancement of their carrier density upon hydrogenation. Our work provided further insights into the development of hydrogen treated $TiO_2$ materials for PEC water oxidation as well as other solar energy conversion devices.

**References**


1. T. Bak, J. Nowotny, M. Rekas and C. C. Sorrell, *Int. J. Hydrogen Energy***2002**, 27, 991-1022.
2. Y. Li and J. Z. Zhang, *Laser Photonics Rev.***2010**, 4, 517-528.
3. X. B. Chen, S. H. Shen, L. J. Guo and S. S. Mao, *Chem. Rev.***2010**, 110, 6503-6570.
4. M. Ni, M. K. H. Leung, D. Y. C. Leung and K. Sumathy, *Renew. Sust. Energ. Rev*.**2007**, 11, 401-425.
5. M. Z. Liu, N. D. Snapp and H. Park, *Chem. Sci.***2011**, 2, 80-87.
6. K. Shankar, J. I. Basham, N. K. Allam, O. K. Varghese, G. K. Mor, X. J. Feng, M. Paulose, J. A. Seabold, K. S. Choi and C. A. Grimes, *J. Phys. Chem. C***2009**, 113, 6327-6359.
7. M. Xu, P. M. Da, H. Y. Wu, D. Y. Zhao and G. F. Zheng, *Nano Lett.***2012**, 12, 1503-1508.

8. Y. R. Smith, B. Sarma, S. K. Mohanty and M. Misra, *Int. J. Hydrogen Energy***2013**, 38, 2062-2069.

9. S. Y. Noh, K. Sun, C. Choi, M. Niu, K. Xu, M. Yang, S. Jin and D. Wang, *Nano Energy***2012**, 2, 351-360.

10. R. Sasikala, V. Sudarsan, C. Sudakar, R. Naik, T. Sakuntala and S. R. Bharadwaj, *Int. J. Hydrogen Energy***2008**, 33, 4966-4973.

11. J. Hensel, G. Wang, Y. Li and J. Z. Zhang, *Nano Lett.***2010**, 10, 478-483.

12. H. Wang, G. Wang, Y. Ling, M. Lepert, C. C. Wang, J. Z. Zhang and Y. Li, *Nanoscale***2012**, 4, 1463-1466.

13. L. P. Liu, G. Wang, Y. Li, Y. D. Li and J. Z. Zhang, *Nano Res.***2011**, 4, 249-258.

14. H. Y. Wang, G. M. Wang, Y. C. Ling, M. Lepert, C. C. Wang, J. Z. Zhang and Y. Li, *Nanoscale***2012**, 4, 1463-1466.

15. G. M. Wang, Y. C. Ling and Y. Li, *Nanoscale***2012**, 4, 6682-6691.

16. X. H. Lu, G. M. Wang, S. L. Xie, J. Y. Shi, W. Li, Y. X. Tong and Y. Li, *Chem. Comm.***2012**, 48, 7717-7719.

17. G. M. Wang, Y. C. Ling, H. Y. Wang, X. Y. Yang, C. C. Wang, J. Z. Zhang and Y. Li, *Energy Environ. Sci.***2012**, 5, 6180-6187.

18. J. K. Cooper, Y. C. Ling, C. Longo, Y. Li and J. Z. Zhang, *J. Phys. Chem. C***2012**, 116, 17360-17368.

19. G. Wang, Y. Ling, X. Lu, F. Qian, Y. Tong, J. Zhang, V. Lordi, C. R. Leao

and Y. Li, *J. Phys. Chem. C***2013**, 117, 10957-10964.

20. A. Janotti, J. B. Varley, P. Rinke, N. Umezawa, G. Kresse and C. G. Van de Walle, *Phys. Rev. B***2010**, 81.

21. G. M. Wang, H. Y. Wang, Y. C. Ling, Y. C. Tang, X. Y. Yang, R. C. Fitzmorris, C. C. Wang, J. Z. Zhang and Y. Li, *Nano Lett.***2011**, 11, 3026-3033.

22. S. Hoang, S. P. Berglund, N. T. Hahn, A. J. Bard and C. B. Mullins, *J. Am. Chem. Soc.***2012**, 134, 3659-3662.

23. X. Lu, G. Wang, T. Zhai, M. Yu, J. Gan, Y. Tong and Y. Li, *Nano Lett.***2012**, 12, 1690-1696.

24. J. G. Cai, J. F. Ye, S. Y. Chen, X. W. Zhao, D. Y. Zhang, S. Chen, Y. R. Ma, S. Jin and L. M. Qi, *Energy Environ. Sci.***2012**, 5, 7575-7581.

25. R. A. Parker, *Phys. Rev.***1961**, 124, 1719-&.

26. G. Boschloo and D. Fitzmaurice, *J. Phys. Chem. B***1999**, 103, 2228-2231.

27. A. L. Linsebigler, G. Q. Lu and J. T. Yates, *Chem. Rev.***1995**, 95, 735-758.

28. T. L. Thompson and J. T. Yates, *Top. Catal.***2005**, 35, 197-210.

29. H. C. Sun, C. F. Huang, Y. T. Chen, T. Y. Wu, C. W. Liu, Y. J. Hsu and J. S. Chen, *IEEE Trans. Electron Devices***2010**, 57, 3186-3189.

30. X. Wang, G. Liu, L. Wang, J. Pan, G. Q. Lu and H. M. Cheng, *J. Mater. Chem.***2011**, 21, 869-873.

31. H. Pan, J. Qian, Y. Cui, H. Xie and X. Zhou, *J. Mater. Chem.***2012**, 22,

6002-6009.

32. M. Jankulovska, T. Berger, T. Lana-Villarreal and R. Gomez, *Electrochim. Acta***2012**, 62, 172-180.

33. J. Y. Liao, B. X. Lei, H. Y. Chen, D. B. Kuang and C. Y. Su, *Energy Environ. Sci.***2012**, 5, 5750-5757.

34. J. M. Wu, *J. Cryst. Growth***2004**, 269, 347-355.

# Chapter 4

## Photo-hole Induced Corrosion of Titanium Dioxide: Mechanism and Solutions


### Abstract

$TiO_2$ has been investigated as photoanode for PEC water oxidation for years as one of the most stable photoanode materials. While,we found that $TiO_2$photoanodes(rutile nanowire, anatase nanotube and P25 nanoparticle film) suffered from substantial photocurrent decay in neutral ($Na_2SO_4$) as well as basic (KOH) electrolyte solutionsurprisingly. Photoelectrochemical measurements and electron microscopy studies show that the photocurrent decay is due to photohole induced corrosion.This reaction competes with water oxidation reaction. Further studies reveal that photocurrent decay in neutral and basic solutions are fundamentally different. Notably, the structural reconstruction of nanowire surface occurs simultaneously with the corrosion of $TiO_2$ in KOH solution and formate an amorphous layer of titanium hydroxide, which slows downthe photo-corrosion. Based on this discovery, we successfully improve the photoelectrochemical stability of $TiO_2$photoanode intentionally coating an amorphous layer of titanium hydroxide on the nanowire surface. The pre-treated $TiO_2$ photaonode exhibits an excellent photocurrent retention rate of 97% after testing in KOH solution for 72 hours, while in comparison the

untreated sample lost 20% of photocurrent in 12 hours under the same measurement conditions. This work provides new insights in understanding of the photoelectrochemical stability of bare $TiO_2$ photoanodes.

## 4.1 Introduction

$TiO_2$has been extensively investigated as photoanode for PEC water splitting since it is believed to be one of the most stable photoanode materials.[1-11]Recently, a general strategy has been demonstrated to fundamentally improve the performance of $TiO_2$ for PEC water splitting by controlled creation of oxygen vacancies in $TiO_2$ using a number of methods including hydrogenation, post-growth annealing in oxygen-deficient environments and flame reduction.[12-17] The $Ti^{3+}$ defect sites serve as shallow donors that increase the carrier density of $TiO_2$ and consequently improve its charge separation efficiency and the photoactivity. [18]However, the stability of H-$TiO_2$ has been a concern because the $Ti^{3+}$ defect sites may be reoxidized during the water oxidation process. More specifically it raises two important questions: 1) whether the enhanced photocurrent observed for H-$TiO_2$ is due to re-oxidation of $Ti^{3+}$,And 2) how stable the H-$TiO_2$ photoanode is in the water oxidation reaction. To address these questions, we investigated the long term stability of rutile pristine $TiO_2$ and hydrogen-treated $TiO_2$ (H-$TiO_2$) nanowire photoanodes for PEC water oxidation.

## 4.2 Experimental Section

### 4.2.1. Preparation of $TiO_2$ nanowire arrays

Rutile $TiO_2$ nanowire arrays were grown on a FTO glass substrate using a previously reported hydrothermal method. 15 ml of concentrated hydrochloric acid was diluted with 15 ml deionized (DI) water, and mixed with 0.5 ml titanium n-butoxide in a 100 ml beaker.This clear solution mixture and a clean FTO glass substrate were transferred to a Teflon-lined stainless steel autoclave (30 ml volume), where the FTO substrate was submerged in the solution with the conductive side facing downward. The sealed autoclave was heated in an electric oven at 150 °C for 5 hours, and then cooled down to room temperature slowly. A white $TiO_2$ nanowire film was uniformly coated on the FTO glass substrate. The sample was washed with DI water and air dried. Finally, the sample was annealed in air at 550 $^oC$ for 3 hours to increase the crystallinity of $TiO_2$ nanowires.

### 4.2.2. Preparation of $TiO_2$anatase nanotube arrays

Anatase nanotube arrays were synthesized on a piece of titanium foil (Alfa Aesar, 0.25 mm thick, 99.5%). First, the titanium foil was sonicated for 5 min in a water bath containing acetone to remove any impurities absorbed on surface. Then, the cleaned titanium foil and a Pt wire were connected to a power supply (BK Precision 1623A DC Power Supply) as positive electrode and negative

electrode, respectively. The two electrodes were inserted into a 20 mL glass wire filled with the electrolyte containing 0.3 wt% $NH_4F$ and 1 wt% $H_2O$ with ethylene glycol as solvent. A constant potential of 60 V was applied for 30 min. After reaction, the titanium foil was rinsed with acetone and blow-dried with compressed air.

### 4.2.3. Preparation of P25 nanoparticle film

0.5 g Degussa P25 $TiO_2$ powder was milled and then added into a solution mixture containing 0.16 g polyethylene glycol (PEG) (MW 20,000), 0.63 mL DI water, and 0.04 mL acetylacetone. This solution was then sonicated for 30 min to form a $TiO_2$ paste. P25-based electrodes were fabricated by depositing 20 μL $TiO_2$ paste on a 1 inch × 1 inch on FTO glass substrate and spin-coated at 1,000 rpm for 50 s to get a uniform P25 nanoparticle film. Finally, the P25 samples were annealed in air at 550 °C for 3 hours to increase their crystallinity and improve their contact to the substrate.

### 4.2.4. Preparation of hydrogen-treated $TiO_2$ nanowire arrays

$TiO_2$ nanowires grown on FTO substrate were further annealed in hydrogen atmosphere at 350 °C for 30 min. The hydrogenation was carried out in a home-built tube furnace filled with ultrahigh purity hydrogen gas at 740 torr, with the hydrogen gas flow of 50 sccm.

### 4.2.5. Electrodeposition of $Ni(OH)_2$ catalyst

$Ni(OH)_2$ was electrochemically deposited onto $TiO_2$ or H-$TiO_2$ nanowires in a 0.01 M $NiCl_2$ solution at 0.7 mA/cm$^2$ at 90 °C for 30 s. After electrodeposition, the sample was rinsed in DI water, and then air dried at room temperature.

### 4.2.6. Deposition of $Ti(OH)_4$ layer on $TiO_2$ nanowires

$Ti(OBu)_4$ liquid dissolved in a 2 M HCl aqueous solution was used as Ti precursor solution. $TiO_2$ nanowires were treated in 10 mL of 0.025 M HCl solution containing 100 μL of the precursor solution at 90 °C for 2 hours. Then the sample was rinsed with DI water and air dried at room temperature.

### 4.2.7. Material Characterization

SEM images were collected with a field-emission SEM (Hitachi S-4800 II). TEM images were collected witha JEOL2100 TEM/STEM operated at 200 kV.XRD spectra were collected with a Rigaku Americas Miniflex Plus powder diffractometer. Diffraction spectra were recorded from a 2θ angle of 20 to 80 degree with a step size of 0.04 degree at a rate of 1 degree/min.

### 4.2.8. PECMeasurements

PEC measurements were carried out in a three-electrode electrochemical cell

using a $TiO_2$ or H-$TiO_2$ nanowire as working electrode, a coiled Pt wire as counter electrode and an Ag/AgCl electrode as reference electrode. Aqueous solutions of 1 M KOH with a pH 13.6 or 0.5 M $Na_2SO_4$ with a pH 6.8 wereused as the electrolyte. $TiO_2$electrodeswere fabricated by soldering a copper wire onto a bare part of FTO substrate. The contact area was sealed by epoxy.A black mask with a rectangular window (0.20 $cm^2$) was placed in the front of the electrochemical cell to fix the illuminated area.All linear sweep voltammograms were measured by a CHI 660D electrochemical workstation (CH instruments, Inc., Austin, TX), with front side illumination using a solar simulator (Newport 69920, 1000 W xenon lamp) coupled with an infrared water filter (Oriel 6127) and an AM 1.5 global filter (Newport 81094). The power density of 100mW/$cm^2$ was measured with a power meter (Molectron, PM5100). The power density of solar simulator before and after the stability test was measured with power meter, and they were the same.

### 4.2.9. Measurement of charge injection efficiency

Charge injection efficiency was estimated by comparing the photocurrent density in 1 M KOH solution with and without 0.5 M $H_2O_2$. The charge injection yield in the presence of an efficient hole scavenger reagent such as $H_2O_2$ was assumed to be 100%. The charge injection efficiency of electrode is therefore calculated by dividing the photocurrent density obtained in KOH

electrolyte solution ($J_{KOH}$) by the photocurrent density obtained in $H_2O_2$ ($J_{H2O2}$)

$$Charge\ injection\ efficiency = (J_{KOH} / J_{H2O2}) \times 100\%$$

### 4.3 Results and Discussion

Pristine $TiO_2$ and H-$TiO_2$ rutile nanowire arrays were prepared on FTO substrates by hydrothermal method [12] Their photoactivities were measured in a three-electrode electrochemical cell in 1 M KOH electrolyte, using Ag/AgCl in 1 M KCl as a reference electrode and a Pt plate as counter electrode, respectively. Figure 4.1a shows the *I-t* curves of pristine rutile $TiO_2$ and H-$TiO_2$ collected at 0 V vs. Ag/AgCl for 12 hours. H-$TiO_2$ exhibits significantly higher photocurrent density than pristine $TiO_2$ in the entire measurement. Meanwhile, a simple calculation based on this*I-t* data can address the question whether the enhanced photocurrent from H-$TiO_2$was due to re-oxidation of $Ti^{3+}$. By weighing the FTO substrate before and after $TiO_2$ growth, the average mass density of H-$TiO_2$ on FTO substrate was determined to be 0.287 mg/cm$^2$, corresponding to $3.59\times10^{-6}$ mol/cm$^2$ of $TiO_2$. Assume all $Ti^{4+}$ states in $TiO_2$were reduced to $Ti^{3+}$ states during hydrogenation, the total charges (Q) required for the process is:

$Q = M_{Ti}^{3+} \times N_A \times e = 3.59\times10^{-6}$ mol/cm$^2$ $\times$ $6.022\times10^{23}$ mol$^{-1}$ $\times$ $1.602\times10^{-19}$ C = 0.346 C/cm$^2$

where$M_{Ti}^{3+}$ is the number of mole of $Ti^{3+}$ per cm$^2$, $N_A$ is Avogadro number, *e* is

electron charge. This number is over-estimated because only a small amount of $Ti^{3+}$are expected to be created in $TiO_2$.[12, 17] The same amount of charges is needed for re-oxidation of H-$TiO_2$. If all the photo-holes are used to re-oxidize $Ti^{3+}$ sites at the current density (I) of ~0.8 mA/cm$^2$ (0 V vs. Ag/AgCl, Figure 1a),it takes 433 s to electrochemically convert all $Ti^{3+}$ back to $Ti^{4+}$, according to the following equation:

Time = Q / $I$ = 0.346 C/cm$^2$/(0.8 mA/cm$^2$ ×10$^{-3}$ C/s) = 433 s

Then the current density is expected to drop to the similar level as pristine $TiO_2$. On the contrary, the *I-t* curve (Figure 4.1a) shows that the photocurrent density of H-$TiO_2$ is still significantly higher than the photocurrent of pristine $TiO_2$ after 12 hours. Although we cannot rule out the possibility of slow re-oxidation of $Ti^{3+}$or partial re-oxidation on $TiO_2$ surface but maintaining $Ti^{3+}$ in the bulk, this data suggests that if any current used for re-oxidation of $Ti^{3+}$is negligible compared to the enhanced photocurrent obtained from H-$TiO_2$.

Furthermore, the *I-t*data show that both pristine $TiO_2$ and H-$TiO_2$ samples exhibit a certain degree of photocurrent decay after 12 hours. *I-V* curves further show that their saturation currents decreased after the 12-hour stability test, while their onset potentials remained unchanged (Figure 4.1b). Surprisingly, the pristine rutile $TiO_2$ is not as stable as it is expected to be. We also tested the photostability of two other commonly used $TiO_2$ photoelectrode materials, anatase nanotubes and P25 (a mixture of anatase and rutile $TiO_2$ nanoparticles).

Interestingly, both $TiO_2$photoanodes also showed significant photocurrent decay after 12 hours (Figure 4.1c and 4.1d). These unexpected results motivated us to investigate the cause of photocurrent decay of $TiO_2$ based photoanodes, which has been considered to be one of the most stable photoanodes for water oxidation.

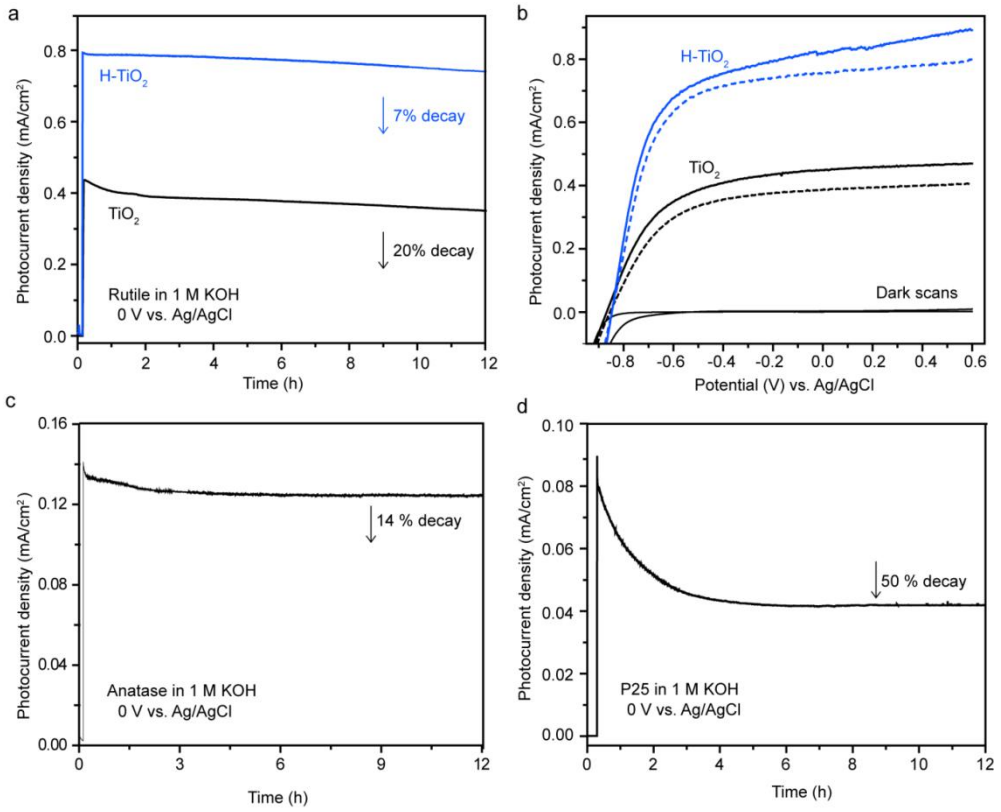


**Figure 4.1.**(a) I-t curves of rutile $TiO_2$ and H-$TiO_2$ photoanode for 12 hours. (b) I-V curves collected at 50 mV/s for rutile $TiO_2$ and H-$TiO_2$ before (solid lines) and following (dash lines) test.Amperometric *I–t* curve of (c) anatase $TiO_2$ nanotube and (d) P25 nanoparticle film photoanodes.

In fact, the photoelectrochemical stability of bare $TiO_2$photoanode has rarely

been studied. In 1998, Khan *et al.* reported that the bare n-$TiO_2$ film electrode is unstable during water splitting reaction under light illumination. They showed that $TiO_2$ stability can be improved by coating a $Mn_2O_3$ layer as oxygen evolution reaction (OER) catalyst, however, the article did not explain the cause of the photoelectrochemical instability of $TiO_2$.[19]In addition,Imanishi and coworkers reported a mechanistic study on photoelectrochemical water oxidation reaction, which is initiated by a nucleophilic attack of an $H_2O$ molecule to a surface-trapped hole.[20] In the study, they reported that atomic level surface roughening occurred with the progress of oxygen photoevolution reaction under anodic bias, in which Ti-O bond breaking was induced at the surface lattice. According to these articles and our stability data, we suspected that the photocurrent decay of $TiO_2$ samples is due to photo-corrosion.

To verify this hypothesis, we carried out several experiments. First, there was no obvious change in the XRD spectra of $TiO_2$ before and after the stability test (Figure 4.2). It suggests that the current decay should not be related to the modification of chemical composition or crystal phase of $TiO_2$. Second, we collected SEMimages for the samples before and following the stability test (Figure 4.3). As shown in Figure 4.3a, we indeed observed significant structural modification of $TiO_2$ after the 12-hour test. Apparently, the crystalline nanowire surface was converted to amorphous structure. The side view SEM images further revealed that the average thickness of nanowire film dropped slightly

from 2.2 μm to 1.8 μm (Figure 4.3b). The samples we compared before and after stability tests were from the same piece of $TiO_2$ film where the thickness variation of the $TiO_2$ film over the substrate can be neglected. These results clearly indicate that the observed photocurrent decay was due to corrosion.

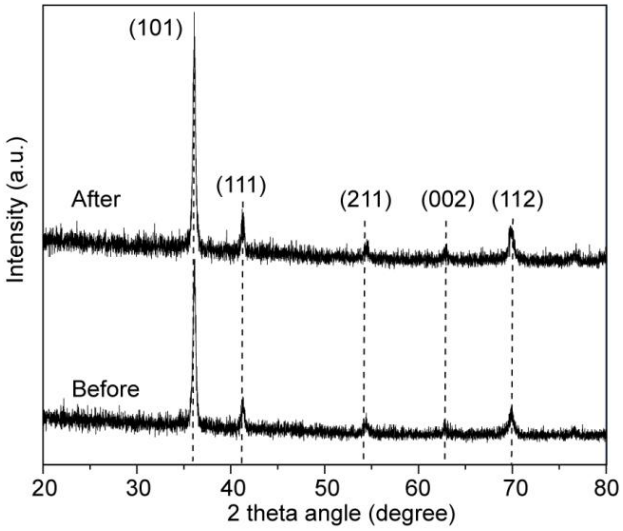


**Figure 4.2**. XRD spectra collected for $TiO_2$ nanowire photoanode before and after the 12-hour stability test

We further carried out a control experiment to test whether the observed corrosion is induced by light illumination. We applied a constant current density of 0.8 mA/cm$^2$ on H-$TiO_2$photaonode in the darkin 1 M KOH electrolyte to split water (Figure 4.4). The applied current density is equivalent to the photocurrent density that can be obtained at 0 V vs. Ag/AgCl under light illumination (100 mW/cm$^2$). Significantly, there was no morphology change observed for $TiO_2$ nanowires after testing in the dark for 3 days (Figure 4.5).

These resultsconfirmed that the instability of $TiO_2$ photoanode was not due to

the electrochemical corrosion or $O_2$ bubble etching, but photoinduced corrosion. Third, photo-corrosion also induced structural modification of $TiO_2$ nanowires that can significantly change the surface kinetics for water oxidation. To evaluate the effect of surface modification on charge transfer, we compared the charge injection efficiency of $TiO_2$ electrode before and after the stability test. Charge injection efficiency can be calculated by dividing the photocurrent obtained in KOH electrolyte by the photocurrent obtained in the same electrolye with the addition of hydrogen peroxide ($H_2O_2$) as hole scavenger, with the assumption that the hole collection efficiency is 100% in the presence of $H_2O_2$.[21] As shown in Figure 4.3c, the charge injection efficiency of $TiO_2$ electrode dropped considerably after 12-hour test. This result suggests that the photo-corrosion induced surface modification indeed slows down the interfacial hole transfer, which could be due to the formation of amorphous layer at $TiO_2$ surface. The finding of $TiO_2$ photoelectrochemical instability is surprising because $TiO_2$ have been considered to be one of the most stable photoanode materials.

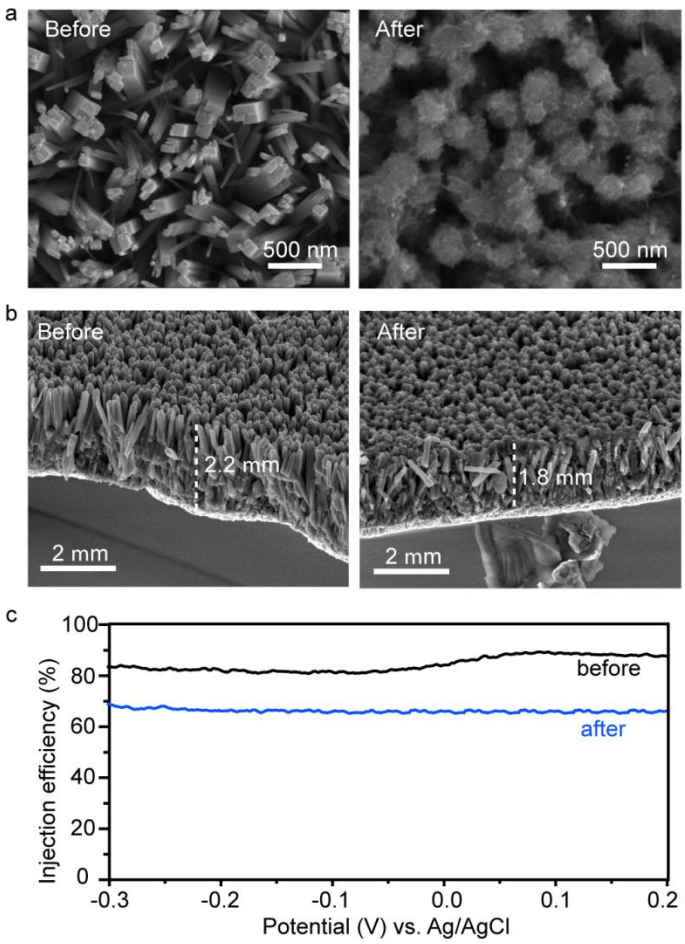


**Figure 4.3.**(a) Top view and (b) side view SEM images of $TiO_2$ photoanode collected before and after test. (c) Charge injection efficiency of $TiO_2$ photoanode as a function of applied potential in basic electrolyte before and after stability test.

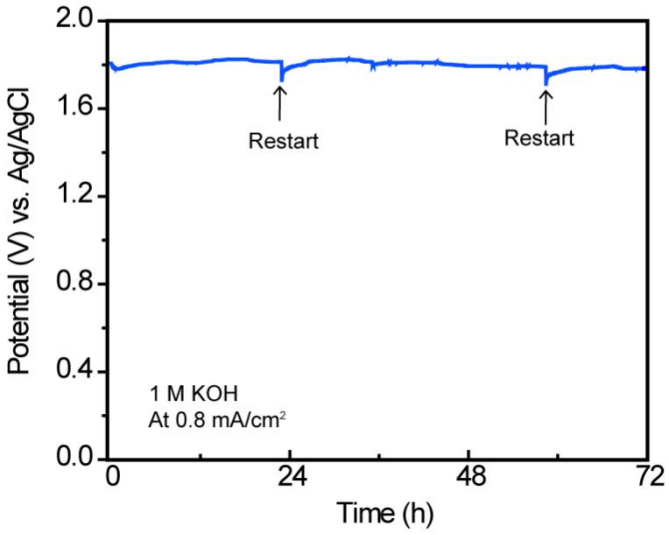


**Figure 4.4.** V-t curve collected for H-$TiO_2$ photoanode in 1 M KOH electrolyte at current density of 0.8 mA/$cm^2$ in the dark.

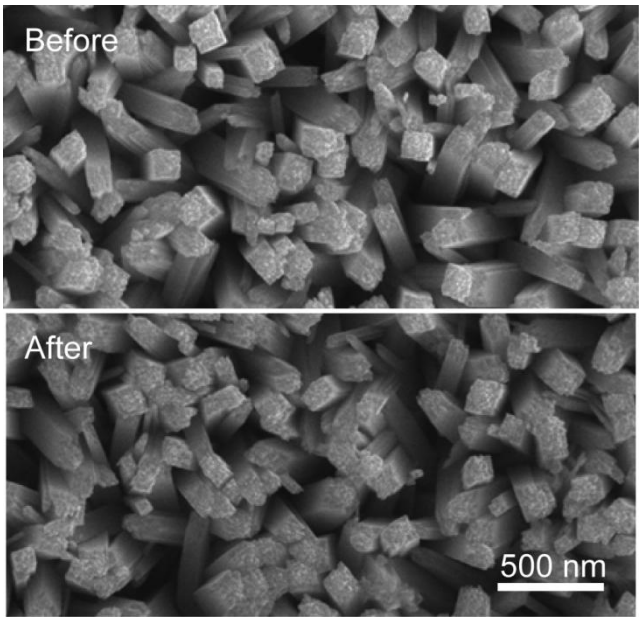


**Figure 4.5.** SEM images collected from $TiO_2$ photoanode before and after constant current test.

While we have identified the photocurrent decay is related to photo-corrosion,

the next step was to understand the photo-corrosion mechanism and explore methods to address the instability of $TiO_2$ photoanode. According to the Imanishi *et al.* article, the atomic level surface roughening occurred with the progress of oxygen photoevolution reaction.[20] We hypothesized that the surface photoinduced holes initiate both water oxidation and surface roughening, and they are competitive reactions. Therefore, we believe that the photo-corrosion of $TiO_2$ photoanode can be suppressed by consuming the surface holes efficiently. To test this hypothesis, we carried out PEC measurements on H-$TiO_2$ photoanode in the electrolyte with the addition of methanol as a hole scavenger. By adding methanol, we introduce an additional pathway competing for photoinduced holes, in addition to water oxidation and photo-corrosion (Figure 4.6a), with a goal of increasing the efficiency for hole transfer/collection and suppressing the path of photo-corrosion. The addition of methanol did not change the photocurrent density.Importantly, the current-time data of H-$TiO_2$ photoanode collected at 0.2 V vs. Ag/AgCl in a 1 M KOH/1 M methanol solution confirmed that there was no photocurrent decay after 12 hours (Figure 4.6b). The current-voltage curves of H-$TiO_2$ collected before and after the 12-hour stability test were also well matched. Likewise, similar results were obtained from anatase $TiO_2$ nanotube photoanode and P25 nanoparticle film photoanode (Figure 4.7). Moreover, we did not observe surface amorphization of $TiO_2$ nanowires after the stability test, which again suggesting the

photocurrent decay and structural modification is correlated. Taken together, these results validate our hypothesis that adding a hole sacrificial reagent can suppress the photo-corrosion and stabilize the photoactivity of $TiO_2$ photoanode.

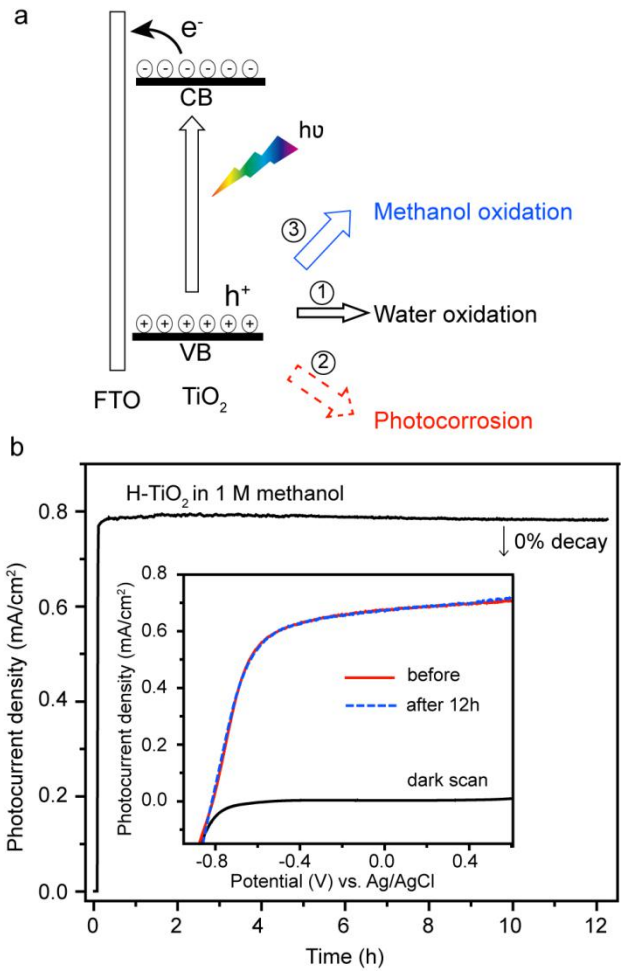


**Figure 4.6** (a) Schematic diagram of three possible hole transfer pathways of $TiO_2$ photoanode in 1 M KOH/1 M methanol electrolyte. (b) *I–t* curve of H-$TiO_2$ photoanode collected in 1 M KOH/1 M methanol electrolyte. Inset: I-V curve of H-$TiO_2$ photoanode collected before and after the 12-hour test.

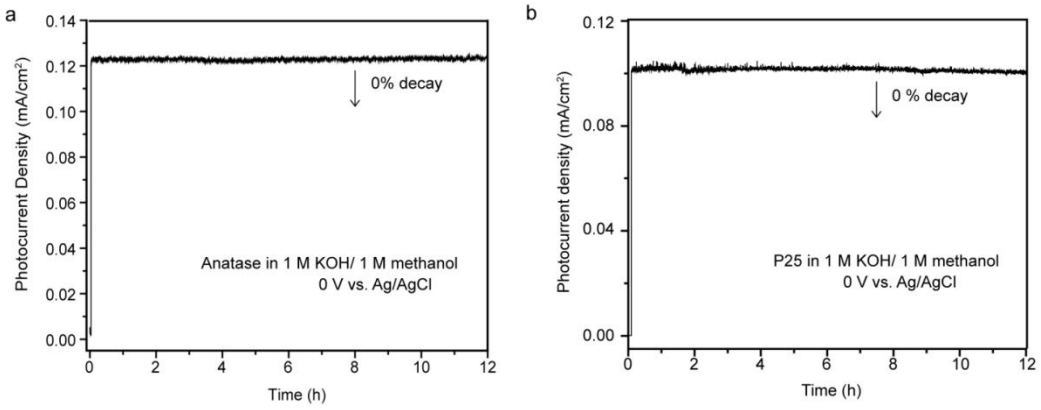


**Figure 4.7.**Amperometric*I–t* curve collected for (a) anatase $TiO_2$ nanotube and (b) P25 film photoanode in 1 M KOH/1 M methanol electrolyte.

The methanol experiment has proved that improved hole transfer can suppress photo-corrosion. However, methanol is an important chemical fuel, it is certainly not desirable to use methanol as sacrificial reagent. Alternatively, we have explored two approaches to increase hole transfer efficiency of $TiO_2$ by adding OER catalysts and/or using renewable hole sacrificial reagent. Recently, Ni based OER catalysts such as nickel hydroxide, nickel oxide and nickel borate have attracted a lot of interest, due to their excellent catalytic performance, low cost and low toxicity.[24-30] We deposited $Ni(OH)_2$ catalyst onto H-$TiO_2$ electrochemically in a solution of 0.01 M $NiCl_2$ at 0.7 mA/cm$^2$ at 90 °C for 30 seconds.[31] The $Ni(OH)_2$ catalyst decorated H-$TiO_2$ is denoted as H-$TiO_2$/$Ni(OH)_2$. To evaluate the effect of $Ni(OH)_2$ catalyst on the photoinduced hole transfer, we again measured and compared the charge injection efficiency of H-$TiO_2$/$Ni(OH)_2$and bare H-$TiO_2$ electrodes. Figure 4.8a inset shows that the

charge injection efficiency of H-$TiO_2$ has been considerably improved after coating $Ni(OH)_2$ catalyst, asexpected. As a result, while the photocurrent remained the same as H-$TiO_2$ photoanode without $Ni(OH)_2$ catalyst,the photocurrent retention rate of H-$TiO_2$ in 12 hours has slightly improved from 93% to 95% (Figure 4.8a). While the addition of $Ni(OH)_2$catalyst enhances the photostability of $TiO_2$ by increasing the hole transfer efficiency, apparently it is less effective than adding a hole scavenger. This is because $Ni^{4+}$ is believed to be the active catalytic species for water oxidation, however, $Ni^{3+}/Ni^{4+}$ transition is known to be slow.[28]The slow formation of $Ni^{4+}$ from $Ni^{2+}$ limits the effect of $Ni(OH)_2$ catalyst. We believe that other OER catalysts should have similar or even better effect in improving the photostability of $TiO_2$.[19, 22]

Furthermore, we aimed to increase hole transfer efficiency by adding urea as an additional hole acceptor. It has been shown that urea oxidation is more favorable than water oxidation in the presence of $Ni(OH)_2$ catalyst.[33] We expected that the addition of urea would provide an alternative and more favorable path for hole transfer, and therefore suppress the photohole induced corrosion. In contrast to other electron acceptors such as methanol, urea is a sustainable hole sacrificial reagent because it is a major component of human/animal urine. Figure 4.8b shows the current-time data of H-$TiO_2$/$Ni(OH)_2$ photoanode collected in a solution mixture of 1 M KOH and 1.5 M urea at 0.2 V vs. Ag/AgCl for 3 days.The addition of urea did not change the photocurrent density.Remarkably,

there was no photocurrent decay in the first 24 hours, and the total reduction of photocurrent in 3 days was 3% only. This data unambiguously showed that adding urea is an effective method to stabilize H-$TiO_2$ photoanode.

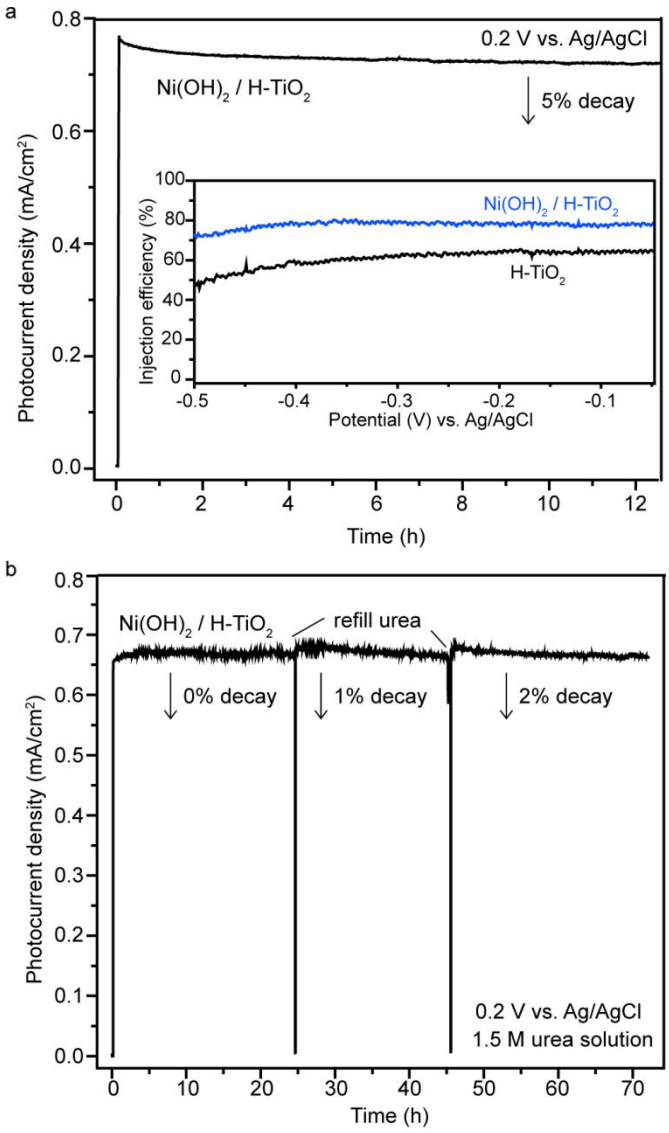


**Figure 4.8.**(a) *I–t* curve of $Ni(OH)_2$/H-$TiO_2$ photoanode collected in basic solution. Inset: a plot of charge injection efficiency of $Ni(OH)_2$/H-$TiO_2$ and H-$TiO_2$ photoanodes. (b) *I–t* curve of H-$TiO_2$/$Ni(OH)_2$ photoanode collected in a

solution mixture of 1 M KOH and 1.5 M urea.

In addition, the photochemical stability of $TiO_2$ can be highly dependent on a number of factors, such as solution pH and the presence of electrolyte ions. For example, Imanishi and coworkers reported that the surface roughening on the $TiO_2$ surfaces can be substantially suppressed in the basic solution.[20] Therefore we also compared the long term stability of rutile$TiO_2$nanowire photoanode tested in basic (1 M KOH) and neutral (0.5 M $Na_2SO_4$) electrolyte solutions. While we observed photocurrent decay in both cases (Figure 4.9), it is noteworthy that the photocurrent decay profiles in these two electrolyte solutions are fundamentally different. In neutral solution, the photocurrent of $TiO_2$ photoanode decays almost linearly with time. In contrast, in basic solution the photocurrent decreased rapidly in the first few hours and then remained relatively stable. Importantly, SEM images revealed thatthe $TiO_2$ nanowires tested in the neutral solutionwere severely etched after the 24-hour test, however, there was no amorphous coating on the wire (Figure 4.9 inset). The results suggest that the surface amorphization of $TiO_2$ nanowiresin the KOH solution can somehow slow down the photo-corrosion process. We collected the high resolution TEM images of $TiO_2$ nanowires after 12-hour stability test when the photocurrent decay became slower. As shown in Figure 4.10, we observed a uniform amorphous coating on $TiO_2$ nanowires, with an average thickness of

around 10 nm. We believe that the amorphous coating could be titanium hydroxide which is insoluble in the basic KOH electrolyte solution. The etching of crystalline $TiO_2$ nanowire during photo-corrosion produces $Ti^{4+}$ cations (Ti precursor) that can further react with hydroxide ($OH^-$) anions presence in the electrolyte solution to form amorphous titanium hydroxide on $TiO_2$ nanowire surface. Nevertheless, the formation of this insoluble amorphous layer in neutral $Na_2SO_4$ solution is impossible, which is consistent with the SEM data. It is likely that the formation of this amorphous layer prevents the crystalline $TiO_2$ nanowire core from contacting electrolyte, and thus, slows down the photo-corrosion processafter the first few hours.

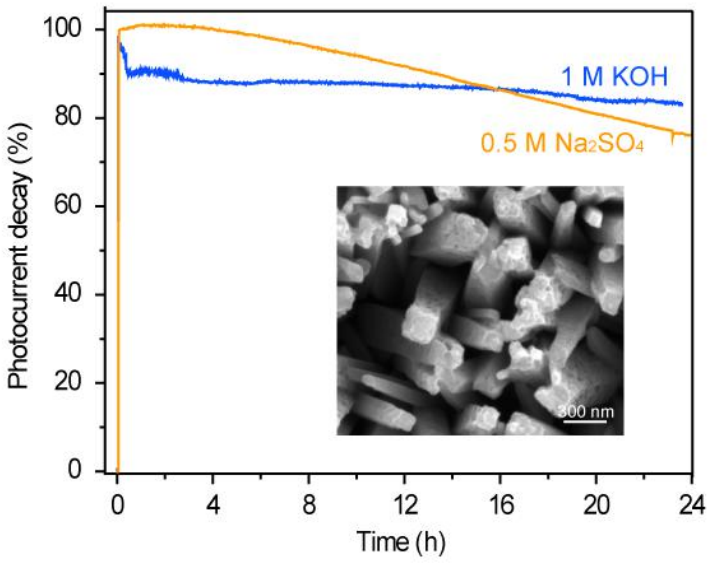


**Figure 4.9.** photocurrent decay as a function of stability test time for $TiO_2$ nanowire photoanode in a 0.5 M $Na_2SO_4$ and 1 M KOH electrolyte solution. Inset: SEM image of $TiO_2$ nanowires collected after stability test in 0.5 M

$Na_2SO_4$electrolyte.

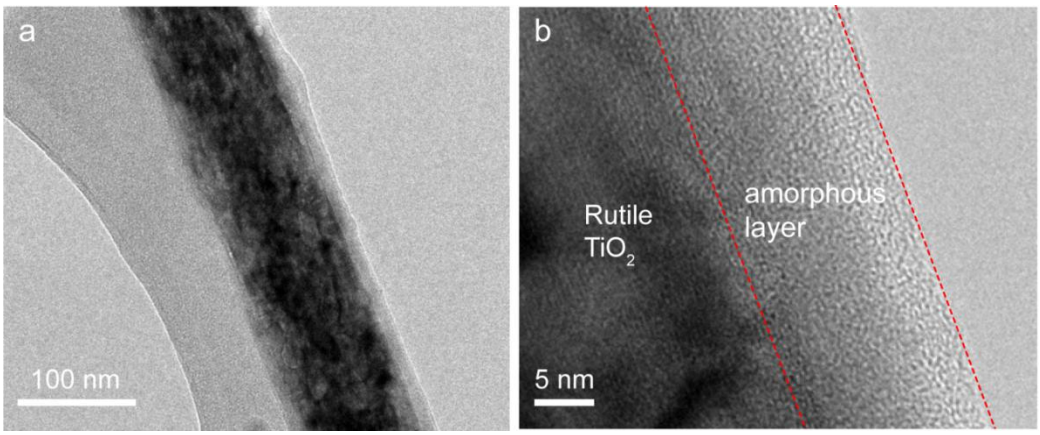


**Figure 4.10.** TEM image (a)and High resolution TEM image (b) of $TiO_2$ nanowire collected after test in basic solution.

Based on the above results, we found coating an additional amorphous titanium hydroxide layer onto crystalline $TiO_2$nanowire can protect it from photo-corrosion. To test this hypothesis, we intentionally deposit an amorphous titanium hydroxide shell on rutile $TiO_2$ nanowires using hydrothermal method.[34] Significantly, the $TiO_2$ photoanode showed even better photochemical stability in KOH solution, with only ~3% decay in 72 hours (Figure 4.11). In addition, SEM image further revealed that there was no obvious morphological change of nanowire surface after the stability test (Figure 4.12). These results proved that theamorphous titanium hydroxide coating can effectively suppress the photo-corrosion of rutile $TiO_2$ nanowires. In addition, these results also suggest that the relatively better photoelectrochemical stability of H-$TiO_2$ (vs. pristine $TiO_2$)

could be due to the higher concentration of hydroxyl groups on nanowire surface,[12] although further studies are required to fully understand the mechanism.

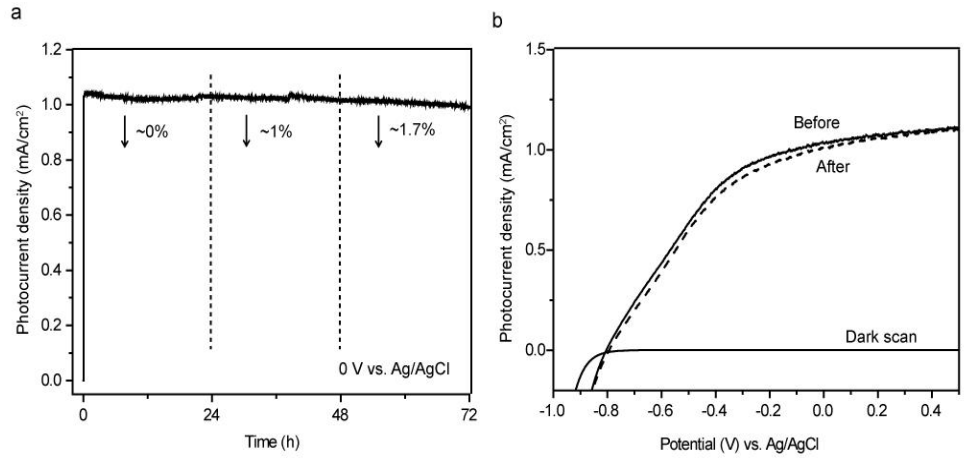


**Figure4.11.**(a) *I–t* curve of $TiO_2$photoanode coated with amorphous film collected in a basic for 72 hours. (b) Linear sweep voltammograms collected fromthe $TiO_2$ nanowire photoanodebefore and after the 72-hour test.

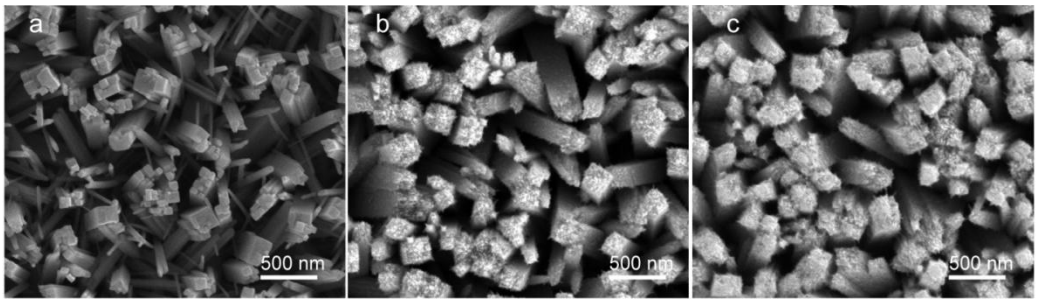


**Figure 4.12.** SEM images collected for (a) bare rutile $TiO_2$ nanowires, rutile $TiO_2$ nanowires coated with amorphous $Ti(OH)_4$ nanoparticle film before (b) and (c) after stability test.

## 4.4 Conclusion

In summary, we reported for the first time the long term photoelectrochemical stability of bare $TiO_2$ photoanodes. The key and surprising finding is the photoelectrochemical instability of $TiO_2$ photoanodes. The studies showed that the photoanode made of rutile $TiO_2$nanowires, anatase $TiO_2$ nanotubes and P25 nanoparticles suffered from substantial photocurrent decay in photoelectrochemical stability test. The photocurrent decay is believed to be due to photo-hole induced corrosion. Importantly, we have demonstrated that thephoto-corrosion can be considerably suppressed by two distinct approaches.First, photo-corrosion can be suppressed by modifying $TiO_2$ electrode with $Ni(OH)_2$OER catalyst and/or adding urea as scarificial reagent to improve extraction of photoholes.Alternatively, an amorphous layer of titanium hydroxide can protect$TiO_2$from photo-corrosion.$TiO_2$ nanowire photoanodes treated by either one of the approaches exhibitoutstanding photoelectrochemical stability in KOH solution, with only ~3% photocurrent decay in 3 days. We believe that the new understanding on the photoelectrochemical instability of $TiO_2$ photoanodes and the capability to stabilize them are critical to the applications of $TiO_2$ photoelectrodes.

## References

1. A. Fujishima; K. Honda. *Nature* **1972,** 238,37-38.

2. M. Z. Liu; N. D. Snapp; H. Park. *Chem. Sci.***2011,** 2,80-87.

3. C. Liu; Y. J. Hwang; H. E. Jeong; P. D. Yang. *Nano Lett.***2011,** 11,3755-3758.

4. G. K. Mor; K. Shankar; M. Paulose; O. K. Varghese; C. A. Grimes. *Nano Lett.***2005,** 5,191-195.

5. S. U. M. Khan; M. Al-Shahry; W. B. Ingler. *Science* **2002,** 297,2243-2245.

6. X. Chen; S. S. Mao. *Chem. Rev.* **2007,** 107,2891-2959.

7. X. B. Chen; S. H. Shen; L. J. Guo; S. S. Mao. *Chem. Rev.* **2010,** 110,6503-6570.

8. Y. H. Hu. *Angew. Chem. Int. Ed.* **2012,** 51,12410-12412.

9. K. S. Joya; Y. F. Joya; K. Ocakoglu; R. Van De Krol. *Angew. Chem. Int. Ed.* **2013,** 52,10426-10437.

10. B. Liu; H. M. Chen; C. Liu; S. C. Andrews; C. Hahn; P. D. Yang. *J. Am. Chem. Soc.* **2013,** 135,9995-9998.

11. Y. J. Hwang; C. Hahn; B. Liu; P. D. Yang. *ACS Nano* **2012,** 6,5060-5069.

12. G. M. Wang; H. Y. Wang; Y. C. Ling; Y. C. Tang; X. Y. Yang; R. C. Fitzmorris; C. C. Wang; J. Z. Zhang; Y. Li. *Nano Lett.***2011,** 11,3026-3033.

13. Y. Yang; Y. C. Ling; G. M. Wang; Y. Li. *Eur. J. Inorg. Chem.***2014,** 760-766.

14. H. Y. Wang; G. M. Wang; Y. C. Ling; M. Lepert; C. C. Wang; J. Z. Zhang; Y. Li. *Nanoscale* **2012,** 4,1463-1466.

15. S. Hoang; S. W. Guo; N. T. Hahn; A. J. Bard; C. B. Mullins. *Nano Lett.***2012,** 12,26-32.

16. I. S. Cho; M. Logar; C. H. Lee; L. L. Cai; F. B. Prinz; X. L. Zheng. *Nano Lett.***2014,** 14,24-31.

17. S. Hoang; S. P. Berglund; N. T. Hahn; A. J. Bard; C. B. Mullins. *J. Am. Chem. Soc.* **2012,** 134,3659-3662.

18. F. M. Pesci; G. M. Wang; D. R. Klug; Y. Li; A. J. Cowan. *J.Phys.Chem.C***2013,** 117,25837-25844.

19. S. U. M. Khan; J. Akikusa. *J. Electrochem. Soc.***1998,** 145,89-93.

20. A. Imanishi; T. Okamura; N. Ohashi; R. Nakamura; Y. Nakato. *J. Am. Chem. Soc.* **2007,** 129,11569-11578.

21. H. Dotan; K. Sivula; M. Gratzel; A. Rothschild; S. C. Warren. *Energy Environ. Sci.***2011,** 4,958-964.

22. S. Hu; M. R. Shaner; J. A. Beardslee; M. Lichterman; B. S. Brunschwig; N. S. Lewis. *Science* **2014,** 344,1005-1009.

23. Y. J. Hwang; A. Boukai; P. D. Yang. *Nano Lett.***2009,** 9,410-415.

24. B. S. Yeo; A. T. Bell. *J.Phys.Chem.C***2012,** 116,8394-8400.

25. P. L. Liao; J. A. Keith; E. A. Carter. *J. Am. Chem. Soc.* **2012,** 134,13296-13309.

26. K. Sun; N. Park; Z. L. Sun; J. G. Zhou; J. Wang; X. L. Pang; S. H. Shen; S. Y. Noh; Y. Jing; S. H. Jin; P. K. L. Yu; D. L. Wang. *Energy Environ. Sci.***2012,** 5,7872-7877.

27. G. M. Wang; X. H. Lu; T. Zhai; Y. C. Ling; H. Y. Wang; Y. X. Tong; Y. Li. *Nanoscale* **2012,** 4,3123-3127.

28. G. M. Wang; Y. C. Ling; X. H. Lu; T. Zhai; F. Qian; Y. X. Tong; Y. Li. *Nanoscale* **2013,** 5,4129-4133.

29. C. Du; X. G. Yang; M. T. Mayer; H. Hoyt; J. Xie; G. Mcmahon; G. Bischoping; D. W. Wang. *Angew. Chem. Int. Ed.* **2013,** 52,12692-12695.

30. C. Du; M. Zhang; J. W. Jang; Y. Liu; G. Y. Liu; D. W. Wang. *J.Phys.Chem.C***2014,** 118,17054-17059.

31. Y. C. Mao; H. Yang; J. X. Chen; J. Chen; Y. X. Tong; X. D. Wang. *Nano Energy* **2014,** 6,10-18.

32. X. H. Xia; J. S. Luo; Z. Y. Zeng; C. Guan; Y. Q. Zhang; J. P. Tu; H. Zhang; H. J. Fan. *Sci. Rep.***2012,** 2.

33. G. M. Wang; Y. C. Ling; X. H. Lu; H. Y. Wang; F. Qian; Y. X. Tong; Y. Li. *Energy Environ. Sci.***2012,** 5,8215-8219.

34. Y. C. Pu; Y. C. Ling; K. D. Chang; C. M. Liu; J. Z. Zhang; Y. J. Hsu; Y. Li. *J.Phys.Chem.C***2014,** 118,15086-15094.

# Chapter 5

## Acid Treatment Enables Suppression of Electron-Hole Recombination in Hematite for Photoelectrochemical Water Splitting


### Abstract

In this chapter, Ireport a new and simple strategy-acid treated methodto suppressthe electron-hole recombination in hematite photoanode. Acid-treated hematitephotoanodesshowsubstantially enhanced photocurrent density compared to untreated sample.Electrochemical impedance spectroscopy (EIS) studiesreveal that the enhanced photocurrent is partlydue to improved efficiency of charge separation.Transient absorption (TA) spectroscopic studiescoupled to electrochemical measurements indicate that in addition to improved bulk electrochemical properties, acid treated hematite has significantly decreased surface electron-hole recombination losses due to a greater yield of the trapped photoelectrons being extracted to the external circuit. The capability of improvingphotoactivity of hematite electrodes using simple acid treatment method should open up new opportunities for solar energy conversion systems including photoelectrochemical cells and solar cells.


### 5.1 Introduction

Metal oxide semiconductors have been extensively studied as photoelectrodes

for water splitting.[1-10] Among them, hematite ($\alpha$-$Fe_2O_3$) has attracted much attention due to its favorable optical band gap, extraordinary chemical stability in oxidative environments, low cost, and abundance.[11-19]Nevertheless, poor hole transfer efficiency and late turn-on characteristics severely limits the photoelectrochemical performance of hematite electrodes.[12, 20-21] Numerous methods have been demonstrated to address this limitation. For example, a number of hematite nanostructures have been developed to minimize hole transfer distance.[11, 13, 22] Surface passivation has been demonstrated to be another effective method to enhance hole transfer efficiency by reducing the number of surface trap states.[20-21, 23] Likewise, hole transfer efficiency can be improved by decorating hematite surface with oxygen evolution reaction (OER) catalysts which can enhance activity either by reducing the over-potential for water oxidation[24-27] or through the suppression of slow recombination due to interfacial electronic effects [28-30]. Previous studies also suggested that the turn-on characteristics of hematite photoanodes may be closely related to their surface nature. Recently, Jang *et al.* reported a re-growth strategy to reduce surface disorders of hematite nanowires and achieved a significantly shifted onset voltage. [31]Yet, the performance of hematite photoanodes can also be limited by the efficiency of initial charge separation and electron transfer, which has been rarely studied. Here we demonstrate that a simple acid treatment method can substantially enhance the efficiency of electrons moving out of traps

in hematite nanowire photoanodes, and therefore reduce the electron-hole recombination loss. The acid-treated hematite photoanode shows significantly improved performance for PEC water oxidation.

## 5.2 Experimental Section

### 5.2.1 Synthesis of Sn-doped hematite nanowires

Hematite ($\alpha$-$Fe_2O_3$) nanowires were prepared on a FTO glass substrate by a previously reported method. A Teflon-lined stainless steel autoclave was filled with 20 ml aqueous solution containing 0.15 M of ferric chloride ($FeCl_3 \cdot 6H_2O$, Acros, 99+%) and 1 M sodium nitrate ($NaNO_3$, Fisher 99.4%). The solution pH was adjusted to 1.5 by HCl. A pre-cleaned piece of FTO glass substrate was put into the autoclave. The autoclave was heated at 95 °C for 4 hrs and allowed to cool down at ambient conditions. A uniform layer of iron oxyhydroxide ($\alpha$-FeOOH) film (yellow in color) was formed on the FTO substrate. The $\alpha$-FeOOH film was washed with deionized (DI) water to remove residual salt. To introduce Sn-doping into the nanowires, we intentionally added 1-2 drops of tin (IV) chloride ($SnCl_4$) ethanol solution (2 mg/ml) onto the$\alpha$-FeOOH film, and then sintered in air at 550 °C for 30 min, followed by annealing at 800 °C for additional 20 min.

### 5.2.2 Acid treatment

Hematite nanowires grown on FTO glass substrate were immersed in pureacetic acid for 5 min, and then let them dry in air without washing. Then the acid-

treated hematite nanowires were further annealed at 450 $^{o}$C in air for 30 min.

### 5.2.3 Material characterization

SEM images were collected with a field-emission SEM (Hitachi S-4800 II). XRD spectra were collected with a Rigaku Americas Miniflex Plus powder diffractometer. Diffraction spectra were recorded from a 2θ angle of 20 to 80 degree with a step size of 0.04 degree at a rate of 1 degree/min. X-ray Photoelectron Spectroscopy (XPS) was performed on a RBD upgraded PHI-5000C ESCA system (Perkin-Elmer) using Al-monochromatic X-ray at a power of 25 W with an X-ray-beam diameter of 10 mm, and a pass energy of 29.35 eV. The pressure of analyzer chamber was maintained below $5\times10^{-8}$ Pa during the measurement. The binding energy was calibrated using the C 1s photoelectron peak at 284.6 eV as the reference.

### 5.2.4 Photoelectrochemical and electrochemical measurements

Hematite nanowires were fabricated into photoanodes by soldering a copper wire onto a bare part of the FTO substrate. The substrate edges and the metal contact region were sealed with insulating epoxy resin. The working electrode area is in the range of 0.2-0.25 cm$^2$. 1 M NaOH aqueous solution (pH = 13.6) was used as electrolyte for hematite electrodes. Linear sweeps, *I-t* curves and electrochemical impedance spectra were collected by a CHI 660D electrochemical station, with Pt sheet as counter electrode and Ag/AgCl as reference, under simulated sunlight (100 mW/cm$^2$) generated from a 150 W

xenon lamp (Newport 6255) coupled with an AM 1.5 global filter (Newport 81094). Incident-photon-to-current-conversion-efficiency (IPCE) data were collected by the CHI 660D electrochemical station with a solar simulator (Newport 69920, 1000 W xenon lamp), coupled with an infrared water filter (Oriel 6127) and aligned monochrometor (Oriel Cornerstone 130 1/8 m). Charge separation efficiency is measured the photocurrent densities under 370nm light illumination in 1 M NaOH solution with $H_2O_2$, according to the following equation:

Where λ is the incident wavelength, which is 370 nm, $J_{H2O2}$is the photocurrent density in 0.5 M $H_2O_2$ aqueous solution, P(λ) is the power density of irradiance at 370 nm, Abs (λ) is the amount of absorption at 370 nm.

EIS was carried out by using the same electrochemical setup as PEC measurement. It was conducted in a range from 0.1 Hz to 100kHz at open circuit potential with a perturbation of 5 mV. ZSimpWin software was used to fit EIS data and obtain parameters of equivalent circuit elements.

### 5.2.5 Transient measurements

The TA apparatus has been described elsewhere. Briefly, the third harmonic of a Nd:YAG laser (Continuum, Surelite I-10, 355 nm, 4-6 ns pulse width) operating at 0.33 Hz is the UV excitation source. The repetition rate of the laser was chosen to ensure that all photogenerated charge carriers had fully decayed

prior to the next excitation event. A laser intensity of ca.200 μJ $cm^{-2}$ at 355 nm was incident on the photoelectrochemical cell, leading to an intensity of ca.100 μJ $cm^{-2}$ at the sample. We note that high pump laser intensities can lead to excessively high electron-hole recombination rates and in mind of this we use the relatively low excitation power of ca.100 μJ $cm^{-2}$ throughout, in order to limit/eliminate this effect. There are a number of past studies on hematite regarding these laser intensities which give us confidence that the parameters used here are relevant in providing useful information. A 75 W Xe lamp (OBB Corp.) coupled to monochromator (OBB Corp., set to 4 nm resolution) acts as the probe light and the change in optical density of the sample is calculated by measuring the transmitted light using a Si Photodiode (Hamamatsu) and a homemade amplification system coupled to both an oscilloscope (Textronix TDS 220) and data acquisition card (National Instruments NI-6221). In order to generate the TA spectra at a range of biases, 200 laser shots per wavelength were recorded. Accurate kinetic traces were recorded in a separate experiment using a minimum of 500 shots per wavelength. All TA experiments were carried out in PEC cell under potentiostatic control at the potential indicated in the text. Transient photocurrent measurements were recorded using the same apparatus with the light from the Xe probe lamp blocked. The current was obtained by measuring the voltage drop across a 47 ohm resistor in series with the working and counter electrode.

## 5.3 Results and Discussion

Hematite ($\alpha$-$Fe_2O_3$) nanowires intentionally doped with Sn were synthesized on a FTO glass substrate according to a literature reported hydrothermal method.[13]SEM image revealed that the nanowires are vertically aligned on the FTO substrate, with average diameter of 100 nm and length of ~1 μm. The hematite nanowire film on FTO substrate was then immersed in pure acetic acid solution for 5 min, followed by annealing in air at 450 $^oC$ for 30 min. The nanowire morphology remained unchanged upon the acid treatment and annealing. The X-ray powder diffraction results also revealed that the acid treated nanowires are still pure hematite crystal (Figure 5.1). Furthermore, lattice-resolved transmission electron microscopy images showed that the acid-treated nanowirehas an equally smooth surface as the untreated hematite, and there is no sign of surface etching or shell coating (Figure 5.2). To investigate the possible influence of acid treatment on the chemical nature of the hematite nanowire surface, we also collected X-ray photoelectron spectroscopy (XPS) spectra for untreated and acid treated hematite samples (Figure 5.3). Both samples exhibit a Fe 2p1/2 peak and a Fe 2p3/2 peak centered at binding energies of724.5eV and 711.4 eV, which are typical values reported for $Fe^{3+}$ in $Fe_2O_3$,[4, 32]In addition, they exhibit a satellite peak located at 716 eV that corresponds to $Fe^{2+}$, which is consistent to the value reported for Sn-doped

hematite. [33] Notably, acid-treated hematite has a slightly higher $Fe^{2+}$ signal than the untreated hematite, suggesting $Fe^{2+}$ sites have been created during acid treatment. Furthermore, both hematite samples have similar O 1s spectra with the main line centered at530.0 eV. Acid-treated hematite exhibits an additional shoulder peak at higher binding energy of 531.9 eV that can be attributed to Fe-OH, which has been reported to be located at the binding energy ~1.5-2.0 eV higher than the O 1s peak of $Fe_2O_3$. [14, 34] Taken together, the XPS data confirm the increased amount of hydroxyl groups on the hematite surface following acid treatment, resulting in the formation of more $Fe^{2+}$ sites to balance the charge.

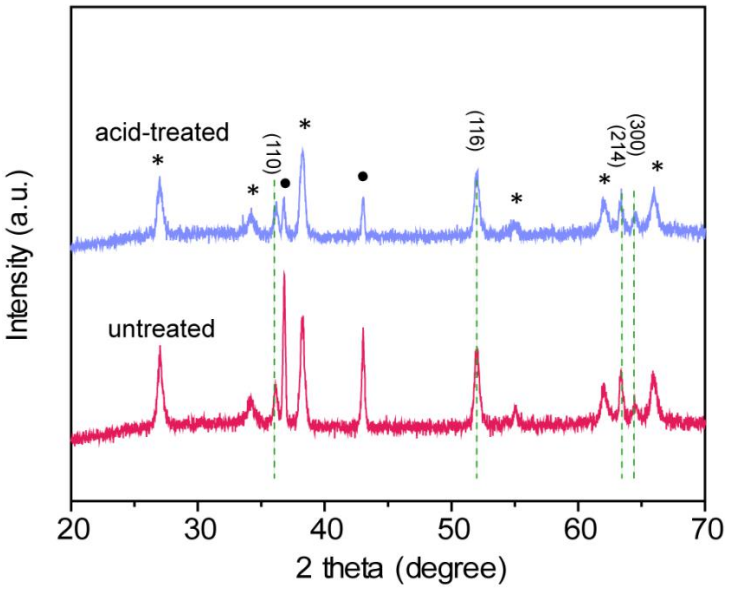


**Figure 5.1.** XRD spectra collected for untreated hematite and acid-treated hematite sample.

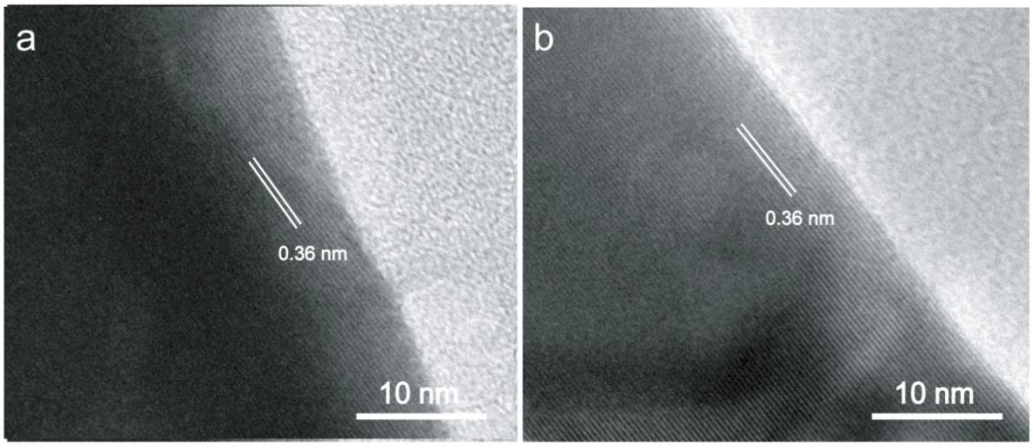


**Figure 5.2.**Lattice-resolved TEM images collected from (a) untreated and (b) acid-treated hematite nanowire.

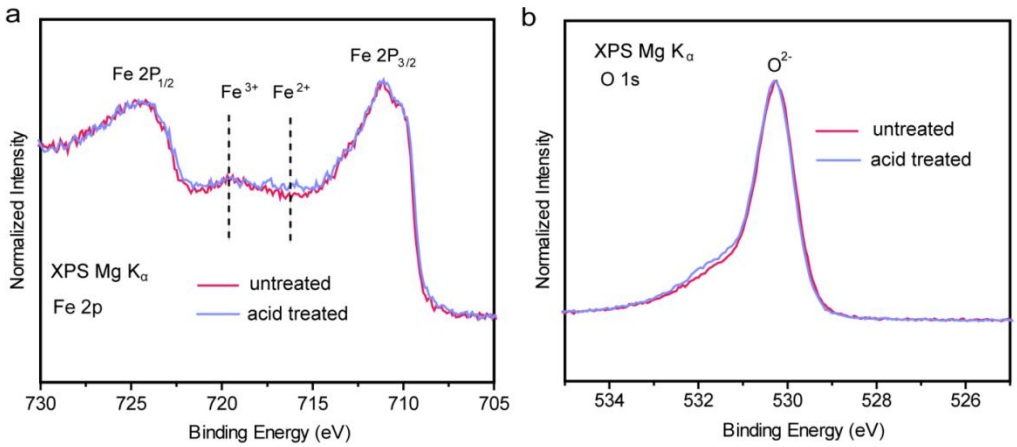


**Figure 5.3.** (a) Fe 2p and (b) O 1s XPS spectra of untreated hematiteandacid-treated hematitesamples.

The photoelectrochemical performance of untreated and acid treated hematite samples were investigated in a three-electrode electrochemical cell using hematite sample as a working electrode, a platinum sheet as counter electrode, and Ag/AgCl (1 M KCl) as a reference electrode. Linear sweep voltammograms

were collected for both hematite samples in 1 M NaOH electrolyte solution (pH = 13.6) under illumination of simulated solar light at 100 mW/cm$^2$. Significantly, acid-treated hematite showed considerably enhanced photocurrent density compared to that of untreated sample (Figure 5.4a). It is also noteworthy that both the untreated and acid-treated hematite electrodes have a similar onset potential of -0.15 V *vs.* Ag/AgCl (equivalent to 0.85 V *vs.* RHE), which is consistent with the values reported for other hematite photoanodes without the addition of oxygen-evolving catalysts. [11, 13, 15] To understand the interplay between the enhanced photocurrent and the photo-response of acid-treated hematite, we collected IPCE for these hematite photoanodes as a function of wavelength at 0.2 V *vs.* Ag/AgCl (Figure 5.4b).

The photocurrent density $I$ measured at 0.2 V vs. Ag/AgCl was calculated according to the equation:

where $E(\lambda)$ is the solar spectral irradiance at a specific wavelength ($\lambda$) and IPCE($\lambda$) is the obtained IPCE profile of the hematite sample as a function of wavelength ($\lambda$) at 0.2 V vs. Ag/AgCl. The calculated photocurrent density, 0.95 mA/cm$^2$, is only slightly smaller than the experimental value of 1.07 mA/cm$^2$ obtained at the same potential (Figure 5.4b inset), indicating the discrepancy due to the mismatch between the simulated light and the standard AM 1.5 G solar spectrum is minor. As shown in Figure 5.4b, the acid-treated hematite exhibits

significantly enhanced IPCE values compared to the untreated sample over the entire wavelength range between 350 and 650 nm. IPCE values of both samples gradually drop to zero at wavelengths beyond 600 nm, in accordance with the bandgap of hematite. Taken together, these results proved that the enhanced photocurrent density of acid-treated hematite is due to improved efficiency of charge collection following light harvesting. While acid-treated samples show substantially enhanced photocurrent, it was unclear if the acid treatment would affect its photostability. We tested the acid-treated hematite photoanode under illumination (AM 1.5 G, 100 mW/cm$^2$) at 0.2 V *vs.* Ag/AgCl for 24 hours. As shown in Figure 5.4c, it exhibits excellent photostability without obvious photocurrent decay.Additionally, it proves that the enhanced photocurrent of acid-treated hematite was not at the expense of photostability.

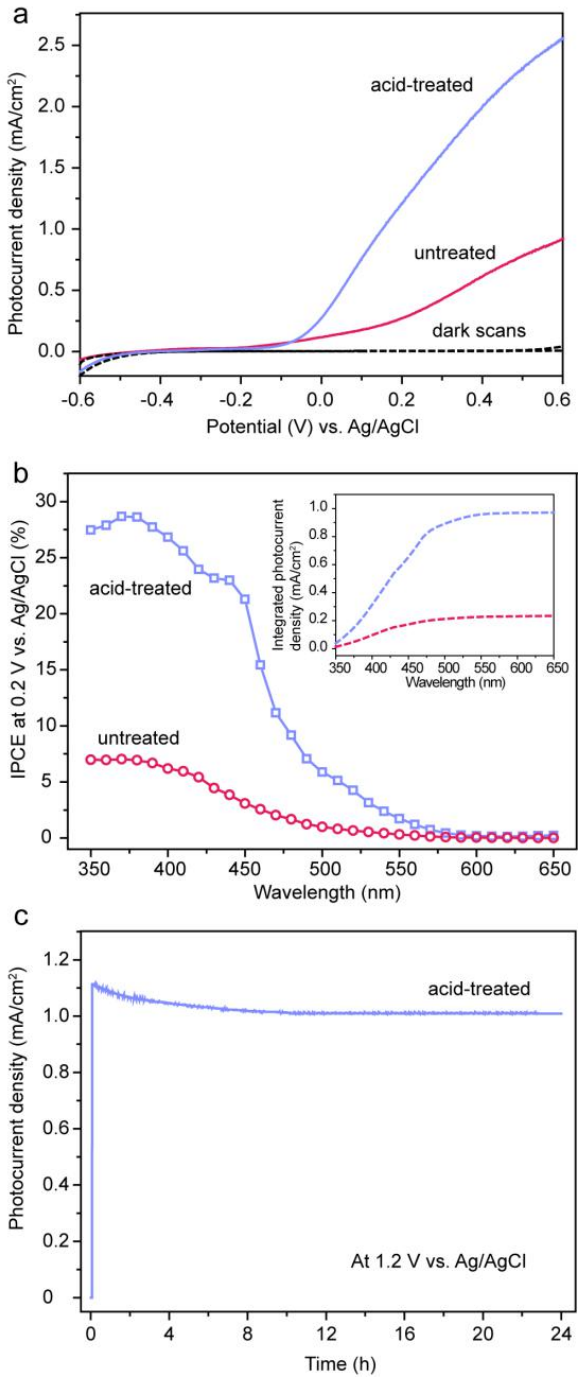


**Figure 5.4.**(a) Linear sweep voltammograms collected for untreated hematite and acid-treated hematite photoaonodes. (b) IPCE spectra of untreated hematite and acid-treated hematite collected at 0.2 V vs. Ag/AgCl. Inset: calculated photocurrent density of untreated and acid-treated hematite.(c) *I–t* curve of acid-

treated hematite.

The improved charge collection efficiency in acid-treated hematite can be attributed to a number of factors. We investigated the influence of acid treatment on the electronic properties of hematite and its possible relation to the enhanced photoactivity. Figure 5.5 a shows the Mott–Schottky plots generated based on the capacitances derived from the electrochemical impedance values obtained at each potential. The donor density of acid-treated hematite was calculated to be $1.11\times10^{20}$ $cm^{-3}$, which is an order of magnitude higher than that of the untreated hematite sample ($1.06\times10^{19}$ $cm^{-3}$). The increased donor density is expected to improve the electrical conductivity of hematite, and therefore reduce the electrode internal resistance and the voltage drop at the interface of hematite and FTO substrate. Furthermore, we also performed EIS measurements to investigate the influence of acid treatment on the charge transfer at the hematite/electrolyte interface. The Nyquist plots of hematite electrodes consist of a semi-circle in the high-frequency domain and a steep line in the low-frequency domain (Figure 5.5b). In comparison to untreated hematite, the acid treated sample exhibits a smaller semi-circle, indicating the charge transfer resistance ($R_{ct}$) was reduced upon acid treatment. [14, 35]Figure 5.5b inset shows the equivalent circuit used to fit the EIS data. $R_s$ is the series resistance, which includes the sheet resistance of the FTO substrate and the external contact

resistance of the cell. The parallel elements, $R_{kt}$, $C_d$, $R_{ct}$ and $C_t$, characterize the charge transfer resistance and the double layer capacitance for the hematite electrode and Pt counter electrode. Significantly, the charge transfer resistance ($R_{ct}$) of hematite was considerably reduced from 113.6 Ω to 5.1 Ω after acid treatment. The reduced $R_{ct}$ can be attributed to the improved electrical conductivity of acid-treated hematite.

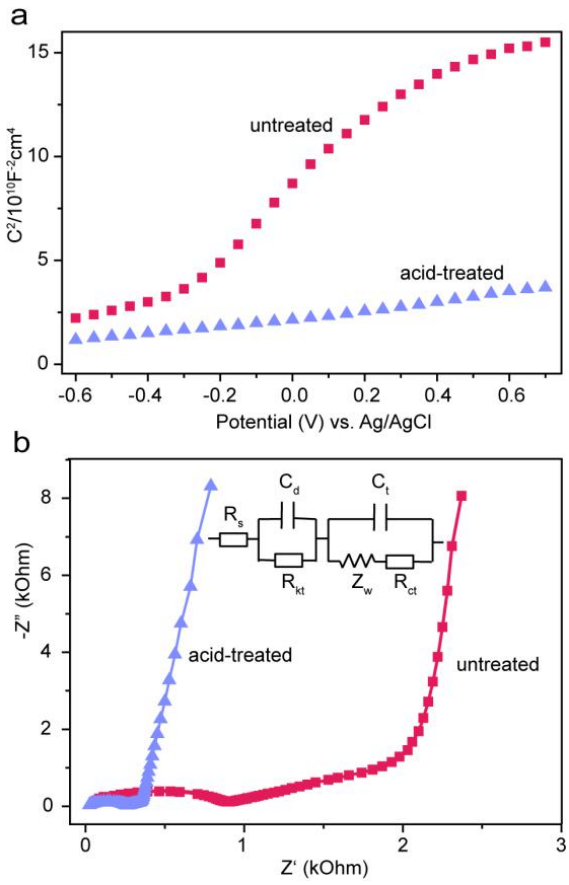


**Figure 5.5.**(a) Mott-Schottky plots of untreated and acid-treated hematite electrodes. (b) EIS spectra of untreated and acid-treated hematite electrodes. Inset : the equivalent circuit to fit the spectra.

It is anticipated that the acid treatment primarily modifies the surface properties of the hematite electrode, however in-light of the measured increased donor density it is also important to assess if the improved activity can be in part at least related to a difference in the yield of initial charge separation, which is defined as the yield of photogenerated holes reaching the surface. Sivula *et al.* have previously described a simple methodology for distinguishing between bulk and surface electron-hole recombination losses [36], where the photoelectrochemical response in the presence of $H_2O_2$, an efficient hole scavenger, is compared to that achieved during water oxidation. Similar experiments here do indicate that we achieve a slight decrease in bulk-electron hole recombination with the yield of photogenerated holes reaching the surface increasing from *ca.* 33% to nearly 50% for acid treated Sn-doped hematite at 0.2 V vs. Ag/AgCl, (Figure 5.6). Whilst significant, this change in charge separation yield alone is not sufficient to explain the very large change in IPCE measured during water splitting, which at 0.2 V vs. Ag/AgCl, 350 nm, increases approximately four-fold (7% to 27%), Figure 1b. This indicates that a change in the surface kinetics is likely to be a more significant factor controlling the enhanced activity.

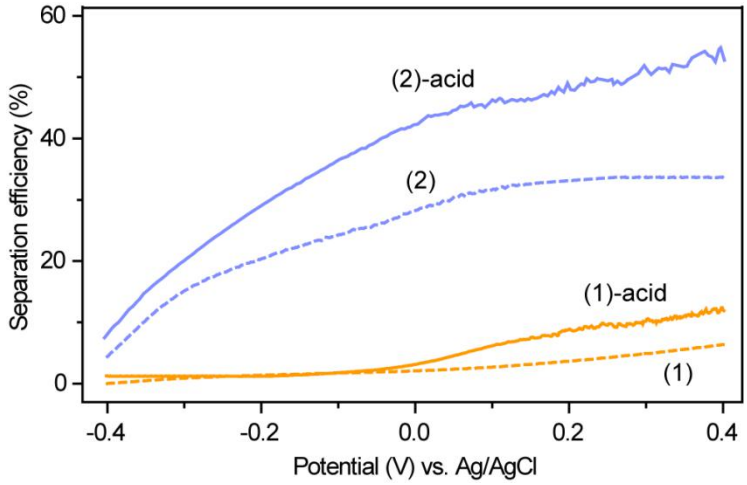


**Figure 5.6.**Plot of yield of charge separation against applied potential for (1) pristine and (2) Sn-doped hematite.

Transient absorption (TA) spectroscopy and transient photocurrent (TPC) measurements allow the direct measurement of the yield and dynamics of photogenerated charges within a photoelectrode. Previous TA spectroscopic studies of hematite photoelectrodes have examined numerous aspects of the photophysics and chemistry of extrinsically and intrinsically doped hematite, including the role of co-catalysts on hole kinetics, the effect of bias on charge trapping and recombination, and the effect of surface passivation on trap states, from the fs–ms timescale. [13, 37-38] In-line with these past studies the TA spectra (500-825 nm) of untreated and acid-treated samples, at a potential where water oxidation is expected to occur (0.2 V), show two distinct features which are well documented in the literature for hematite [38-40]; a broad positive transient absorption at wavelengths greater than ~600 nm and a sharp bleach at ~575 nm

which are assigned to photoholes and trapped photoelectrons respectively (Figure 5.7 a,b). The similar magnitude of the maximum transient signal at 575 nm (*ca.* -1x$10^{-4}$ O.D. Figure 5.8a,b), indicates that following initial charge separation a similar yield of photoelectrons are trapped at inter-band states in both films. However we find that the rate of recovery of the 575 nm bleach, i.e. the rate of loss of trapped electrons, is markedly accelerated following the acid treatment and can be well fitted to a single exponential decay function with a time constant of 7.1 ± 1 ms for the acid treated sample and 40 ± 4 ms for the untreated sample. Trap mediated electron-hole recombination at, or close to the hematite surface has been shown to be a significant loss pathway in several studies [37, 41-43] and here we explore the fate of the de-trapped electrons measured by TA through comparison to the recorded transient photocurrent (Figure 5.8a, b). In both samples the rate of decay of the 575 nm TA signal is similar to the rate of charge extraction as measured by TPC (Figure 5.8b), indicating that a portion of the de-trapped electrons are able to reach the external circuit. However despite the similar initial concentration of trapped electrons, we note a far lower charge extraction yield in the untreated sample (Figure 5.8b). This indicates that in parallel to electron transport to the external circuit, a 2nd process is occurring which dominates in the untreated sample. We assign the parallel process to recombination, which on this timescale is anticipated to be with surface trapped holes. Here we propose a simple parallel kinetics model

where the trapped electrons can either be extracted to the external circuit to give rise to a photocurrent, or be lost through recombination with trapped holes with the two processes having rate constants $k_{extract}$ and $k_{recomb}$ respectively (Figure 5.9). In our kinetics model the overall rate of loss of the trapped electrons is given by the sum of the parallel rate constants and the yield of each pathway (charge extraction or charge recombination) is determined by the relative rate constants of the processes, a full kinetic analysis is in the Figure 5.10. [44]The greater rate constant for the detrapping and charge extraction pathway following acid treatment gives rise to a higher charge extraction yield. This is in line with the measured improved conductivity and it may also indicate that acid treatments modify either the nature or position of the available trap sites. In this study we are unable to definitively ascertain the spatial positioning of the trap sites within the film however the acid-treatment would be expected to primarily affect surface states. Jang et al., also recently proposed a “re-growth” approach to hematite that modifies surface defects. [31]

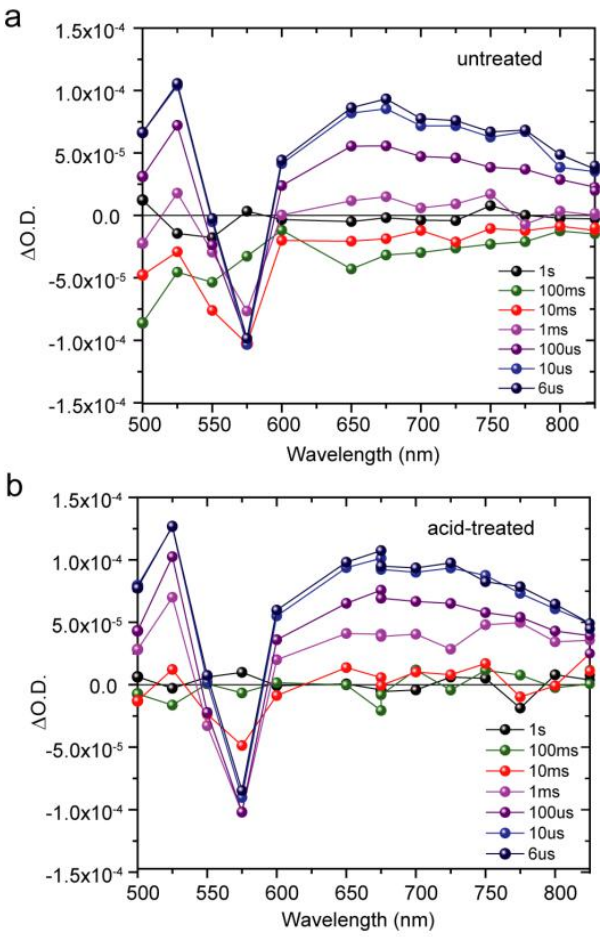


**Figure 5.7.** TA under working photoelectrochemical conditions at 0.2 V vs. Ag/AgCl for (a) untreated and (b) acidtreated hematite.

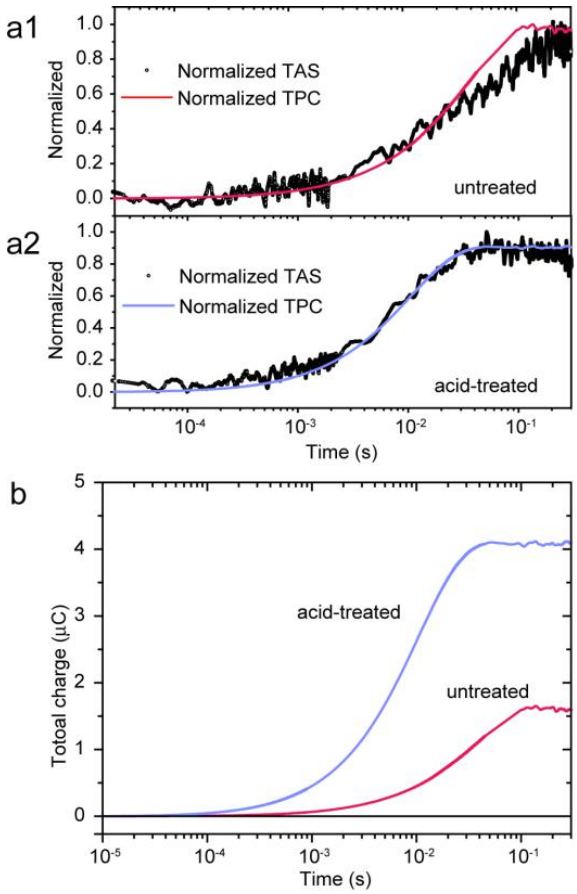


**Figure 5.8.** 575 nm TA signal of photoelectron trapping with the total charge passed derived from TPC for (a1) untreated and (a2) acidtreated hematite under 0.2 V vs. Ag/AgCl. (b) The charge extracted with time before normalization.

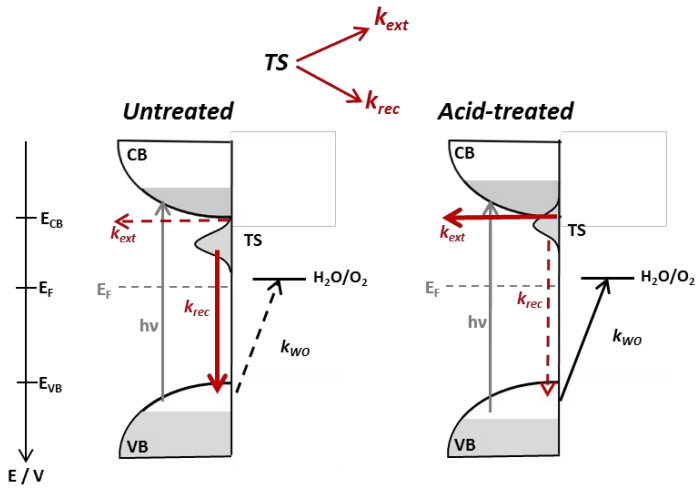

**Figure 5.9**. Proposed kinetic scheme of the untreated and acid-treated hematite.

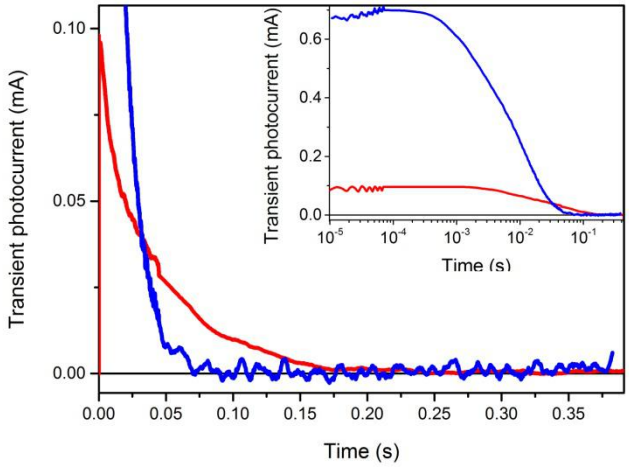


**Figure 5.10**. Transient photocurrent response of the acid treated and untreated hematite samples. Inset: the same data on a logarithmic scale.

In addition to acetic acid, we also tested other inorganic acids including HCl, $HNO_3$ and $H_3PO_4$ for treating hematite nanowire films. Hematite films treated with different acids all show pronounced enhancement in photocurrent (Figure 5.11) proving that acid treatment is a general strategy for enhancing the performance of hematite photoanode. Interesting, we found that acid treated pristine hematite without Sn doping do not show photocurrent enhancement. A possible reason is that the performance of pristine hematite is critically limited by charge separation; the improved rate of electron moving out of traps as a result of acid treatment may have minor effect on the overall performance. To confirm this hypothesis, we have measured the charge separation efficiency of

pristine hematite before and after acid treatment. As shown in Figure 5.6, the acid-treated pristine hematite sample exhibits considerably lower charge separation efficiency compared to the Sn-doped hematite samples, indicating the performance of acid-treated pristine hematite is still mainly limited by the yield of initial charge separation.

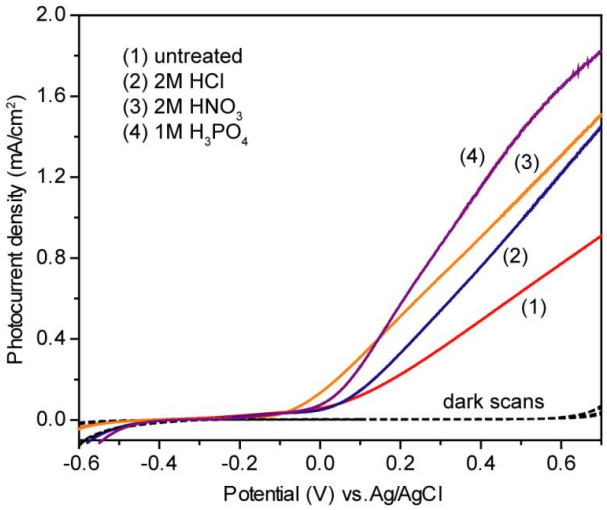


**Figure 5.11**. I-V curves collected for hematite untreated and treated with different acids.

## 5.4 Conclusion

In summary, we have demonstrated that acid treatment can substantially increase the performance of hematite for photoelectrochemical water splitting. Electrochemical impedance spectroscopy studies have shown that enhanced photocurrent is partly due to improved efficiency of charge separation; and moreover, transient absorption and transient photocurrent spectroscopic studies

provide evidence that the improved efficiency can be also related to a minimization of surface electron-hole recombination brought about by an increased detrapping rate, in line with the improved conductivity and potential passivation of surface electron traps. More generally, we believe that present studies open up new opportunities for design and fabrication of high performance hematite electrodes for photoelectrochemical reactions.

**References**


1. R. Liu, Y. J. Lin, L. Y. Chou, S. W. Sheehan, W. S. He, F. Zhang, H. J. M. Hou, D. W. Wang, *Angew. Chem. Int. Ed.* **2011**, *50*, 499-502.
2. K. Sivula, F. Le Formal, M. Gratzel, *Chem. Mater.* **2009**, *21*, 2862-2867.
3. Y. J. Lin, S. Zhou, S. W. Sheehan, D. W. Wang, *J. Am. Chem. Soc.* **2011**, *133*, 2398-2401.
4. G. M. Wang, H. Y. Wang, Y. C. Ling, Y. C. Tang, X. Y. Yang, R. C. Fitzmorris, C. C. Wang, J. Z. Zhang, Y. Li, *Nano. Lett.* **2011**, *11*, 3026-3033.
5. Y. C. Pu, Y. C. Ling, K. D. Chang, C. M. Liu, J. Z. Zhang, Y. J. Hsu, Y. Li, *J. Phys. Chem. C* **2014**, *118*, 15086-15094.
6. Y. Yang, Y. C. Ling, G. M. Wang, Y. Li, *Eur. J. Inorg. Chem.* **2014**, 760-766.
7. F. M. Pesci, G. M. Wang, D. R. Klug, Y. Li, A. J. Cowan, *J. Phys. Chem.*

*C* **2013**, *117*, 25837-25844.

8. Y. C. Pu, G. M. Wang, K. D. Chang, Y. C. Ling, Y. K. Lin, B. C. Fitzmorris, C. M. Liu, X. H. Lu, Y. X. Tong, J. Z. Zhang, Y. J. Hsu, Y. Li, *Nano. Lett.* **2013**, *13*, 3817-3823.

9. X. Y. Yang, A. Wolcott, G. M. Wang, A. Sobo, R. C. Fitzmorris, F. Qian, J. Z. Zhang, Y. Li, *Nano. Lett.* **2009**, *9*, 2331-2336.

10. H. Y. Wang, G. M. Wang, Y. C. Ling, M. Lepert, C. C. Wang, J. Z. Zhang, Y. Li, *Nanoscale* **2012**, *4*, 1463-1466.

11. A. Kay, I. Cesar, M. Gratzel, *J. Am. Chem. Soc.* **2006**, *128*, 15714-15721.

12. K. Sivula, R. Zboril, F. Le Formal, R. Robert, A. Weidenkaff, J. Tucek, J. Frydrych, M. Gratzel, *J. Am. Chem. Soc.* **2010**, *132*, 7436-7444.

13. Y. C. Ling, G. M. Wang, D. A. Wheeler, J. Z. Zhang, Y. Li, *Nano. Lett.* **2011**, *11*, 2119-2125.

14. Y. C. Ling, G. M. Wang, H. Y. Wang, Y. Yang, Y. Li, *Chemsuschem* **2014**, *7*, 848-853.

15. Y. C. Ling, G. M. Wang, J. Reddy, C. C. Wang, J. Z. Zhang, Y. Li, *Angew. Chem. Int. Ed.* **2012**, *51*, 4074-4079.

16. C. X. Kronawitter, I. Zegkinoglou, S. H. Shen, P. Liao, I. S. Cho, O. Zandi, Y. S. Liu, K. Lashgari, G. Westin, J. H. Guo, F. J. Himpsel, E. A. Carter, X. L. Zheng, T. W. Hamann, B. E. Koel, S. S. Mao, L. Vayssieres, *Energy Environ. Sci.* **2014**, *7*, 3100-3121.

17. W. Li, D. He, Y. He, X. Yao, R. L. Grimm, G. W. Brudvig, D.Wang, *Angew. Chem. Int. Ed.* **2015**, *54*, 11428–11432.

18. C. Du, M. T. Mayer, H. Hoyt, J. Xie, G. McMahon, G. Bischoping, D. Wang, *Angew. Chem. Int. Ed.* **2013**, *52*, 12692–12695

19. M. Zhou, H. B. Wu, J. Bao, L. Liang, X. W. Lou, Y. Xie, *Angew. Chem. Int. Edit.* **2013**, *52*, 8579-8583.

20. T. Hisatomi, F. Le Formal, M. Cornuz, J. Brillet, N. Tetreault, K. Sivula, M. Gratzel, *Energy Environ. Sci.* **2011**, *4*, 2512-2515.

21. F. Le Formal, N. Tetreault, M. Cornuz, T. Moehl, M. Gratzel, K. Sivula, *Chem. Sci.* **2011**, *2*, 737-743.

22. J. Brillet, M. Gratzel, K. Sivula, *Nano. Lett.* **2010**, *10*, 4155-4160.

23. R. Liu, Z. Zheng, J. Spurgeon, X. G. Yang, *Energy Environ. Sci.* **2014**, *7*, 2504-2517.

24. B. S. Yeo, A. T. Bell, *J. Phys. Chem. C* **2012**, *116*, 8394-8400.

25. P. L. Liao, J. A. Keith, E. A. Carter, *J. Am. Chem. Soc.* **2012**, *134*, 13296-13309.

26. K. Sun, N. Park, Z. L. Sun, J. G. Zhou, J. Wang, X. L. Pang, S. H. Shen, S. Y. Noh, Y. Jing, S. H. Jin, P. K. L. Yu, D. L. Wang, *Energy Environ. Sci.* **2012**, *5*, 7872-7877.

27. G. M. Wang, Y. C. Ling, X. H. Lu, T. Zhai, F. Qian, Y. X. Tong, Y. Li, *Nanoscale* **2013**, *5*, 4129-4133.

28. M. Barroso, A. J. Cowan, S. R. Pendlebury, M. Gratzel, D. R. Klug, J. R. Durrant, *J. Am. Chem. Soc.* **2011**, *133*, 14868-14871.

29. Y. Ma, A. Kafizas, S. R. Pendleburya, J. R. Durrant, *J. Mater. Chem. A* **2015**, DOI: 10.1039/C5TA05826K

30. C. Y. Cummings, F. Marken, L. M. Peter, A. A. Tahir, K. G. U. Wijayantha, *Chem. Commun.* **2012**, *48*, 2027-2029.

31. J. W. Jang, C. Du, Y. F. Ye, Y. J. Lin, X. H. Yao, J. Thorne, E. Liu, G. McMahon, J. F. Zhu, A. Javey, J. H. Guo, D. W. Wang, *Nat. Commun.* **2015**, DOI:10.1038/ncomms8447.

32. Y. C. Ling, Y. Li, *Part. Part. Syst .Char.* **2014**, *31*, 1113-1121.

33. L. F. Xi, S. Y. Chiam, W. F. Mak, P. D. Tran, J. Barber, S. C. J. Loo, L. H. Wong, *Chem. Sci.* **2013**, *4*, 164-169.

34. T. H. Jeon, W. Choi, H. Park, *J. Phys. Chem. C* **2011**, *115*, 7134-7142.

35. T. Liu, Y. Ling, Y.i Yang, L. Finn, E. Collazo, T. Zhai, Y. Tong, Y. Li, *Nano Energy* **2015**, *12*, 169-177.

36. H. Dotan, K. Sivula, M. Gratzel, A. Rothschild, S. C. Warren, *Energy Environ. Sci.* **2011**, *4*, 958-964.

37. M. Forster, Y. Ling, Y. Yang, D. R. Klug, Y. Li, A. J. Cowan*, *Chem. Sci.***2015,** DOI:10.1039/C5SC00423C

38. M. Barroso, S. R. Pendlebury, A. J. Cowan, J. R. Durrant, *Chem. Sci.* **2013**, *4*, 2724-2734.

39. A. J. Cowan, C. J. Barnett, S. R. Pendlebury, M. Barroso, K. Sivula, M. Gratzel, J. R. Durrant, D. R. Klug, *J. Am. Chem. Soc.* **2011**, *133*, 10134-10140.

40. S. R. Pendlebury, A. J. Cowan, M. Barroso, K. Sivula, J. H. Ye, M. Gratzel, D. R. Klug, J. W. Tang, J. R. Durrant, *Energy Environ. Sci.* **2012**, *5*, 6304-6312.

41. K. Sivula, *J. Phys. Chem. Lett.* **2013**, *4*, 1624-1633.

42. L. Steier, I. Herraiz-Cardona, S. Gimenez, F. Fabregat-Santiago, J. Bisquert, S. D. Tilley, M. Gratzel, *Adv.Funct. Mater.* **2014**, *24*, 7681-7688.

43. O. Zandi, T. W. Hamann, *J. Phys. Chem. Lett.* **2014**, *5*, 1522-1526.

44. P. W. S. Michael J. Pilling, *Reaction Kinetics (Oxford Science Publications) 2nd Edition*, Oxford University Press, **1996**.

**Bibliography**


Li, Y.; Zhang, J. Z. *Laser & Photonics Reviews* **2010,** 4, (4), 517-528.

Wheeler, D. A.; Wang, G.; Ling, Y.; Li, Y.; Zhang, J. Z. *Energy Environ. Sci.* **2012,** 5, (5), 6682-6702.

Gratzel, M. *Nature* **2001,** 414, (6861), 338-344.

Sivula, K.; Zboril, R.; Le Formal, F.; Robert, R.; Weidenkaff, A.; Tucek, J.; Frydrych, J.; Gratzel, M. *J Am Chem Soc* **2010,** 132, (21), 7436-7444.

Sivula, K.; Le Formal, F.; Grätzel, M. *ChemSusChem* **2011,** 4, (4), 432-449.

Wang, G.; Ling, Y.; Li, Y. *Nanoscale* **2012,** 4, (21), 6682-6691.

Wang, G.; Ling, Y.; Wang, H.; Xihong, L.; Li, Y. *Journal of Photochemistry and Photobiology C: Photochemistry Reviews* **2014,** 19, (0), 35-51.

Grätzel M., *Nature,* **2001***,* 414, 338-344

Coridan, R. H.; Shaner, M.; Wiggenhorn, C.; Brunschwig, B. S.; Lewis, N. S. *The Journal of Physical Chemistry C* **2013,** 117, (14), 6949-6957.

Liu, C.; Tang, J.; Chen, H. M.; Liu, B.; Yang, P. *Nano Lett* **2013,** 13, (6), 2989-2992.

Park, H. S.; Lee, H. C.; Leonard, K. C.; Liu, G.; Bard, A. J. *Chemphyschem* **2013,** 14, (10), 2277-2287.

Heller, A. *Science* **1984,** 223, (4641), 1141-1148.

Wang, H.; Wang, G.; Ling, Y.; Lepert, M.; Wang, C.; Zhang, J. Z.; Li, Y.

*Nanoscale* **2012,** 4, (5), 1463-1466.

Aharon-Shalom, E.; Heller, A. *J Electrochem Soc* **1982,** 129, (12), 2865-2866.

Hensel, J.; Wang, G.; Li, Y.; Zhang, J. Z. *Nano Lett.* **2010,** 10, 478-483.

Wang, G.; Wang, H.; Ling, Y.; Tang, Y.; Yang, X.; Fitzmorris, R. C.; Wang, C.; Zhang, J. Z.; Li, Y. *Nano Lett* **2011,** 11, (7), 3026-3033.

Boettcher, S. W.; Warren, E. L.; Putnam, M. C.; Santori, E. A.; Turner-Evans, D.; Kelzenberg, M. D.; Walter, M. G.; McKone, J. R.; Brunschwig, B. S.; Atwater, H. A.; Lewis, N. S. *J Am Chem Soc* **2011,** 133, (5), 1216-1219.

Hwang, Y. J.; Hahn, C.; Liu, B.; Yang, P. *ACS Nano* **2012,** 6, (6), 5060-5069.

Su, J. Z.; Guo, L. J.; Bao, N. Z.; Grimes, C. A. *Nano Lett* **2011,** 11, (5), 1928-1933.

Wang, G.; Ling, Y.; Wang, H.; Yang, X.; Wang, C.; Zhang, J. Z.; Li, Y. *Energy Environ. Sci.* **2012,** 5, (3), 6180-6187.

Zhang, X.; Lu, X.; Shen, Y.; Han, J.; Yuan, L.; Gong, L.; Xu, Z.; Bai, X.; Wei, M.; Tong, Y.; Gao, Y.; Chen, J.; Zhou, J.; Wang, Z. L. *Chem. Commun. (Camb.)* **2011,** 47, (20), 5804-5806.

Jin, T.; Diao, P.; Wu, Q.; Xu, D.; Hu, D.; Xie, Y.; Zhang, M. *Applied Catalysis B: Environmental* **2014,** 148-149, 304-310.

Sayama, K.; Nomura, A.; Arai, T.; Sugita, T.; Abe, R.; Yanagida, M.; Oi, T.; Iwasaki, Y.; Abe, Y.; Sugihara, H. *The Journal of Physical Chemistry B* **2006,** 110, (23), 11352-11360.

Wang, G.; Ling, Y.; Lu, X.; Qian, F.; Tong, Y.; Zhang, J. Z.; Lordi, V.; Rocha Leao, C.; Li, Y. *The Journal of Physical Chemistry C* **2013,** 117, (21), 10957-10964.

Sivula, K. *The Journal of Physical Chemistry Letters* **2013,** 4, (10), 1624-1633.

Zhou, M.; Wu, H. B.; Bao, J.; Liang, L.; Lou, X. W.; Xie, Y. *Angew. Chem. Int. Ed.* **2013,** 52, (33), 8579-8583.

Wang, G.; Ling, Y.; Wheeler, D. A.; George, K. E. N.; Horsley, K.; Heske, C.; Zhang, J. Z.; Li, Y. *Nano Lett* **2011,** 11, (8), 3503-3509.

Ling, Y.; Wang, G.; Reddy, J.; Wang, C.; Zhang, J. Z.; Li, Y. *Angew. Chem.* **2012,** 124, (17), 4150-4155.

Lin, Y.; Zhou, S.; Sheehan, S. W.; Wang, D. *J. Am. Chem. Soc.* **2011,** 133, 2398-2401.

Lin, Y.; Yuan, G.; Sheehan, S.; Zhou, S.; Wang, D. *Energy Environ. Sci.* **2011,** 4, (12), 4862-4869.

Li, L.; Yu, Y.; Meng, F.; Tan, Y.; Hamers, R. J.; Jin, S. *Nano Lett* **2012,** 12, (2), 724-731.

Jing, D. W.; Guo, L. J.; Zhao, L. A.; Zhang, X. M.; Liu, H. A.; Li, M. T.; Shen, S. H.; Liu, G. J.; Hu, X. W.; Zhang, X. H.; Zhang, K.; Ma, L. J.; Guo, P. H., *Int. J. Hydrogen Energy* **2010,** 35, 7087-7097

Hensel, J.; Wang, G. M.; Li, Y.; Zhang, J. Z., *Nano Lett.* **2010,** 10, 478-483.

Wang, G. M.; Yang, X. Y.; Qian, F.; Zhang, J. Z.; Li, Y., *Nano Lett.* **2010,** 10,

1088-1092.

Liu, L. P.; Wang, G. M.; Li, Y.; Li, Y. D.; Zhang, J. Z., *Nano Res.* **2011,** 4, 249-258.

Larsen, G. K.; Fitzmorris, B. C.; Longo, C.; Zhang, J. Z.; Zhao, Y. P., *J.Mater. Chem.* **2012,** 22, 14205-14218.

Walter, M. G.; Warren, E. L.; McKone, J. R.; Boettcher, S. W.; Mi, Q. X.;Santori, E. A.; Lewis, N. S., *Chem. Rev.* **2010,** 110, 6446-6473.

Shin, K.; Yoo, J. B.; Park, J. H., *J. Power Sources* **2013,** 225, 263-268.

Swierk, J. R.; Mallouk, T. E., *Chem. Soc. Rev.* **2013,** 42, 2357-2387.

Khaselev, O.; Turner, J. A., *Science* **1998,** 280, 425-427.

Brillet, J.; Yum, J. H.; Cornuz, M.; Hisatomi, T.; Solarska, R.; Augustynski, J.; Graetzel, M.; Sivula, K., *Nature Photon.* **2012,** 6, 823-827.

Chen, Y. W.; Prange, J. D.; Duhnen, S.; Park, Y.; Gunji, M.; Chidsey, C. E.D.; McIntyre, P. C., *Nature Mater.* **2011,** 10, 539-544.

C. M. Lieber, *MRS Bull.*, 2003, **28**, 486-491.

Y. Li, F. Qian, J. Xiang and C. M. Lieber, *Materials Today*, 2006, **9**, 18-27.

X. C. Jiang, Q. H. Xiong, S. Nam, F. Qian, Y. Li and C. M. Lieber, *Nano Letters*, 2007, **7**, 3214-3218.

L. S. Li, Y. H. Yu, F. Meng, Y. Z. Tan, R. J. Hamers and S. Jin, *Nano Letters*, 2012, **12**, 724-731.

O. Ambacher, *Journal of Physics D-Applied Physics*, 1998, **31**, 2653-2710.

S. K. Lim, M. Brewster, F. Qian, Y. Li, C. M. Lieber and S. Gradecak, *Nano Letters*, 2009, **9**, 3940-3944.

S. A. Dayeh, C. Soci, X. Y. Bao and D. L. Wang, *Nano Today*, 2009, **4**, 347-358.

Y. J. Dong, B. Z. Tian, T. J. Kempa and C. M. Lieber, *Nano Letters*, 2009, **9**, 2183-2187.

Y. Li, J. Xiang, F. Qian, S. Gradecak, Y. Wu, H. Yan, H. Yan, D. A. Blom and C. M. Lieber, *Nano Letters*, 2006, **6**, 1468-1473.

M. Azize, A. L. Hsu, O. I. Saadat, M. Smith, X. Gao, S. P. Guo, S. Gradecak and T. Palacios, *Ieee Electron Device Letters*, 2011, **32**, 1680-1682.

S. A. Dayeh, D. Susac, K. L. Kavanagh, E. T. Yu and D. Wang, *Nano Letters*, 2008, **8**, 3114-3119.

X. F. Duan, Y. Huang, Y. Cui, J. F. Wang and C. M. Lieber, *Nature*, 2001, **409**, 66-69.

Z. H. Zhong, F. Qian, D. L. Wang and C. M. Lieber, *Nano Letters*, 2003, **3**, 343-346.

H. M. Kim, Y. H. Cho, H. Lee, S. I. Kim, S. R. Ryu, D. Y. Kim, T. W. Kang and K. S. Chung, *Nano Letters*, 2004, **4**, 1059-1062.

F. Qian, Y. Li, S. Gradecak, D. L. Wang, C. J. Barrelet and C. M. Lieber, *Nano Letters*, 2004, **4**, 1975-1979.

Y. Huang, X. F. Duan and C. M. Lieber, *Small*, 2005, **1**, 142-147.

M. H. Huang, S. Mao, H. Feick, H. Q. Yan, Y. Y. Wu, H. Kind, E. Weber, R.

Russo and P. D. Yang, *Science*, 2001, **292**, 1897-1899.

J. C. Johnson, H. J. Choi, K. P. Knutsen, R. D. Schaller, P. D. Yang and R. J. Saykally, *Nature Materials*, 2002, **1**, 106-110.

X. F. Duan, Y. Huang, R. Agarwal and C. M. Lieber, *Nature*, 2003, **421**, 241-245.

R. Agarwal, C. J. Barrelet and C. M. Lieber, *Nano Letters*, 2005, **5**, 917-920.

F. Qian, Y. Li, S. Gradecak, H. G. Park, Y. J. Dong, Y. Ding, Z. L. Wang and C. M. Lieber, *Nature Materials*, 2008, **7**, 701-706.

F. Qian, M. Brewster, S. K. Lim, Y. C. Ling, C. Greene, O. Laboutin, J. W. Johnson, S. Gradecak, Y. Cao and Y. Li, *Nano Letters*, 2012, **12**, 3344-3350.

T. Kuykendall, P. J. Pauzauskie, Y. F. Zhang, J. Goldberger, D. Sirbuly, J. Denlinger and P. D. Yang, *Nature Materials*, 2004, **3**, 524-528.

S. H. Lee, Y. H. Mo, K. S. Nahm, E. K. Suh and K. Y. Lim, *Phys. Stat. Sol. (c)*, 2002, **0**, 148-151.

W. Guo, M. Zhang, P. Bhattacharya and J. Heo, *Nano Lett.*, 2011, **11**, 1434-1438.

Y. Tomida, S. Nitta, S. Kamiyama, H. Amano, I. Akasaki, S. Otani, H. Kinoshita, R. Liu, A. Bell and F. A. Ponce, *Applied Surface Science*, 2003, **216**, 502-507.

J. Ohta, H. Fujioka and M. Oshima, *Applied Physics Letters*, 2003, **83**, 3060-3062.

J. R. LaRoche, B. Luo, F. Ren, K. H. Baik, D. Stodilka, B. Gila, C. R. Abernathy, S. J. Pearton, A. Usikov, D. Tsvetkov, V. Soukhoveev, G. Gainer, A. Rechnikov, V. Dimitriev, G. T. Chen, C. C. Pan and J. I. Chyi, *Solid-State Electronics*, 2004,

**48**, 193-196.

C. Pendyala, J. B. Jasins, J. H. Kim, V. K. Vendra, S. Lisenkov, M. Menon and M. K. Sunkara, *Nanoscale*, 2012, **4**, 6269-6275.

S. H. Jo, D. Z. Wang, J. Y. Huang, W. Z. Li, K. Kempa and Z. F. Ren, *Applied Physics Letters*, 2004, **85**, 810-812.

X. H. Zhang, L. Gong, K. Liu, Y. Z. Cao, X. Xiao, W. M. Sun, X. J. Hu, Y. H. Gao, J. A. Chen, J. Zhou and Z. L. Wang, *Advanced Materials*, 2010, **22**, 5292-5296.

Q. Cheng, J. Tang, J. Ma, H. Zhang, N. Shinya and L. C. Qin, *Journal of Physical Chemistry C*, 2011, **115**, 23584-23590.

G. Wang, X. Lu, Y. Ling, T. Zhai, H. Wang, Y. Tong and Y. Li, *ACS Nano*, 2012, **6**, 10296-10302.

X. F. Duan and C. M. Lieber, *Journal of the American Chemical Society*, 2000, **122**, 188-189.

T. Kuykendall, P. Pauzauskie, S. K. Lee, Y. F. Zhang, J. Goldberger and P. D. Yang, *Nano Letters*, 2003, **3**, 1063-1066.

C. Liu, Z. Hu, Q. Wu, X. Z. Wang, Y. Chen, H. Sang, J. M. Zhu, S. Z. Deng and N. S. Xu, *Journal of the American Chemical Society*, 2005, **127**, 1318-1322.

Z. Chen, C. B. Cao and H. S. Zhu, *Journal of Physical Chemistry C*, 2007, **111**, 1895-1899.

H. S. Jung, Y. J. Hong, Y. Li, J. Cho, Y. J. Kim and G. C. Yi, *Acs Nano*, 2008, **2**,

637-642.

D. F. Wang, A. Pierre, M. G. Kibria, K. Cui, X. G. Han, K. H. Bevan, H. Guo, S. Paradis, A. R. Hakima and Z. T. Mi, *Nano Letters*, 2011, **11**, 2353-2357.

W. Gotz, N. M. Johnson, C. Chen, H. Liu, C. Kuo and W. Imler, *Applied Physics Letters*, 1996, **68**, 3144-3146.

I. M. Huygens, K. Strubbe and W. P. Gomes, *Journal of the Electrochemical Society*, 2000, **147**, 1797-1802.

T. Bak, J. Nowotny, M. Rekas and C. C. Sorrell, *Int. J. Hydrogen Energy***2002**, 27, 991-1022.

Y. Li and J. Z. Zhang, *Laser Photonics Rev.***2010**, 4, 517-528.

X. B. Chen, S. H. Shen, L. J. Guo and S. S. Mao, *Chem. Rev.***2010**, 110, 6503-6570.

M. Ni, M. K. H. Leung, D. Y. C. Leung and K. Sumathy, *Renew. Sust. Energ. Rev.***2007**, 11, 401-425.

M. Z. Liu, N. D. Snapp and H. Park, *Chem. Sci.***2011**, 2, 80-87.

K. Shankar, J. I. Basham, N. K. Allam, O. K. Varghese, G. K. Mor, X. J. Feng, M. Paulose, J. A. Seabold, K. S. Choi and C. A. Grimes, *J. Phys. Chem. C***2009**, 113, 6327-6359.

M. Xu, P. M. Da, H. Y. Wu, D. Y. Zhao and G. F. Zheng, *Nano Lett.***2012**, 12, 1503-1508.

Y. R. Smith, B. Sarma, S. K. Mohanty and M. Misra, *Int. J. Hydrogen*

*Energy***2013**, 38, 2062-2069.

S. Y. Noh, K. Sun, C. Choi, M. Niu, K. Xu, M. Yang, S. Jin and D. Wang, *Nano Energy***2012**, 2, 351-360.

R. Sasikala, V. Sudarsan, C. Sudakar, R. Naik, T. Sakuntala and S. R. Bharadwaj, *Int. J. Hydrogen Energy***2008**, 33, 4966-4973.

J. Hensel, G. Wang, Y. Li and J. Z. Zhang, *Nano Lett.***2010**, 10, 478-483.

H. Wang, G. Wang, Y. Ling, M. Lepert, C. C. Wang, J. Z. Zhang and Y. Li, *Nanoscale***2012**, 4, 1463-1466.

L. P. Liu, G. Wang, Y. Li, Y. D. Li and J. Z. Zhang, *Nano Res.***2011**, 4, 249-258.

H. Y. Wang, G. M. Wang, Y. C. Ling, M. Lepert, C. C. Wang, J. Z. Zhang and Y. Li, *Nanoscale***2012**, 4, 1463-1466.

G. M. Wang, Y. C. Ling and Y. Li, *Nanoscale***2012**, 4, 6682-6691.

X. H. Lu, G. M. Wang, S. L. Xie, J. Y. Shi, W. Li, Y. X. Tong and Y. Li, *Chem. Comm.***2012**, 48, 7717-7719.

G. M. Wang, Y. C. Ling, H. Y. Wang, X. Y. Yang, C. C. Wang, J. Z. Zhang and Y. Li, *Energy Environ. Sci.***2012**, 5, 6180-6187.

J. K. Cooper, Y. C. Ling, C. Longo, Y. Li and J. Z. Zhang, *J. Phys. Chem. C***2012**, 116, 17360-17368.

G. Wang, Y. Ling, X. Lu, F. Qian, Y. Tong, J. Zhang, V. Lordi, C. R. Leao and Y. Li, *J. Phys. Chem. C***2013**, 117, 10957-10964.

A. Janotti, J. B. Varley, P. Rinke, N. Umezawa, G. Kresse and C. G. Van de

Walle, *Phys. Rev. B***2010**, 81.

G. M. Wang, H. Y. Wang, Y. C. Ling, Y. C. Tang, X. Y. Yang, R. C. Fitzmorris, C. C. Wang, J. Z. Zhang and Y. Li, *Nano Lett.***2011**, 11, 3026-3033.

S. Hoang, S. P. Berglund, N. T. Hahn, A. J. Bard and C. B. Mullins, *J. Am. Chem. Soc.***2012**, 134, 3659-3662.

X. Lu, G. Wang, T. Zhai, M. Yu, J. Gan, Y. Tong and Y. Li, *Nano Lett.***2012**, 12, 1690-1696.

J. G. Cai, J. F. Ye, S. Y. Chen, X. W. Zhao, D. Y. Zhang, S. Chen, Y. R. Ma, S. Jin and L. M. Qi, *Energy Environ. Sci.***2012**, 5, 7575-7581.

R. A. Parker, *Phys. Rev.***1961**, 124, 1719-&.

G. Boschloo and D. Fitzmaurice, *J. Phys. Chem. B***1999**, 103, 2228-2231.

A. L. Linsebigler, G. Q. Lu and J. T. Yates, *Chem. Rev.***1995**, 95, 735-758.

T. L. Thompson and J. T. Yates, *Top. Catal.***2005**, 35, 197-210.

H. C. Sun, C. F. Huang, Y. T. Chen, T. Y. Wu, C. W. Liu, Y. J. Hsu and J. S. Chen, *IEEE Trans. Electron Devices***2010**, 57, 3186-3189.

X. Wang, G. Liu, L. Wang, J. Pan, G. Q. Lu and H. M. Cheng, *J. Mater. Chem.***2011**, 21, 869-873.

H. Pan, J. Qian, Y. Cui, H. Xie and X. Zhou, *J. Mater. Chem.***2012**, 22, 6002-6009.

M. Jankulovska, T. Berger, T. Lana-Villarreal and R. Gomez, *Electrochim. Acta***2012**, 62, 172-180.

J. Y. Liao, B. X. Lei, H. Y. Chen, D. B. Kuang and C. Y. Su, *Energy Environ. Sci.***2012**, 5, 5750-5757.

J. M. Wu, *J. Cryst. Growth***2004**, 269, 347-355.

A. Fujishima; K. Honda. *Nature* **1972,** 238,37-38.

M. Z. Liu; N. D. Snapp; H. Park. *Chem. Sci.***2011,** 2,80-87.

C. Liu; Y. J. Hwang; H. E. Jeong; P. D. Yang. *Nano Lett.***2011,** 11,3755-3758.

G. K. Mor; K. Shankar; M. Paulose; O. K. Varghese; C. A. Grimes. *Nano Lett.***2005,** 5,191-195.

S. U. M. Khan; M. Al-Shahry; W. B. Ingler. *Science* **2002,** 297,2243-2245.

X. Chen; S. S. Mao. *Chem. Rev.* **2007,** 107,2891-2959.

X. B. Chen; S. H. Shen; L. J. Guo; S. S. Mao. *Chem. Rev.* **2010,** 110,6503-6570.

Y. H. Hu. *Angew. Chem. Int. Ed.* **2012,** 51,12410-12412.

K. S. Joya; Y. F. Joya; K. Ocakoglu; R. Van De Krol. *Angew. Chem. Int. Ed.* **2013,** 52,10426-10437.

B. Liu; H. M. Chen; C. Liu; S. C. Andrews; C. Hahn; P. D. Yang. *J. Am. Chem. Soc.* **2013,** 135,9995-9998.

Y. J. Hwang; C. Hahn; B. Liu; P. D. Yang. *ACS Nano* **2012,** 6,5060-5069.

G. M. Wang; H. Y. Wang; Y. C. Ling; Y. C. Tang; X. Y. Yang; R. C. Fitzmorris; C. C. Wang; J. Z. Zhang; Y. Li. *Nano Lett.***2011,** 11,3026-3033.

Y. Yang; Y. C. Ling; G. M. Wang; Y. Li. *Eur. J. Inorg. Chem.***2014,** 760-766.

H. Y. Wang; G. M. Wang; Y. C. Ling; M. Lepert; C. C. Wang; J. Z. Zhang; Y. Li.

*Nanoscale* **2012,** 4,1463-1466.

S. Hoang; S. W. Guo; N. T. Hahn; A. J. Bard; C. B. Mullins. *Nano Lett.***2012,** 12,26-32.

I. S. Cho; M. Logar; C. H. Lee; L. L. Cai; F. B. Prinz; X. L. Zheng. *Nano Lett.***2014,** 14,24-31.

S. Hoang; S. P. Berglund; N. T. Hahn; A. J. Bard; C. B. Mullins. *J. Am. Chem. Soc.* **2012,** 134,3659-3662.

F. M. Pesci; G. M. Wang; D. R. Klug; Y. Li; A. J. Cowan. *J.Phys.Chem.C***2013,** 117,25837-25844.

S. U. M. Khan; J. Akikusa. *J. Electrochem. Soc.***1998,** 145,89-93.

A. Imanishi; T. Okamura; N. Ohashi; R. Nakamura; Y. Nakato. *J. Am. Chem. Soc.* **2007,** 129,11569-11578.

H. Dotan; K. Sivula; M. Gratzel; A. Rothschild; S. C. Warren. *Energy Environ. Sci.***2011,** 4,958-964.

S. Hu; M. R. Shaner; J. A. Beardslee; M. Lichterman; B. S. Brunschwig; N. S. Lewis. *Science* **2014,** 344,1005-1009.

Y. J. Hwang; A. Boukai; P. D. Yang. *Nano Lett.***2009,** 9,410-415.

B. S. Yeo; A. T. Bell. *J.Phys.Chem.C***2012,** 116,8394-8400.

P. L. Liao; J. A. Keith; E. A. Carter. *J. Am. Chem. Soc.* **2012,** 134,13296-13309.

K. Sun; N. Park; Z. L. Sun; J. G. Zhou; J. Wang; X. L. Pang; S. H. Shen; S. Y. Noh; Y. Jing; S. H. Jin; P. K. L. Yu; D. L. Wang. *Energy Environ. Sci.***2012,**

5,7872-7877.

G. M. Wang; X. H. Lu; T. Zhai; Y. C. Ling; H. Y. Wang; Y. X. Tong; Y. Li. *Nanoscale* **2012,** 4,3123-3127.

G. M. Wang; Y. C. Ling; X. H. Lu; T. Zhai; F. Qian; Y. X. Tong; Y. Li. *Nanoscale* **2013,** 5,4129-4133.

C. Du; X. G. Yang; M. T. Mayer; H. Hoyt; J. Xie; G. Mcmahon; G. Bischoping; D. W. Wang. *Angew. Chem. Int. Ed.* **2013,** 52,12692-12695.

C. Du; M. Zhang; J. W. Jang; Y. Liu; G. Y. Liu; D. W. Wang. *J.Phys.Chem.C***2014,** 118,17054-17059.

Y. C. Mao; H. Yang; J. X. Chen; J. Chen; Y. X. Tong; X. D. Wang. *Nano Energy* **2014,** 6,10-18.

X. H. Xia; J. S. Luo; Z. Y. Zeng; C. Guan; Y. Q. Zhang; J. P. Tu; H. Zhang; H. J. Fan. *Sci. Rep.***2012,** 2.

G. M. Wang; Y. C. Ling; X. H. Lu; H. Y. Wang; F. Qian; Y. X. Tong; Y. Li. *Energy Environ. Sci.***2012,** 5,8215-8219.

Y. C. Pu; Y. C. Ling; K. D. Chang; C. M. Liu; J. Z. Zhang; Y. J. Hsu; Y. Li. *J.Phys.Chem.C***2014,** 118,15086-15094.

R. Liu, Y. J. Lin, L. Y. Chou, S. W. Sheehan, W. S. He, F. Zhang, H. J. M. Hou, D. W. Wang, *Angew. Chem. Int. Ed.* **2011**, *50*, 499-502.

K. Sivula, F. Le Formal, M. Gratzel, *Chem. Mater.* **2009**, *21*, 2862-2867.

Y. J. Lin, S. Zhou, S. W. Sheehan, D. W. Wang, *J. Am. Chem. Soc.* **2011**, *133*,

2398-2401.

G. M. Wang, H. Y. Wang, Y. C. Ling, Y. C. Tang, X. Y. Yang, R. C. Fitzmorris, C. C. Wang, J. Z. Zhang, Y. Li, *Nano. Lett.* **2011**, *11*, 3026-3033.

Y. C. Pu, Y. C. Ling, K. D. Chang, C. M. Liu, J. Z. Zhang, Y. J. Hsu, Y. Li, *J. Phys. Chem. C* **2014**, *118*, 15086-15094.

Y. Yang, Y. C. Ling, G. M. Wang, Y. Li, *Eur. J. Inorg. Chem.* **2014**, 760-766.

F. M. Pesci, G. M. Wang, D. R. Klug, Y. Li, A. J. Cowan, *J. Phys. Chem. C* **2013**, *117*, 25837-25844.

Y. C. Pu, G. M. Wang, K. D. Chang, Y. C. Ling, Y. K. Lin, B. C. Fitzmorris, C. M. Liu, X. H. Lu, Y. X. Tong, J. Z. Zhang, Y. J. Hsu, Y. Li, *Nano. Lett.* **2013**, *13*, 3817-3823.

X. Y. Yang, A. Wolcott, G. M. Wang, A. Sobo, R. C. Fitzmorris, F. Qian, J. Z. Zhang, Y. Li, *Nano. Lett.* **2009**, *9*, 2331-2336.

H. Y. Wang, G. M. Wang, Y. C. Ling, M. Lepert, C. C. Wang, J. Z. Zhang, Y. Li, *Nanoscale* **2012**, *4*, 1463-1466.

A. Kay, I. Cesar, M. Gratzel, *J. Am. Chem. Soc.* **2006**, *128*, 15714-15721.

K. Sivula, R. Zboril, F. Le Formal, R. Robert, A. Weidenkaff, J. Tucek, J. Frydrych, M. Gratzel, *J. Am. Chem. Soc.* **2010**, *132*, 7436-7444.

Y. C. Ling, G. M. Wang, D. A. Wheeler, J. Z. Zhang, Y. Li, *Nano. Lett.* **2011**, *11*, 2119-2125.

Y. C. Ling, G. M. Wang, H. Y. Wang, Y. Yang, Y. Li, *Chemsuschem* **2014**, *7*,

848-853.

Y. C. Ling, G. M. Wang, J. Reddy, C. C. Wang, J. Z. Zhang, Y. Li, *Angew. Chem. Int. Ed.* **2012**, *51*, 4074-4079.

C. X. Kronawitter, I. Zegkinoglou, S. H. Shen, P. Liao, I. S. Cho, O. Zandi, Y. S. Liu, K. Lashgari, G. Westin, J. H. Guo, F. J. Himpsel, E. A. Carter, X. L. Zheng, T. W. Hamann, B. E. Koel, S. S. Mao, L. Vayssieres, *Energy Environ. Sci.* **2014**, *7*, 3100-3121.

W. Li, D. He, Y. He, X. Yao, R. L. Grimm, G. W. Brudvig, D.Wang, *Angew. Chem. Int. Ed.* **2015**, *54*, 11428–11432.

C. Du, M. T. Mayer, H. Hoyt, J. Xie, G. McMahon, G. Bischoping, D. Wang, *Angew. Chem. Int. Ed.* **2013**, *52*, 12692–12695

M. Zhou, H. B. Wu, J. Bao, L. Liang, X. W. Lou, Y. Xie, *Angew. Chem. Int. Edit.* **2013**, *52*, 8579-8583.

T. Hisatomi, F. Le Formal, M. Cornuz, J. Brillet, N. Tetreault, K. Sivula, M. Gratzel, *Energy Environ. Sci.* **2011**, *4*, 2512-2515.

F. Le Formal, N. Tetreault, M. Cornuz, T. Moehl, M. Gratzel, K. Sivula, *Chem. Sci.* **2011**, *2*, 737-743.

J. Brillet, M. Gratzel, K. Sivula, *Nano. Lett.* **2010**, *10*, 4155-4160.

R. Liu, Z. Zheng, J. Spurgeon, X. G. Yang, *Energy Environ. Sci.* **2014**, *7*, 2504-2517.

B. S. Yeo, A. T. Bell, *J. Phys. Chem. C* **2012**, *116*, 8394-8400.

P. L. Liao, J. A. Keith, E. A. Carter, *J. Am. Chem. Soc.* **2012**, *134*, 13296-13309.

K. Sun, N. Park, Z. L. Sun, J. G. Zhou, J. Wang, X. L. Pang, S. H. Shen, S. Y. Noh, Y. Jing, S. H. Jin, P. K. L. Yu, D. L. Wang, *Energy Environ. Sci.* **2012**, *5*, 7872-7877.

G. M. Wang, Y. C. Ling, X. H. Lu, T. Zhai, F. Qian, Y. X. Tong, Y. Li, *Nanoscale* **2013**, *5*, 4129-4133.

M. Barroso, A. J. Cowan, S. R. Pendlebury, M. Gratzel, D. R. Klug, J. R. Durrant, *J. Am. Chem. Soc.* **2011**, *133*, 14868-14871.

Y. Ma, A. Kafizas, S. R. Pendleburya, J. R. Durrant, *J. Mater. Chem. A* **2015**, DOI: 10.1039/C5TA05826K

C. Y. Cummings, F. Marken, L. M. Peter, A. A. Tahir, K. G. U. Wijayantha, *Chem. Commun.* **2012**, *48*, 2027-2029.

J. W. Jang, C. Du, Y. F. Ye, Y. J. Lin, X. H. Yao, J. Thorne, E. Liu, G. McMahon, J. F. Zhu, A. Javey, J. H. Guo, D. W. Wang, *Nat. Commun.* **2015**, DOI:10.1038/ncomms8447.

Y. C. Ling, Y. Li, *Part. Part. Syst .Char.* **2014**, *31*, 1113-1121.

L. F. Xi, S. Y. Chiam, W. F. Mak, P. D. Tran, J. Barber, S. C. J. Loo, L. H. Wong, *Chem. Sci.* **2013**, *4*, 164-169.

T. Liu, Y. Ling, Y.i Yang, L. Finn, E. Collazo, T. Zhai, Y. Tong, Y. Li, *Nano Energy* **2015**, *12*, 169-177.

H. Dotan, K. Sivula, M. Gratzel, A. Rothschild, S. C. Warren, *Energy Environ.*

*Sci.* **2011**, *4*, 958-964.

M. Forster, Y. Ling, Y. Yang, D. R. Klug, Y. Li, A. J. Cowan*, *Chem. Sci.* **2015,** DOI:10.1039/C5SC00423C

M. Barroso, S. R. Pendlebury, A. J. Cowan, J. R. Durrant, *Chem. Sci.* **2013**, *4*, 2724-2734.

A. J. Cowan, C. J. Barnett, S. R. Pendlebury, M. Barroso, K. Sivula, M. Gratzel, J. R. Durrant, D. R. Klug, *J. Am. Chem. Soc.* **2011**, *133*, 10134-10140.

S. R. Pendlebury, A. J. Cowan, M. Barroso, K. Sivula, J. H. Ye, M. Gratzel, D. R. Klug, J. W. Tang, J. R. Durrant, *Energy Environ. Sci.* **2012**, *5*, 6304-6312.

K. Sivula, *J. Phys. Chem. Lett.* **2013**, *4*, 1624-1633.

L. Steier, I. Herraiz-Cardona, S. Gimenez, F. Fabregat-Santiago, J. Bisquert, S. D. Tilley, M. Gratzel, *Adv.Funct. Mater.* **2014**, *24*, 7681-7688.

O. Zandi, T. W. Hamann, *J. Phys. Chem. Lett.* **2014**, *5*, 1522-1526.

P. W. S. Michael J. Pilling, *Reaction Kinetics (Oxford Science Publications) 2nd Edition*, Oxford University Press, **1996**.